



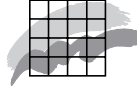
**National Environmental Research Institute**  
University of Aarhus · Denmark

NERI Technical Report No. 609, 2007

# OML: Review of model formulation



*[Blank page]*



**National Environmental Research Institute**  
University of Aarhus · Denmark

---

NERI Technical Report No. 609, 2007

# **OML: Review of model formulation**

Helge Rørdam Olesen  
Ruwim Berkowicz  
Per Løfstrøm.

## Data sheet

Title: OML: Review of model formulation  
Authors: Helge Rørdam Olesen, Ruwim Berkowicz, Per Løfstrøm.  
Department: Department of Atmospheric Environment

Serial title and no.: NERI Technical Report no. 609

Publisher: National Environmental Research Institute ©  
University of Aarhus  
URL: <http://www.neri.dk>

Year of publication: 2007  
Editing complete: December 21, 2006  
Referee: Matthias Ketzel

Financial support: Action Plan for the Aquatic Environment III (VMP III) under the Ministry of Food, Agriculture and Fisheries.

Please cite as: Olesen, H.R., Berkowicz, R.B, Løfstrøm, P., 2007: OML: Review of model formulation. National Environmental Research Institute, Denmark. 130pp. -NERI Technical Report No. 609, <http://www.dmu.dk/Pub/FR609>.

Reproduction is permitted, provided the source is explicitly acknowledged.

Abstract: OML is a local-scale operational air pollution model for estimating dispersion from point sources and area sources. Based on the original OML model, several model versions have been developed over the years to treat different regulatory aspects in Denmark, including assessment of industrial air pollution, regulation of odour and assessment of ammonia deposition. The model was reviewed in 2005-06, and model performance was evaluated with more experimental data than previously. A number of problems were identified, and various issues have been resolved with introduction of new parameterisations in certain parts of the model. The outcome of the process is a revised model, referred to as the "Research Version" of OML.

Keywords: OML, validation, Research Version, air pollution dispersion model, atmospheric dispersion.

Layout: Helge Rørdam Olesen, Ruwim Berkowicz & Majbritt Ulrich  
Drawings: Britta Munter

ISBN: 978-87-7772-971-3  
ISSN (electronic): 1600-0048

Number of pages: 130

Internet version: The report is available in electronic format (pdf) at NERI's webpage <http://www.dmu.dk/Pub/FR609>

Printed copies for sale at: Ministry of the Environment  
Frontlinien  
Rentemestervej 8  
DK-2400 Copenhagen NV  
Denmark  
Tel. +45 7012 0211  
[frontlinien@frontlinien.dk](mailto:frontlinien@frontlinien.dk)

# Contents

## Abstract 5

## Sammenfatning 7

### 1 Introduction 11

### 2 Overview of OML 13

- 2.1 OML model versions 13
- 2.2 The OML modelling system 13
- 2.3 Additional sources of information 14
- 2.4 Guiding principles 15

### 3 Original model formulation 17

- 3.1 The Gaussian dispersion scheme 17
- 3.2 Dispersion parameters 18
- 3.3 Principle of decomposition 20
- 3.4 Vertical dispersion of non-buoyant plumes 21
  - 3.4.1 Vertical dispersion - convective part 21
  - 3.4.2 Vertical dispersion - mechanical part 24
- 3.5 Horizontal dispersion of non-buoyant plumes 28
  - 3.5.1 Contribution from ambient turbulence 28
  - 3.5.2 Modification of horizontal dispersion due to systematic change of wind direction 30
- 3.6 Plume rise 31
  - 3.6.1 Introductory remarks on plume rise 31
  - 3.6.2 References in literature 32
  - 3.6.3 Buoyancy flux and momentum flux 32
  - 3.6.4 Choosing  $\Delta h$  among several candidates 33
  - 3.6.5 Initial plume rise 33
  - 3.6.6 Final plume rise 33
  - 3.6.7 Final rise due to buoyancy 34
  - 3.6.8 Final rise due to momentum 38
  - 3.6.9 Summary of plume rise calculation 38
- 3.7 Penetration 39
- 3.8 Dispersion of buoyant plumes 41
  - 3.8.1 Modification of the turbulent dispersion parameters due to plume buoyancy 41
  - 3.8.2 Buoyancy-induced plume dispersion (internal turbulence) 42
  - 3.8.3 Plume dispersion at the top of the convective boundary layer 44
- 3.9 Stack tip downwash 45
- 3.10 Summary of dispersion parameterization 45
  - 3.10.1 Summary: Components of horizontal dispersion 46
  - 3.10.2 Summary: components of vertical dispersion 47
- 3.11 Wind speed 48
- 3.12 Influence of nearby buildings 49
  - 3.12.1 Decrease of plume rise due to initial dilution. 50
  - 3.12.2 Determination of initial plume dilution radius,  $R_0$  51
  - 3.12.3 Implementation of the  $R_0$ -algorithm in the operational model. 52
- 3.13 Terrain effects 54
- 3.14 Area sources 55

## **4 Problems identified 56**

- 4.1 Overview of problems 56

## **5 Revisions to model formulation 59**

- 5.1 New formulation of the effective wind speed ( $U_{eff}$ ) 59
  - 5.1.1 Background 59
  - 5.1.2 Details of the new formulation 60
- 5.2 New formulation of horizontal dispersion ( $\sigma_y$ ) 61
  - 5.2.1 Background 61
  - 5.2.2 Details of the new formulation 63
- 5.3 New formulation of vertical dispersion 65
  - 5.3.1 Background 65
  - 5.3.2 Details of the new formulation 65
- 5.4 Model performance for non-buoyant plumes 68
  - 5.4.1 Prairie Grass 68
  - 5.4.2 Borex 69
  - 5.4.3 Copenhagen 71
  - 5.4.4 Wind-tunnel experiments 73
- 5.5 Reformulation of plume rise 77
  - 5.5.1 Background 77
  - 5.5.2 Initial Plume Rise 78
  - 5.5.3 Final rise 79
  - 5.5.4 Dispersion of rising plumes 83
- 5.6 Model performance with revised formulation – buoyant plumes 86

## **6 Studies on building effects 89**

- 6.1 Introduction 89
- 6.2 Physical description 89
- 6.3 The models 91
  - 6.3.1 Standard OML 91
  - 6.3.2 AERMOD Prime 91
  - 6.3.3 MISKAM 91
  - 6.3.4 Research Version of OML 91
- 6.4 Investigations based on Thompson's wind tunnel data 92
  - 6.4.1 OML and AERMOD studies 93
  - 6.4.2 Miskam simulations 106
- 6.5 Discussion of building effects 108
- 6.6 Implications for OML development 111

## **7 Conclusions 114**

## **8 Acknowledgements 117**

## **9 References 118**

## **Appendix A 123**

## Abstract

OML is a local-scale operational air pollution model for estimating dispersion from point sources and area sources. It can be applied to both urban and rural settings extending to distances up to approximately 20 km from the sources.

OML is a Gaussian dispersion model. It was basically developed in the 1980's. Compared to previous Gaussian models, several improvements were added: more elaborate schemes for estimating the plume rise, dispersion coefficients that are continuous functions of basic physical parameters (friction velocity, heat flux, stability and mixing height), partial penetration through the top of the mixing layer, terrain features, and a flexible array of user options to control computations and output of statistics and other information.

Based on the original OML model, several model versions have been developed over the years to treat different regulatory aspects in Denmark, including assessment of industrial air pollution, regulation of odour and assessment of ammonia deposition.

The model was reviewed in 2005-06, and model performance was evaluated with more experimental data than previously. A number of problems were identified, and various issues have been resolved with introduction of new parameterisations in certain parts of the model. The outcome of the process is a revised model in a prototype version. In the following, this model version will be referred to as the "Research Version" of OML. The version is not yet fully ready to replace the current regulatory version of OML ("standard OML"). It is recommended that the parameterisations in the Research Version are consolidated by a limited number of additional studies. Further, some additional work concerning the algorithm for building downwash must take place before a complete, revised model is ready to replace the currently operational version.

A substantial effort has been devoted to the study of building effects. At the beginning of the model review it was anticipated that the building algorithm incorporated in the US EPA model AERMOD (PRIME) would be a candidate for inclusion within OML. PRIME is the result of a considerable development effort spent in the USA during the 1990's.

However, it appears that directly adopting an AERMOD approach in OML for building effect will in essence not result in a much more correct model for building effects.

The model review in 2006 was conducted as part of a project on improving dispersion modelling as applied to animal farming. This took place in the context of a larger research programme, Action Plan for the Aquatic Environment III (VMP III) under the Ministry of Food, Agriculture and Fisheries.

The present report is written at the end of the project period within this programme. The report supplies a detailed account of the parameterisa-

tions underlying the currently operational OML model, while also explaining the modifications introduced in the Research Version of the model. Furthermore, a number of outstanding issues are presented.

# Sammenfatning

OML er en operationel luftforureningsmodel, der benyttes til at beregne spredning af luftforurening for punktkilder og arealkilder. Der er tale om en lokalskala model med et gyldighedsområde, som strækker sig til en afstand på omkring 20 km fra kilden. OML er en gaussisk røgfane-model.

Den grundlæggende udvikling af OML-modellen skete i 1980'erne. OML var et af de første eksempler på en ny type af modeller. I stedet for at tage afsæt i en simpel klassificering af spredningsforholdene i diskrete klasser benytter OML sig af en parametrisering, der er baseret på en moderne fysisk forståelse af processerne i atmosfærens grænselag. Adskillige forbedringer blev indført i OML sammenlignet med tidligere modeller, såsom mere detaljerede procedurer til at beregne røgfaneløft, spredningsparametre der er kontinuerte funktioner af basale fysiske parametre (friktionshastighed, varmefluks, stabilitet og blandingshøjde) og delvis penetration gennem grænselagets top.

Fra 1990 er OML blevet benyttet operationelt i Danmark. Det sker bl.a. i tilknytning til Miljøstyrelsens Luftvejledning. Modellen har holdt sig stort set uændret i den forløbne periode indtil 2006, men den er dog blevet udbygget på visse punkter.

Ved siden af den operationelle model – men baseret på den – er der i tidens løb blevet udviklet afledte modelversioner, bl.a. med henblik på lugtproblemer og med henblik på vurdering af ammoniakdeposition.

I forbindelse med Vandmiljøplan III er modellen i 2005-06 blevet underkastet en omfattende gennemgang. Det er sket som et af leddene i et større projekt om lugt fra husdyrproduktion.

Ved gennemgangen i 2005-06 blev modellen testet imod flere eksperimentelle datasæt end tidligere. Disse analyser pegede på en række problemer, som i løbet af projektet er blevet løst gennem ændrede parametriseringer i visse af modellens komponenter.

Som resultat af processen foreligger nu en revideret model i en prototype-version. Denne omtales her i rapporten som "Research Version of OML", mens den operationelle model betegnes "Standard OML".

Nærværende rapport giver en beskrivelse af principperne og modelformuleringen i OML-modellen – både hvad angår den eksisterende standardversion og den ny *Research Version*.

Som nævnt er modellen blevet testet over for et udvalg af eksperimentelle datasæt fra ind- og udland. Det er vigtigt at påpege, at modeleværing med eksperimentelle datasæt på ingen måde er en simpel aktivitet.

Der er i den forbindelse talrige problemer, hvoriblandt følgende kan fremhæves:

- Eksperimentelle datasæt er begrænsede i mange henseender. De er dyre at indsamle, og de vil derfor uvægerligt kun repræsentere en lille del af de mulige scenarier mht. meteorologi og kildens beskaffenhed.
- Det er alt andet end trivielt at tilrettelægge eksperimentelle datasæt til valideringsformål. Dette udsagn dækker over en lang række problemer. Sådanne problemer behandles mere dybtgående i en supplerende rapport (under udarbejdelse, Olesen et al., 2007).
- Der er en uundgåelig variabilitet i målte data, fordi atmosfærisk turbulens er en stokastisk proces. Det indebærer, at uanset om en model er perfekt, så vil dens resultater afvige fra observationer. Når der som her er tale om en enkelt punktkilde og koncentrationssværdier, som måles time for time, gør dette problem sig langt kraftigere gældende end udenforstående normalt gør sig klart.

Disse omstændigheder har som konsekvens, at det ofte er vanskeligt at drage sikre konklusioner om en models træfsikkerhed.

De analyser, der er beskrevet her i rapporten, viser imidlertid gennemgående en bedre grad af træfsikkerhed for den ny *Research Version* end for standard OML. For visse situationer er forbedringen markant, mens den i andre situationer er marginal.

Det er tanken, at den nye *Research Version* skal erstatte standardmodellen. Det anbefales, at inden den eksisterende model erstattes med *Research Version* til operationel brug, gennemføres der modelsimuleringer for et bredt udsnit af kilder og meteorologi. I det omfang det er muligt, er det ønskeligt at gennemføre yderligere validering med nogle eksperimentelle datasæt, der repræsenterer et supplerende udsnit af fysiske forhold.

I forbindelse med de foretagne analyser har vi ikke blot betragtet OML, men også inddraget den amerikanske model AERMOD, der er beslægtet med OML. AERMOD er udarbejdet på foranledning af den amerikanske miljøstyrelse EPA. Vi har foretaget modelvalidering på grundlag af en række eksperimentelle datasæt med simple kildekonfigurationer, hvor bygninger ikke har betydning. I disse sammenligninger giver *Research Version* af OML sammenlignelige eller bedre resultater i forhold til AERMOD.

Herudover har projektet omfattet en del arbejde, hvor bygningers indvirkning på spredning har været i fokus. I forbindelse med dette arbejde er der gjort udstrakt brug af et datasæt fra EPA's vindtunnel, tilvejebragt af R. Thompson (1993). Dette datasæt er særdeles omfattende og har hidtil ikke været genstand for den opmærksomhed, det fortjener.

Den bygningsalgoritme, der indgår i AERMOD - benævnt PRIME - blev oprindeligt anset for at være en naturlig kandidat til at indgå i OML og dermed erstatte OML's nuværende bygningsalgoritme. PRIME er resultatet af en betydelig udviklingsindsats i USA i 1990'erne.

Thompson's datasæt har givet mulighed for at vurdere AERMOD og OML med den nuværende bygningsalgoritme, når modellerne fik til opgave at simulere en lang række konfigurationer af bygningsgeometri og skorstensplacering.

Analyserne på grundlag af Thompsons datasæt viste imidlertid - noget overraskende - at ved at benytte AERMOD's metode til at beregne bygningseffekt, vil man i det store og hele ikke få meget mere præcise resultater for bygningseffekten.

OML har visse erkendte problemer med håndtering af bygninger, men også AERMOD har i mange situationer alvorlige problemer med at simulere bygningseffekter korrekt. Det er derfor ikke nogen anbefalelsesværdig løsning blot at indarbejde AERMOD's metode i OML. Som sagerne står, så må en bruger af enten AERMOD eller OML acceptere temmelig store afvigelser mellem modelforudsigelser og observationer for mange situationer med bygninger. I store afstande fra kilden er forudsigelserne rimelige, men tæt ved kilden kan der let være over- eller under-vurderinger på en faktor 2 eller mere. Problemet bunder i, at bygningseffekter er særdeles komplekse. Det er svært for en simpel model - som OML, AERMOD og mange andre modeller - at simulere dem korrekt. For en modelbruger ser tingene således ud, at hvis han ønsker forudsigelser tæt ved en bygning, så kan han vælge at bruge en simpel model à la OML, men han må i så fald være villig til at acceptere en begrænset nøjagtighed. Alternativt kan han vælge en model af en helt anden type, som er adskillige størrelsesordner mere krævende mht. datakraft, og også krævende på anden vis. Den tyske CFD model MISKAM er et eksempel på en sådan model. MISKAM har været inddraget i undersøgelserne, og i situationer med bygninger giver den klart bedre resultater end AERMOD og OML.

At bruge MISKAM – eller andre CFD-modeller – kræver tilegnelse af specialviden, en stor arbejdsindsats ved tilrettelæggelse af data, samt massive mængder datakraft. Derfor kan MISKAM ikke benyttes til operationelle formål på samme måde som de simple modeller.

Det skal bemærkes, at et af de erkendte problemer med OML formentlig kan imødegås med ret simple ændringer i OML's bygningsalgoritme. Det drejer sig om det problem, at der i modellen er et brat ophør af bygningseffekten, når afstanden mellem skorsten og bygning bliver større end to bygningshøjder. I realiteten er der en effekt også for større afstande, og den aftager gradvis.

Sammenfattende må det anbefales at *Research Version* af OML efter en relativt kort fase med konsolidering afløser den nuværende standard OML model. Enkelte oplagte forbedringer af den nuværende OML bygningsalgoritme bør indføres.

På længere sigt er det ønskeligt med en væsentligt forbedret bygningsalgoritme. At skabe en sådan algoritme vil imidlertid kræve endnu en betydelig udviklingsindsats, uden garanti for succes. Resultaternes kvalitet kan formentlig øges lidt i forhold til den nuværende OML og til AERMOD. Imidlertid er spørgsmålet om bygningseffekt så komplekst, at man må forvente at en hvilken som helst simpel model vil komme til kort i en del situationer.

Som et nyttigt biprodukt fra det foreliggende projekt har arbejdet resulteret i mange iagttagelser, der er af generel interesse for evaluering af spredningsmodeller. Vi har arbejdet indgående med en række eksperimentelle datasæt og har i den forbindelse identificeret en del problemer og faldgruber ved brug af de foreliggende eksperimentelle datasæt. Der gøres rede herfor i en separat rapport om modelvalidering (Olesen et al., 2007).

# 1 Introduction

Air pollution models for local-scale dispersion were developed during the 1980's at the Air Pollution Laboratory under the Danish National Environmental Protection Agency<sup>1</sup>. This work was pursued within an overall project with the Danish title '*Operationelle Meteorologiske Luftkvalitetsmodeller*', or OML, meaning *Operational Meteorological Air Quality Models*.

In 1990, the OML model became operational for regulatory purposes in Denmark. It has remained without major changes in the subsequent period until 2006, although with some additions.

Based on the original OML model, several model versions have been developed over the years to treat different regulatory aspects in Denmark, including assessment of industrial air pollution, regulation of odour and assessment of ammonia deposition.

The model was reviewed in 2005-06, and model performance was evaluated with more experimental data than previously. A number of problems were identified, and various issues have been resolved with introduction of new parameterisations in certain parts of the model. The outcome of the process is a revised model in a prototype version. In the following, this model version will be referred to as the "Research Version" of OML. The version is not yet fully ready to replace the current regulatory version of OML ("standard OML"). It is recommended that the parameterisations in the Research Version are consolidated by a limited number of additional studies. Further, some additional work concerning the algorithm for building downwash must take place before a complete, revised model is ready to replace the currently operational version.

The model review in 2006 was conducted as part of a project on improving dispersion modelling as applied to animal farming. This took place in the context of a larger research programme, Action Plan for the Aquatic Environment III (VMP III) under the Ministry of Food, Agriculture and Fisheries.

The present report is written at the end of the project period within this programme. The report supplies in the first place a detailed account of the parameterisations underlying the currently operational OML model. Secondly, it explains the modifications introduced in the Research Version of the model and presents some of the consequences of these in terms of model performance. Finally, it reports on investigations concerning building effects, which were performed as a stepping stone to the development of improved building algorithms in the model.

Within the project, an extensive set of model evaluation activities have taken place, and have resulted in many findings that are of general interest for model evaluation. Some model evaluation results are included

---

<sup>1</sup> In 1989, the Air Pollution Laboratory became part of the National Environmental Research Agency (NERI) in Denmark. In Danish, NERI is called Danmarks Miljøundersøgelser (or *DMU*).

here, while a separate report provides many additional details on the work with model evaluation (in preparation, Olesen et al., 2007).

Both reports address a specialised, technical audience.

The structure of the present report is as follows:

- Chapter 2 gives an overview of the OML model versions.
- Chapter 3 contains a comprehensive description of the formulation of the original OML model.
- Chapter 4 gives a brief overview of problems identified with the regulatory version during the review of the model in 2005-06.
- Chapter 5 describes the modified formulations in the new Research Version of OML that resolves the problems identified in Chapter 4. Model evaluation results are briefly presented.
- Chapter 6 presents results from the studies on building effects that were conducted as part of the current project.
- The conclusion in Chapter 7 summarises main findings and recommendations.

## 2 Overview of OML

### 2.1 OML model versions

The OML model is comparable to the US EPA model AERMOD (Cinderella et al., 2004) and the British ADMS in respect to the theory underlying the model. At the time of writing, the version of OML available to the public is based on the original model formulation described in Chapter 3. Eventually, it can be expected to be replaced by the final version of the "Research Version" of the model, described in Chapter 5.

The OML model is a computationally fast model, well suited for regulatory purposes. It has a user interface that makes the model easy to use for the large number of non-expert users in Denmark.

The standard model is currently distributed in two versions with a Windows user interface: OML-Point 2.1 (available with Danish menu only) and OML-Multi 5.0, (available in both Danish and English).

OML-Point is applied for a single source (or several collocated sources), while OML-Multi is more flexible and allows multiple point and area sources. The physical basis for all versions of the model is the same.

A model version, suitable for computing short-term concentration fluctuations, has been developed in a first version (Løfstrøm et al., 1994; Løfstrøm et al., 1996). It is designated OML-Lugt (meaning *OML-Odour*), and it consists of a module for short-term concentrations, built into the conventional OML model. Through inclusion of this module, OML has the potential for better handling of odour problems than most regulatory models.

A further variant of the model is OML-DEP. In this version, a deposition module has been added to a restructured 'surface depletion' version of the model in order to compute deposition of ammonia on a local scale.

The present report concerns the core of the model, which is common for all of the versions mentioned.

### 2.2 The OML modelling system

Besides the OML dispersion model itself, the OML modelling system also comprises a meteorological pre-processor. The basic structure of the complete OML modelling system is depicted in Figure 2.1.

The OML meteorological pre-processor is a separate software package that can prepare meteorological measurements for use in the OML model. The package is freely available upon request. The standard version of the pre-processor has as input hourly meteorological measurements from a synoptic or analogous surface station, and twice-daily vertical profiles of temperature from a nearby radiosonde station. Output is

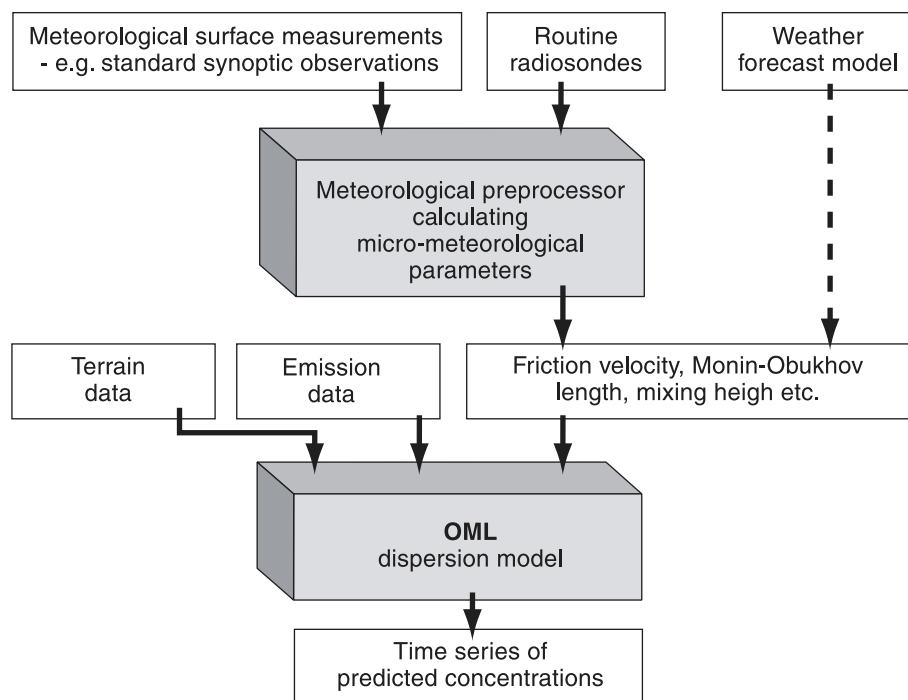


**Figure 2.1** Basic structure of the complete OML modelling system consisting of the meteorological pre-processor as well as the dispersion model.

in this case hourly values of turbulence parameters: most essentially sensible heat flux, Monin-Obukhov length, friction velocity and mixing height. More specialised versions of the pre-processor have been designed for non-standard input such as mast measurements instead of synoptic surface data. The main elements of the meteorological pre-processor have been documented in a number of publications (Nielsen et al., 1981; Berkowicz and Prahm, 1982b; Berkowicz and Prahm, 1982a; Olesen, 2006; Olesen and Brown, 1992; Olesen et al., 1992a). As an alternative to use of the meteorological pre-processor it is possible to derive the necessary meteorological data from a weather forecast model, such as MM5.

### 2.3 Additional sources of information

A large number of publications on OML and its applications exist. For practical application of the Windows version of the model, it is recommended to read the short Getting Started guide (National Environmental Research Institute, 2005), complemented by the help text of the program. There are also older publications describing the file structure etc., namely the User's Guide to OML-Point (Olesen, 1993) and the User's Guide to OML-Multi (Løfstrøm and Olesen, 1994)

Updated information on OML is available on the web: <http://oml-international.dmu.dk> (English) and <http://www.oml.dmu.dk> (Danish).

Further publications include Berkowicz et al., 1986; Olesen, 1995a; Olesen, 1995b; Olesen et al., 1992b

The present report supplies a detailed account of the theory and parameterisations underlying the OML model. Some validation results are in-

cluded here, but a supplementary report (Olesen et al., 2007) gives a much more detailed account of model validation results.

## 2.4 Guiding principles

When the OML project was first initiated in 1980, it had as purpose to improve methods for the simulation of dispersion processes. This improvement was to be obtained by describing dispersion processes in terms of certain physical parameters, shown by recent research to be of basic importance to boundary-layer turbulence. This was in contrast to earlier models that were essentially based upon the empirical Pasquill-Turner stability classification.

The main guiding principles during the early development of the OML model were:

- to construct a model that takes into account the most important physical phenomena governing dispersion of plumes;
- to ensure that the model performs well in a variety of atmospheric conditions;
- to avoid discontinuities in the description of the dispersion processes;
- to ensure that the model results are applicable for regulatory purposes.

These guiding principles still hold truth in 2006.

The fact that the OML model is designed to be used on a routine basis requires, however, that the degree of complexity should be limited. With this in mind, results from studies with more sophisticated models have been condensed and incorporated in the parameterisations. Overall, the most significant simplification in OML is the use of the Gaussian plume formulation.

In 2006, thanks to the power of modern computers, it is possible to use more sophisticated parameterisations than at the time the model was first developed. This is utilized, e.g., in a revised formulation of vertical dispersion in the Research Version of OML, as outlined in Chapter 5.

With regard to the parameterisations described in the remainder of the present report, they were formulated with a basis in literature and physical considerations. However, it must be recognised that the correctness of individual parameterisations cannot be stringently proved. What we observe in the atmosphere is the combined effect of many physical processes. In the model, often these processes are treated separately in mathematical terms, until they are combined mathematically. The advantage of this approach is that for individual processes it is possible to force a correct model response to the variation of physical parameters. But as mentioned, the correctness of the individual parameterisations and the way they are combined is difficult to prove in a stringent manner. The question of whether a certain parameterisation should be

adopted depends on comparisons with experimental data. Numerous tests provide the basis for the parameterisations chosen, but the parameterisations can by no means be regarded as an ultimate truth.

The main characteristics that distinguish the original OML model from previous models are:

- new methods for calculation of plume rise;
- modification of turbulent dispersion due to plume rise;
- special treatment of penetration processes;
- special treatment of plume lofting effect (lofting: as a result of plume rise, the plume may remain close to the top of the boundary layer)
- special treatment of horizontal dispersion in the case of light wind conditions or systematic changes of wind direction;

During the review in 2005-06 certain changes were applied to the model. Despite the earlier attempts to avoid discontinuities, during the review it became clear that the original model was prone to discontinuities in several respects. Also some other problems were identified - see Chapter 4. They have been resolved in the Research Version of the model.

The OML model is designed for short range dispersion in urban and rural environments. It should be noted that the OML model does include some methods to account for hilly terrain; however, the terrain correction methods are crude and can only be applied in slightly hilly terrain typical for, e.g., Danish conditions.

### 3 Original model formulation

In this chapter, the original formulation of the OML model is described in detail. Thus, the chapter describes the formulation before the review in 2005-6. Such a complete description of the model has not previously been available in a single publication. Parts of the description will become outdated when a new OML version is officially released. Nevertheless, it seems appropriate to include it here as reference for the modifications described in Chapter 5.

An operational model intended for regulatory use such as the OML model must be applicable under a wide range of conditions. The OML dispersion model is based on the Gaussian plume formulation. The original OML model assumed a Gaussian distribution in both the horizontal and the vertical directions. This is recognised as a gross simplification, as the Gaussian concept does not adequately describe the vertical structure of a plume. However, the Gaussian model type was chosen for the OML model as a compromise between operational expedience and physical soundness. When the model was developed, a Gaussian model type appeared to be the only type of model capable of dealing satisfactorily with buoyant sources and with a wide range of stability conditions. Further, it was found that even with the Gaussian simplification, significant improvements over earlier models could be achieved, when using a parameterization based on the basic principles of the atmospheric boundary layer.

Several other methods were examined during the course of the early model development. A stochastic Monte-Carlo model, based on non Gaussian probability density function (PDF) was developed (Baerentsen and Berkowicz, 1984). This model was shown capable of simulating dispersion in extremely convective conditions. Performance in other atmospheric dispersion conditions and treatment of buoyant sources was, however, not satisfactory. For this reason the simple Gaussian plume formulation was retained until the review in 2005-6.

The computing power of today is much greater than during the early development of OML, thus making a more sophisticated approach feasible. During the review in 2005-06 it was found appropriate to replace the principle of a purely Gaussian distribution in the vertical with a more sophisticated parameterisation of vertical dispersion. This approach leads to improved model results and is described in Chapter 5.

#### 3.1 The Gaussian dispersion scheme

According to the Gaussian plume model the concentration is given by Eq. (3-1)

$$c(x, y, z) = \frac{Q}{2\pi\bar{u}\sigma_z\sigma_y} * \left[ \exp(-0.5\left(\frac{z-h_{ef}}{\sigma_z}\right)^2) + \exp(-0.5\left(\frac{z+h_{ef}}{\sigma_z}\right)^2) \right] \exp(-0.5\left(\frac{y}{\sigma_y}\right)^2) \quad (3-1)$$

Here,  $Q$  is the source strength,  $h_{ef}$  is the effective plume height,  $\bar{u}$  the effective transport velocity, while  $\sigma_z$  and  $\sigma_y$  are the vertical and horizontal dispersion parameters, respectively. Reflection from the bottom and top of the mixing layer is taken into account by the introduction of imaginary sources. For simplicity, the equation shown as Eq. ( 3-1 ) only includes reflection from the bottom. When the vertical dispersion parameter,  $\sigma_z$ , becomes larger than 1.2 times the height of the mixing layer, the OML model assumes a uniform vertical concentration distribution throughout the entire mixing layer.

In the following, the methods used for determination of the model parameters are described.

### 3.2 Dispersion parameters

Compared to previous models, the main innovation in the OML model is the way in which the dispersion parameters -  $\sigma_z$  and  $\sigma_y$  - are determined. The great majority of older Gaussian models make use of the dispersion parameters and classification methods proposed by (Pasquill, 1961) and later slightly modified by Gifford (1961) and Turner (1964). The Pasquill-Gifford-Turner (PGT) dispersion parameters were deduced from tracer experiments using sources near the ground. In spite of this, however, they are frequently applied for high sources. Dispersion experiments with elevated sources show that the PGT dispersion parameters do in fact perform quite poorly. In an effort to prescribe meaningful dispersion parameters for elevated releases, Briggs (1973) analyzed the PGT curves together with curves determined for high sources: the Brookhaven National Laboratory (BNL) curves, described by Singer and Smith (1966), and the Tennessee Valley Authority (TVA) curves, described by Carpenter et al. (1970). Briggs deduced a new set of dispersion parameters (Gifford, 1976; Gifford, 1975) which gave proper weight to the BNL and TVA data when these deviated from the PGT values. These empirical parameters are used in the Weil and Brower (1982) model.

In the OML model, the dispersion parameters are directly related to the basic physical parameters describing the turbulent state of the atmospheric boundary layer. As the turbulent properties may in general change with the height above the ground, the same is true for the dispersion parameters. In the OML model this dependence is expressed explicitly, making the model applicable for sources of any height.

In view of the simplified nature of the model it was not attempted to provide an "exact" derivation of the dispersion parameters (as well as other model parameters). Instead the known properties in some limiting cases were incorporated, and in order to avoid discontinuity, simple formulas were provided for the "in-between" conditions.

Basically, the dispersion parameters in OML are considered as being composed by a number of different contributions, each being due to one specific dispersion mechanism. It is illustrated in Figure 3.1.

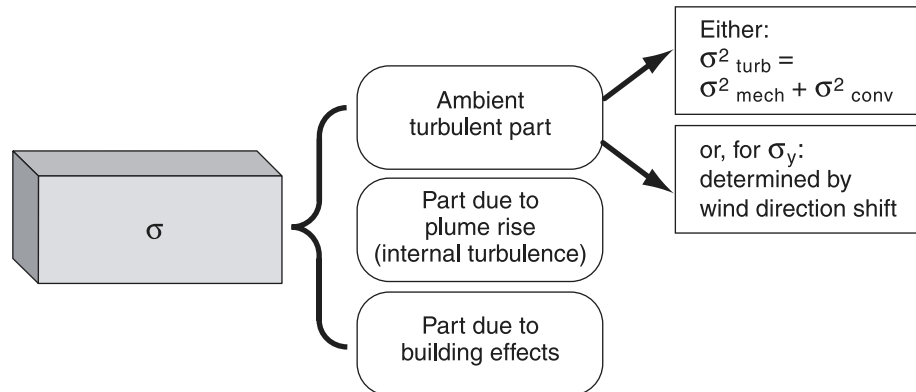


**Figure 3.1** Dispersion parameters in the OML model broken down into their components. A minor contribution from stack tip downwash is not included in the figure. A summary of the components can be found in Section 3.10.

As a main rule, either of the  $\sigma$ 's ( $\sigma_y$  or  $\sigma_z$ ) is composed of the following three parts:

$$\sigma^2 = \sigma_{\text{turb}}^2 + \sigma_{\text{internal}}^2 + \sigma_{\text{building}}^2 \quad (3-2)$$

Here,  $\sigma_{\text{turb}}$  represents dispersion due to the atmospheric turbulence. It can be further decomposed into contributions from mechanical and convective turbulence. Modelling of  $\sigma_{\text{turb}}$  will be described in details in the next sections.

$\sigma_{\text{internal}}$  is only relevant for plumes experiencing plume rise. It represents a contribution due to entrainment of the ambient air into a rising plume, and is referred to as dispersion due to *internal turbulence*. Modelling of  $\sigma_{\text{internal}}$  will be described in connection with discussion of dispersion of buoyant plumes in Section 3.8.2. The contribution is sometimes called *buoyancy-induced dispersion*, as it is usually connected with plumes with significant buoyancy.

$\sigma_{\text{building}}$  is a contribution due to enhancement of dispersion in the wake of buildings near the source. Discussion of buildings effects is presented in Section 3.12. There is an additional minor contribution from stack tip downwash, which is not explicitly shown in Eq. ( 3-2 ). It affects only vertical dispersion, and is discussed in Section 3.9.

Thus, the  $\sigma$  parameters are determined taking all the contributions discussed into account.

After some introductory remarks on the principle of decomposition (Section 3.3), the expressions used for the turbulent part of the dispersion parameters are derived in Sects. 3.4 and 3.5.

Dispersion parameters for passive plumes are not directly applicable to buoyant plumes. This is discussed in Section 3.8. As it is shown there, the plume rise not only has the effect of introducing an additional dilution of

the plume (expressed via  $\sigma_{internal}$ ), but also acts upon the turbulent part of  $\sigma$ ,  $\sigma_{turb}$ .

The derivations of the expressions for the different contributions to the  $\sigma$  parameters are rather lengthy; therefore, a summary of the final results is appropriate; it is found in Section 3.10.

### 3.3 Principle of decomposition

Before presenting the derivation of the expressions for the different parts of the dispersion parameters, a few words must be said about the main principle used for modelling of the ambient turbulence induced dispersion.

In the OML model,  $\sigma_{turb}$  is being regarded as being composed of two contributions: one for mechanical turbulence, the other for convectively induced turbulence:

$$\sigma_{turb}^2 = \sigma_{mech}^2 + \sigma_{conv}^2 \quad (3-3)$$

In (3-3), it is assumed that dispersion is governed by two independent processes. As this procedure is not a trivial one, it requires some explanation.

According to Taylor (1921), the mean square displacement of particles moving in a turbulent field can be expressed as

$$\sigma^2 = \int_0^t \int_0^t \overline{w(t_1)w(t_2)} dt_1 dt_2 \quad (3-4)$$

Here,  $w$  is a turbulent velocity at a given time, and the overbars indicate averaging with respect to different realizations. The turbulent velocities can be described by a Markov chain process (Baerentsen and Berkowicz, 1984).

$$w(t_1) = w_c(t_0)R_c + \eta_{1c}(1 - R_c^2)^{1/2} + w_m(t_0)R_m + \eta_{1m}(1 - R_m^2)^{1/2} \quad (3-5)$$

In (3-5), it is assumed that at a time  $t_1$  a particle has a velocity  $w(t_1)$ , where at time  $t_0$  it had a component  $w_c(t_0)$  due to convective eddies, and a component,  $w_m(t_0)$  due to mechanical eddies.  $R_c$  and  $R_m$  are the respective correlation functions, and  $\eta_{1c}$  and  $\eta_{1m}$  are random variables with a Gaussian distribution and standard deviations  $\sigma_{wc}$  and  $\sigma_{wm}$ , respectively.  $\sigma_{wc}$  and  $\sigma_{wm}$  are the convective and mechanical contributions to the total turbulent energy:

$$\sigma_w^2 = \sigma_{wm}^2 + \sigma_{wc}^2 \quad (3-6)$$

The principle of decomposition of the turbulent energy into a convective and mechanical part is discussed by Berkowicz and Prahm (1984)

Writing a corresponding expression for  $w(t_2)$ , and assuming that the mechanical and convective velocities are uncorrelated, we obtain:

$$\overline{w(t_1)w(t)} = \sigma_{wc}^2 R_c + \sigma_{wm}^2 R_m \quad (3-7)$$

From (3-4) and (3-7), it follows that the dispersion can be separated into two independent parts, convective and mechanical. Each part is governed by the respective contributions to the total turbulent energy and the correlation functions.

In the following, we describe the derivation of the respective contributions to the dispersion parameters.

In Section 3.4, the *vertical dispersion parameter* is discussed. First (Subsect. 3.4.1), an expression for the *convective contribution*  $\sigma_{zc}$  is derived, using simplifying assumptions about the vertical structure of the turbulence and its relation to turbulent diffusion. Next (Subsection 3.4.2), an expression for the *mechanical contribution*  $\sigma_{zm}$  is derived.

In Section 3.5, an expression for the *horizontal dispersion parameter*  $\sigma_y$  is presented. Further (Subsect. 3.5.2), a method is presented for modifying  $\sigma_y$  in order to take account of systematic change of wind direction.

### 3.4 Vertical dispersion of non-buoyant plumes

Considering the vertical dispersion, one must take into account the different nature of the mechanical and convective turbulence. The *convective* turbulence is governed by large and long living eddies. The size of those eddies is determined by the thickness of the boundary layer, i.e. the mixing height  $z_i$ . The *mechanical* turbulence is mainly governed by small, short living eddies, the size of which is determined by the height above the ground. Considering the *intensity* of convective turbulence, it increases with height (at least in the lowest part of the boundary layer), while the height dependence of the intensity of the mechanical turbulence is negligible (e. g. Berkowicz and Prahm, 1984). The large convective eddies lead to strongly correlated motions, while the correlation time of the mechanically generated motions depends on the height above the ground.

Mechanically generated turbulence is in principle present under all atmospheric stability conditions. The convective turbulence is only active in the case of unstable stratified atmosphere and is absent in the case of stable stratification.

Due to the different nature of the convective and the mechanical turbulence, different modelling procedures are required for the respective contributions to turbulent dispersion.

#### 3.4.1 Vertical dispersion - convective part

Theoretical investigations by Deardorff (1972) and laboratory models by Willis and Deardorff (1981; 1978; 1976; 1974) indicate that turbulence and dispersion in a convective boundary layer are controlled by two important parameters: the mixing height  $z_i$  and the convective velocity scale,  $w^*$ :

$$w_* = \left( \frac{g}{T\rho c_p} H z_i \right)^{1/3} \quad (3-8)$$

where  $H$  is the surface sensible heat flux,  $g$  the gravitational acceleration of the earth,  $\rho$  the air density,  $T$  the air temperature, and  $c_p$  the specific heat of the air under constant pressure.

The *intensity of convective turbulence* shows considerable height dependence in the lower part of the boundary layer and is almost constant in the upper part of the boundary layer.

We use here the following simplified expression for  $\sigma_{wc}$ :

$$\sigma_{wc} = \begin{cases} Aw_* \left( \frac{z}{z_i} \right)^{1/3} & \text{for } z < bz_i \\ Ab^{1/3} w_* & \text{for } z \geq bz_i \end{cases} \quad (3-9)$$

The constants are:  $A = 1.241$  and  $b = 0.1$  (the corresponding constants for  $\sigma_{wc}^2$  are, respectively  $A^2 = 1.54$ , and  $(Ab^{1/3})^2 = 0.33$ ).

The value of the constant  $A$  in (3-9) is obtained from analyses of surface-layer measurements of  $\sigma_w$  in convective conditions (Kaimal et al., 1976; Berkowicz and Prahm, 1984).  $\sigma_w$  is known to be almost constant with height in the upper 90% of the boundary layer and this explains the value of the constant  $b$  used in (3-9).

The basis for the formulas for  $\sigma_{zc}$  is the rate equation:

$$\frac{d\sigma_{zc}}{dt} = \sigma_{wc}(z'); \quad \sigma_{zc} = 0 \text{ for } t = 0 \quad (3-10)$$

In writing (3-10), we assume that the rate of growth of the convective dispersion is proportional to the local value of turbulence intensity and that the turbulent motions are perfectly correlated. This assumption is justified by the fact that the convective turbulence is characterized by turbulent motions with a very large time scale. In fact, it follows from the work by Bærentsen and Berkowicz (1984) that this time scale is considerably larger than the time required for particles to be spread through the whole boundary layer.

The further assumption used here is that the turbulence should be estimated at a height  $z'$  corresponding to the centre of mass of the plume. As an approximation we use:

$$z' = h_s \quad \text{for } \sigma_{zc} \leq h_s \quad (3-11)$$

$$z' = \sigma_{zc} \quad \text{for } \sigma_{zc} > h_s$$

where  $h_s$  is the source height.

The explanation of this procedure is the following:

In the initial stage of plume dispersion (i.e. as long as the plume has no contact with the ground), the appropriate height at which turbulence should be evaluated must be the source height (or plume centre line). After the lower boundary of the plume has reached the ground, or more precisely, when  $\sigma_{zc}$  gets larger than  $h_s$ , we expect that the centre-of-mass starts to rise above the source height. Furthermore, the rate of ascent of  $z'$  is assumed to be the same as the growth rate of  $\sigma_{zc}$ .

Using (3-9) for  $\sigma_{wc}$  and with the condition (3-11), Eq. (3-10) can be integrated analytically yielding a set of expressions for  $\sigma_{zc}$ .

When the source is in the upper part of the convective boundary layer, i.e. when  $h_s \geq 0.1z_i$ , then

$$\sigma_{zc}^2 = 0.33w_*^2 t^2 \quad ; \quad t = x/u \quad (3-12)$$

When the source is in the lower part of the boundary layer, i.e.  $h_s < 0.1 z_i$ , then

$$\sigma_{zc}^2 = 1.54w_*^2 \left( \frac{h_s}{z_i} \right)^{2/3} t^2 \quad \text{for } \sigma_{zc} < h_s \quad (3-13)$$

$$\sigma_{zc}^2 = (0.83w_*z_i^{-1/3}t + 0.33h_s^{2/3})^3 \quad \text{for } h_s \leq \sigma_{zc} < 0.1z_i \quad (3-14)$$

$$\sigma_{zc}^2 = (0.581 w_*t + 0.231 h_s^{2/3} z_i^{1/3} - 0.05 z_i)^2 \quad \text{for } \sigma_{zc} \geq 0.1z_i \quad (3-15)$$

In the case of a ground-level source ( $h_s = 0$ ), the vertical dispersion is given by (3-14) and (3-15). Eq. (3-14) is in agreement with results from the free convection theory (Nieuwstadt, 1980).

These equations can be written in a more convenient form using appropriate intervals for the travel time  $t$  and introducing dimensionless variables:

$$\begin{aligned} T &= w_* \frac{t}{z_i} \\ H_s &= \frac{h_s}{z_i} \\ SZ &= \frac{\sigma_{zc}}{z_i} \end{aligned} \quad (3-16)$$

We obtain now the following set of equations:

for  $H_s \geq b$  (for all T)

$$SZ = Ab^{1/3} T \quad (3-17)$$

for  $H_s < b$

$$(short\ travel\ time) \left\{ \begin{array}{l} T < H_s^{2/3} / A \\ SZ = AH_s^{1/3} T \end{array} \right. \quad (3-18)$$

$$(medium\ time) \left\{ \begin{array}{l} H_s^{2/3} / A \leq T < \frac{3}{2} b^{2/3} / A - \frac{1}{2} H_s^{2/3} / A \\ SZ = \left[ \frac{2}{3} AT + \frac{1}{3} H_s^{2/3} \right]^{3/2} \end{array} \right.$$

$$(long\ travel) \left\{ \begin{array}{l} T \geq \frac{3}{2} b^{2/3} / A - \frac{1}{2} H_s^{2/3} / A \\ SZ = Ab^{1/3} T + \frac{1}{2} b^{1/3} H_s^{2/3} - \frac{1}{2} b \end{array} \right.$$

### 3.4.2 Vertical dispersion - mechanical part

We now consider the contribution to vertical dispersion of plumes which is due to mechanically generated turbulence.

According to the aforementioned principle of decomposition, this contribution is treated as an independent part. One should, however, note that properties of the mechanical turbulence depend on stability conditions, and this affects the way in which the mechanical turbulence contributes to dispersion.

Contrary to the convective turbulence, the intensity of mechanically generated turbulence has no significant vertical gradients, at least not in the lower part of the boundary layer. However, the time scale of the mechanical turbulence is much smaller than for the convective case, and also changes with height. These properties must be taken into account when modelling the mechanically induced dispersion.

We make use here of the classical statistical theory of Taylor (1921) which relates dispersion to the correlation function of the turbulent flow. Although this approach is strictly only valid for homogeneous turbu-

lence, we extend it also to the case of non-homogeneity in the Lagrangian time scale.

According to Taylor's statistical theory we can write,

$$\sigma_{zm}^2 = 2\sigma_{wm}^2 \int_0^t \int_0^t R(\tau) d\tau dt' \quad (3-19)$$

Here,  $\sigma_{wm}$  is the mechanical contribution to the vertical turbulent energy and  $R(\tau)$  is the correlation function of the turbulent flow.

For  $\sigma_{wm}$  we use here (Berkowicz and Prahm, 1984)

$$\sigma_{wm}^2 = 1.2u_*^2 \quad (3-20)$$

where  $u_*$  is the friction velocity.

For Lagrangian correlation coefficient  $R$ , we apply here

$$R(\tau) = \exp(-\tau / T_L) \quad (3-21)$$

$T_L$  is the Lagrangian time scale, and it must be considered as some effective time scale at the actual stage of plume dispersion. This means that  $T_L$  becomes effectively a function of travel time  $t$ . This is the aforementioned extension of Taylor's statistical theory to the case of non-homogeneous turbulence. We now need a suitable expression for  $T_L$ .

In Bærentsen and Berkowicz (1984), it is suggested that under convective conditions the Lagrangian time scale can be expressed as,

$$T_L = \frac{\sigma_w^2}{\alpha \varepsilon} \quad (3-22)$$

where  $\varepsilon$  is the turbulent energy dissipation rate and  $\alpha$  is an empirical constant. Here, we use the same procedure also for the mechanical turbulence. We will now express  $T_L$  in terms of basic parameters.

The turbulent energy is given by (3-20). The dissipation rate is both a function of height and the thermal stratification of the boundary layer. In the case of unstable stratification, the part of dissipation related to mechanical turbulence is given by

$$\varepsilon = \frac{u_*^3}{\kappa z} \quad (\text{unstable stratification}) \quad (3-23)$$

where  $\kappa$  is the von Karman constant, and  $z$  is the height above the ground.

For the value of the von Karman constant, the value  $\kappa = 0.35$  has been consistently used until the review in 2005-6. On the occasion of the review it was considered pertinent instead to adopt the value 0.40, which is more commonly used nowadays. This change triggers a series of

changes in the affected formulations in the model, as well as in the meteorological pre-processor. More details follow in Chapters 4 and 5.

However, in this chapter we consider the original model formulation. In the case of a stable stratification, we use

$$\varepsilon = \frac{u_*^3}{\kappa} \left( \frac{1}{z} + \frac{3.7}{L} \right) \quad (\text{stable stratification}) \quad (3-24)$$

Here,  $L$  is the Monin-Obukhov length scale, defined as

$$L = - \frac{u_*^3 \rho c_p}{\kappa \frac{g}{T} H} \quad (3-25)$$

The dissipation rate model used here is based on the assumption that the dissipation of the mechanically created energy is equal to the production rate of the turbulent energy. In the case of a stable stratification, the destruction of the turbulent energy due to thermal stratification is also taken into account (Tennekes and Lumley, 1972). For the constant  $\alpha$  we use here as in Bærentsen and Berkowicz (1984),

$$\alpha = 0.25 \quad (3-26)$$

Finally, the Lagrangian time scale used here becomes

$$T_L = \frac{1.68}{u_*} \left( \frac{1}{z} + I \frac{3.7}{L} \right)^{-1} \quad (3-27)$$

where  $I = 0$  for unstable conditions, and  $I = 1$  for stable conditions.

The height  $z'$ , at which  $T_L$  must be evaluated, is determined here in a way similar to what was done in the case of convective turbulence:

$$\begin{aligned} z' &= h_s \quad \text{for } tu_* < h_s \\ z' &= u_* t \quad \text{for } tu_* \geq h_s \end{aligned} \quad (3-28)$$

This height can be considered as the length scale of eddies responsible for plume dispersion. Eddies of a length  $h_s$  are responsible for plume dispersion as long as the plume has no contact with the ground. Because the mechanical dispersion is proportional to  $u_*$ , the time it takes a mechanically dispersed plume to reach the ground is approximately equal to  $h_s/u_*$ . Thereafter, the upward motion dominates and larger eddies come into play. This gives rise to an increase of the length scale  $z'$  as indicated by (3-28). In the case of a stable stratification, the size of eddies is not only a function of the height above the ground, but through the dependence on the Monin-Obukhov length scale  $L$  it also depends on the stability conditions.

Expression (3-27) for  $T_L$  could now be substituted into (3-21) and (3-19) and integration performed. This procedure would, however, be very lengthy, and in view of all the crude approximations and assumptions,

not worthwhile. Instead, we will perform calculations for extreme cases and finally give appropriate interpolation expressions.

Under unstable conditions ( $L < 0$ ),  $T_L$  becomes proportional to  $z'$ . For a ground-level source, furthermore,  $z'$  is proportional to the travel time  $t$ . In this case, we obtain

$$\sigma_{zm}^2 = 2 (1.2 u_*^2) \int_0^t \left[ \int_0^{t'} \exp(-0.6) d\tau \right] dt' = 1.2 u_*^2 t^2 \exp(-0.6) \quad (3-29)$$

For an elevated source,  $z'$  becomes proportional to the travel time when  $t \gg h_s/u_*$ . The long-time limit for an elevated source is thus the same as given by (3-29). In order to obtain a smooth transition for both elevated and ground-level sources, we use the following approximation of  $\sigma_{zm}$  under unstable conditions:

(unstable)

$$\sigma_{zm,u}^2 = \begin{cases} 1.2 u_*^2 t^2 \exp(-0.6 t u_* / h_s) & \text{for } t u_* / h_s < 1 \\ 1.2 u_*^2 t^2 \exp(-0.6) & \text{for } t u_* / h_s \geq 1 \end{cases} \quad (3-30)$$

Under extremely stable conditions, the Lagrangian time scale becomes constant with height and depends only on the Monin-Obukhov length  $L$ . In this limiting case, i.e. when  $L \ll z$ , it follows from (3-27) that

$$T_{L,stable} = 0.45 \frac{L}{u_*} \quad (3-31)$$

When the Lagrangian time scale is constant, one can use the results from Taylor's (1921) diffusion theory, which predicts that for large travel time, the dispersion becomes proportional to the square root of the travel time. For the case of stable stratification we use thus the following expression:

$$\sigma_{zm}^2 = \frac{\sigma_{zm,n}^2}{1 + 0.5 \frac{t}{T_L}} \quad (3-32)$$

where  $\sigma_{m,n}$  is the neutral limit given by (3-30). Substituting (3-31) into (3-32), we obtain

(stable)

$$\sigma_{zm,s}^2 = \frac{\sigma_{zm,n}^2}{1 + 1.11 \frac{t u_*}{L}} \quad (3-33)$$

To summarise for  $\sigma_{zm}$ :

- In the case of unstable conditions ( $L < 0$ ) the mechanical contribution to  $\sigma_w$  is calculated using Eq. (3-30).
- In the case of stable conditions ( $L > 0$ ) the mechanical contribution to  $\sigma_w$  is calculated using Eq. (3-33).

### 3.5 Horizontal dispersion of non-buoyant plumes

Horizontal dispersion is much more difficult to classify than vertical dispersion because the dependence on large scale effects may be as important as the dependence on the boundary layer parameters.

It is widely accepted that the best method is to relate the horizontal standard deviation  $\sigma_y$  of a plume to the standard deviation  $\sigma_\theta$  of the wind direction fluctuations (Hanna et al., 1982).

$$\sigma_y = \sigma_\theta \overline{ut} F_y(t/T_y) \quad (3-34)$$

Here,  $\sigma_y$  is a universal function of the travel time  $t$  and the horizontal time scale  $T$ . However,  $\sigma_\theta$  is not a standard parameter obtainable from routine meteorological observations.

#### 3.5.1 Contribution from ambient turbulence

In the OML model, the horizontal dispersion is modelled using the concept of superposition of the mechanical and convective parts,

$$\sigma_y^2 = \sigma_{ym}^2 + \sigma_{yc}^2 \quad (3-35)$$

As will be shown in the next section, this procedure is, however, modified in the case of systematic change of wind direction due to large scale effects.

For the convective contribution to the turbulent horizontal dispersion we use an expression proposed by Deardorff (1972) on basis of results from water tank convective boundary layer experiments (Willis and Deardorff, 1976).

$$\sigma_{yc} = \frac{0.5w_* \frac{x}{u}}{\sqrt{1 + 0.9 \frac{xw_*}{z_i u}}} \quad (3-36)$$

For the mechanical contribution, we use

$$\sigma_{ym} = \frac{u_*}{u} x \quad (3-37)$$

which is equivalent to the assumption that,

$$\sigma_{\theta} = \frac{u^*}{u} \quad (3-38)$$

This expression is motivated by the observation that, in the case of neutral or slightly stable conditions, the horizontal standard deviation of a plume is close to  $0.1 x$ . The ratio of  $u^*/\bar{u}$  is, for typical rural conditions, also about 0.1, but this depends upon roughness as well as stability.

A special treatment is used in the case of light wind conditions.

When we consider the situation with stable conditions and light winds, the ratio  $u^*/\bar{u}$  decreases with increasing stability, while many observations show that the horizontal dispersion of hourly averaged plumes may even be greater than under unstable conditions (Van der Hoven, 1976). Hanna (Hanna, 1983) reports that under such conditions (stable, light winds), the hourly averaged horizontal velocity fluctuation does not decrease with decreasing wind speed, but remains almost constant at a value of approximately 0.5 m/s, but with significant scatter. This means that the standard deviation of the wind direction,  $\sigma_{\theta}$ , increases with decreasing wind speed under such conditions. Figure 3.2 shows  $\sigma_{\theta}$  measured at 11 meter height as a function of wind speed. The measurements are from an 11 m meteorological mast in Beldringe, Denmark. From the figure it is clearly seen that wind direction fluctuations increase considerably in the case of low wind speed conditions. In order to take this phenomena into account,  $u^*$  in Eq. (3-37) is therefore replaced by 0.5 m/s in the case of stable stratification when  $u^* < 0.5$  m/s.

Note that during the review of the OML model in 2005-06 it was considered inappropriate to use this value for the lower limit of the horizontal wind velocity fluctuations, and to use it for stable conditions only. The procedure is modified in the Research Version of OML, see Section 5.2.

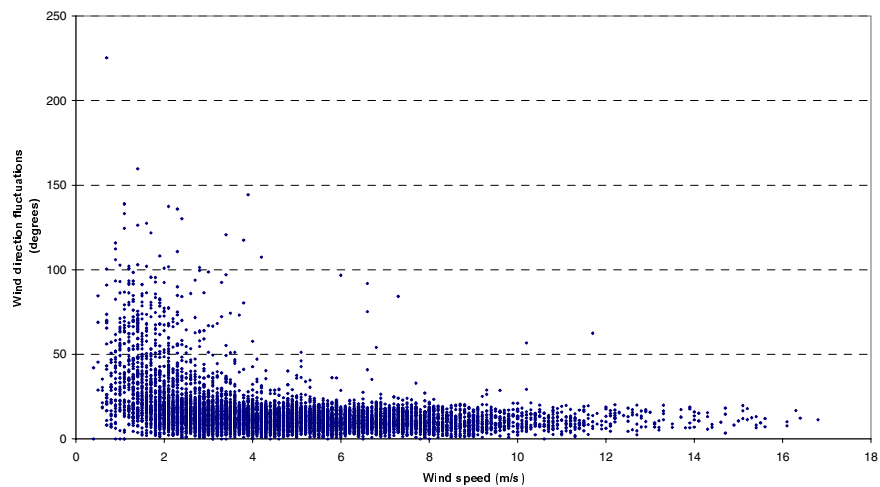


**Figure 3.2**  $\sigma_{\theta}$  as function of wind speed. Measurements from an 11 m mast at Beldringe. Data from the year of 1985.

It should be noted here that the original Pasquill-Gifford-Turner (PGT) curves give much smaller values for  $\sigma_y$  for stable conditions. One must,

however, remember, that the original PGT curves are derived for short term averages, while here we are dealing with hourly averages.

Finally, combining the convective and mechanical contributions, we arrive at the expression used for  $\sigma_y$ :

$$\sigma_y = \left( \frac{0.25w_*^2}{1 + 0.9 \frac{xw_*}{z_i u}} + \max(0.5 \cdot I, u_*)^2 \right)^{1/2} \frac{x}{u} \quad (3-39)$$

where  $I = 0$  for unstable conditions and  $I = 1$  for stable conditions.

Another case, which requires a special treatment, and which usually also is connected with light wind conditions, is a situation with systematic change of wind direction. This case is discussed in the subsequent subsection.

### 3.5.2 Modification of horizontal dispersion due to systematic change of wind direction

In the Gaussian plume model it is assumed that the mean wind direction is stationary for the averaging period under consideration. Frequently, however, a substantial change in mean wind direction takes place between consecutive hours. When this occurs, it is likely that the plume will produce ground-level impact over a larger horizontal area than prescribed by the Gaussian formula with  $\sigma_y$  given by ( 3-39 ). At the same time, the hourly averaged center-line concentration is expected to decrease as the horizontal dilution increases. Hanna (1983) incorporated the effect of systematic change in hourly averaged wind direction into a model of  $\sigma_y$  for stable conditions. In the OML model, we take this effect into account regardless of the stability conditions. The procedure is as follows:

Let  $\Delta_-$  be the change in wind direction (in radians) from the previous to the actual hour. Similarly,  $\Delta_+$  is the change in wind direction between the actual and the following hour.

It is then assumed that the horizontal angle covered by the plume is at least

$$\Delta d = 0.5(\Delta_- + \Delta_+) \quad \text{when } \Delta_- \text{ and } \Delta_+ \text{ are} \quad (3-40)$$

in the same direction

or

$$\Delta d = 0.5\max(\text{abs}(\Delta_-), \text{abs}(\Delta_+)) \quad \text{when } \Delta_- \text{ and } \Delta_+ \text{ are}$$

in opposite directions

A  $\sigma$  value corresponding to this 'change-of-wind-direction-effect' is

$$\sigma_{y\_shift} = (\Delta d / \sqrt{2\pi}) \cdot x \quad (3-41)$$

This is regarded as the minimum value for  $\sigma_y$ . Thus, when  $\sigma_{y\_shift}$  is greater than  $\sigma_y$  given by (3-39), Eq. (3-41) is used for  $\sigma_y$ ; otherwise (3-39) is used.

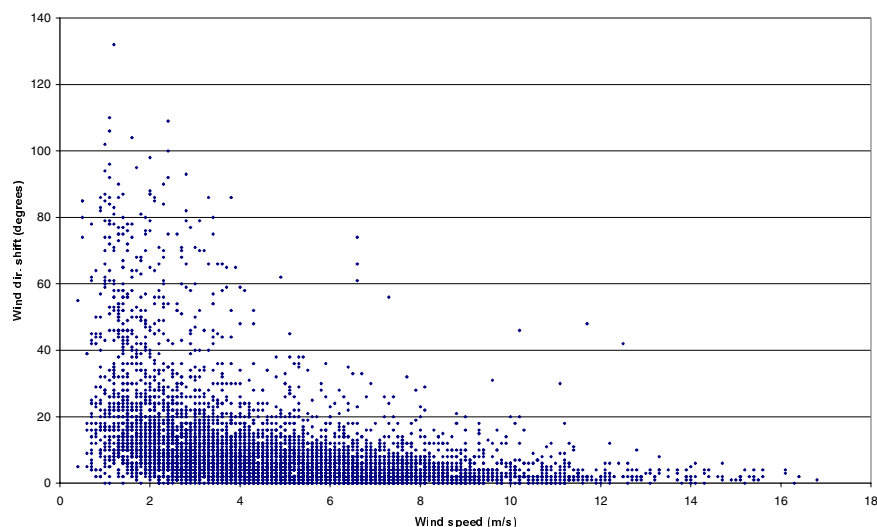


**Figure 3.3** Hourly differences of mean wind direction ( $\Delta d$  in Eq. (3-40)) as a function of wind speed. Data from Beldringe, Denmark (same data set as Figure 3.2).

Figure 3.3 shows the hourly differences of mean wind direction from the Beldringe mast. As seen from this figure, the hour-by-hour change of wind direction frequently increases considerably in the case of low winds. No significant difference between stable and unstable conditions is observed (this cannot be deduced from the figure). Calculation of horizontal dispersion without taking this effect into account will result in underprediction of dilution and thus overprediction of the center-line concentrations.

## 3.6 Plume rise

### 3.6.1 Introductory remarks on plume rise

In the previous chapters we have restricted ourselves to discussing dispersion of passive, i.e. non-buoyant, contaminants. However, a main task of the present model is to estimate dispersion of plumes from industrial sources, which usually have significant amounts of buoyancy.

The main effect of buoyancy is twofold, namely in increasing the effective plume height (plume rise) and in changing the dispersion parameters  $\sigma_y$  and  $\sigma_z$ .

Discussion of the latter effect - change of dispersion parameters - will be postponed to Section 3.8, while *plume rise* will be examined here.

Rising plumes may, under certain conditions, partially or completely penetrate into an elevated stable layer; this has a major influence upon ground level concentrations. The *effect of penetration* on ground level concentrations is discussed in the Section 3.7.

The methods applied in the OML model to account for all the above-mentioned effects are to a wide extent based upon empirical evidence.

The methods are entirely connected with the Gaussian plume model used, and should not be considered to give an exact description of the physical phenomena.

### 3.6.2 References in literature

A variety of methods exists for calculation of plume rise. As part of the OML project, Markvorsen (1982) reviewed available methods. Basically, formulae suggested by Briggs (1975; 1984) for the final plume rise are used in the present model. These formulae are believed to be more physically justified than the earlier, empirical methods by Briggs (1971). The main improvement is that under unstable conditions, the rise is assumed to terminate when the dissipation rate has decayed to that of the surrounding turbulent air (break-up model). Still, unstable conditions represent the most challenging problem in plume rise modelling, and Briggs (1984) warns that his methods are only tentative and suffer from a lack of experimental data for verification. Concerning Briggs' methods, we will only quote the final results here. For more details, the reader is referred to the original papers by Briggs (1975, 1984), and to the report by Weil and Brower (1982) which comments on some of the methods. In addition to the standard methods to be quoted, for convective conditions we have added a "penetration case" meant to represent the fate of a rising plume near an inversion.

In the following description of the computational scheme in the OML model, please note the distinction between the *initial plume rise* close to the source,  $\Delta h_{init}$ , and the *final plume rise*,  $\Delta h_f$ . To represent the position of the plume center at any given distance from the source, the lower of the two is chosen.

In those cases where the plume partially penetrates into an elevated stable layer, a further concept needs to be defined: the *effective plume height*,  $h_{ef}$ , which is assumed to be a height representative for *that part of the plume* which remains in the mixing layer. Derivation of an expression for this height will be postponed to Section 3.7.

### 3.6.3 Buoyancy flux and momentum flux

There are two variables of major importance for plume rise, namely the *buoyancy flux*  $F_B$ , and the *momentum flux*,  $F_M$  (both are initial values for the plume as it is emitted from the stack). The buoyancy flux is by definition given as:

$$F_B = \frac{gV_q}{\pi} \frac{T_s - T_a}{T_s} \quad (3-42)$$

Here,  $V_q$  is the volume flux,  $T_s$  the plume exit temperature and  $T_a$  the ambient air temperature.

The momentum flux is given by:

$$F_M = \frac{w_s V_q}{\pi} \frac{T_a}{T_s} \quad (3-43)$$

Here,  $w_s$  is the exit velocity of the plume, and  $r$  is the stack radius.

For hot industrial emissions, buoyancy flux has by far the dominating effect. In our equations for plume rise, both  $F_B$  and  $F_M$  will be considered during the initial plume rise, while only one of the two parameters is considered for the final rise. An option in the OML model allows the user to neglect the effect of  $F_M$  (if for instance the outlet is horizontal).

### 3.6.4 Choosing $\Delta h$ among several candidates

The entire procedure for determining an  $\Delta h$  value consists of computing various candidates for  $\Delta h$  and choosing among these. The details will be discussed in the following. The total procedure is quite lengthy, and a summary is given in Section 3.6.9.

### 3.6.5 Initial plume rise

First, let us consider *initial plume rise*,  $\Delta h_{init}$ . We follow Briggs (1984; his equation 8.57), and consider this rise to be a (cubic) combination of two components, one dependent on  $F_M$  with an  $x^{1/3}$ -dependence, and the other dependent on  $F_B$  with an  $x^{2/3}$ -dependence:

$$\Delta h_{init} = \left[ \frac{3}{\left(0.4 + 1.2 \frac{u}{w_s}\right)^2} \frac{F_M}{u^2} x + 1.6^3 \frac{F_B}{u^3} x^2 \right]^{1/3} \quad (3-44)$$

Here, and in all the subsequent formulas for plume rise in the present chapter, the wind speed  $u$  is calculated at the stack height.

### 3.6.6 Final plume rise

Next – over the following pages – we shall consider *final plume rise*,  $\Delta h_f$ . The final rise is considered to be due either to plume buoyancy (the rise depends on  $F_B$ ) or plume momentum (the rise depends on  $F_M$ ). Thus, two principal candidates for the final plume rise are calculated on the basis of respectively  $F_B$  and  $F_M$ . The final rise due to buoyancy,  $\Delta h_{f\_buoyancy}$ , is computed by several alternative procedures. Among the several possible  $\Delta h_{f\_buoyancy}$  values, the lowest is chosen as the appropriate. In a similar manner, the final rise due to momentum,  $\Delta h_{f\_momentum}$ , is chosen as the lowest of several candidates. Thus, we end with two principal candidates for the *final plume rise*. The larger of the two is chosen as the appropriate final rise:

$$\Delta h_{f\_dominating} = \max(\Delta h_{f\_buoyant}, \Delta h_{f\_momentum}) \quad (3-45)$$

(Note that there is still another candidate for actual plume rise which is relevant close to the source: the *initial rise*.)

### 3.6.7 Final rise due to buoyancy

Each of the two candidates for final rise will be discussed in turn; first the candidate depending on buoyancy.

#### Neutral break-up, buoyant plume

A value of  $\Delta h_f$ , which is appropriate for plumes rising in a close to neutral atmosphere, and called here *the neutral break-up case*, is calculated from the expression

(neutral break-up)

$$\Delta h_f = 1.17 \left( \frac{F_B}{uu_*^2} \right)^{3/5} \left( \frac{h_s + \Delta h_f}{1 + 3.7 \frac{h_s + \Delta h_f}{L}} \right)^{2/5} \quad (3-46)$$

where  $h_s$  is the stack height and the  $L$ -dependent term in the second denominator is included only for stable conditions. This expression corresponds to equation 8.97 in Briggs (1984). It has been derived in the same manner, but here the constant is slightly corrected (from 1.2 to 1.17) in accordance with Briggs' assumptions; furthermore, a stability correction has been added (the expression depends on the dissipation rate  $\epsilon$ , which we have taken from our equations (3-23) and (3-24)).

Eq. (3-46) is solved using an iterative procedure. A value for  $\Delta h_f$  given by (3-46) is *always* calculated, regardless of stability.

#### Bent-over stable, buoyant plume

For *stable conditions* ( $H < 0$ ), an alternative value for the final rise is calculated in accordance with Briggs (1984, his equation 8.71). The following formula is used when the ambient air can be assumed to have a constant potential temperature gradient  $\partial\theta / \partial z$  above stack height:

(stable, I)

$$\Delta h_f = 2.6 \left( \frac{F_B}{us} \right)^{1/3} \quad (3-47)$$

Here, the stability parameter  $s$  is defined by

$$s = \frac{g}{T} \frac{\partial\theta}{\partial z} \quad (3-48)$$

The determination of  $s$  poses the problem that radio soundings used for measurements of temperature profiles are often not very reliable at low heights; furthermore they are sparse in terms of time and space. Therefore, we have chosen generally to use predictions from the similarity theory for calculation of the temperature gradient to determine  $s$ .

Applying Businger's profiles (Businger et al., 1971), we can write:

$$\frac{\partial \theta}{\partial z} = \frac{\theta_*}{\kappa} \left( \frac{0.74}{z} + \frac{4.7}{L} \right) \quad (3-49)$$

where

$$\theta_* = \frac{u_*^2}{\kappa L \frac{g}{T_a}} \quad (3-50)$$

From (3-49) and (3-50), we obtain

$$s = \frac{u_*^2}{\kappa^2} \left( \frac{0.74}{zL} + \frac{4.7}{L^2} \right) \quad (3-51)$$

Eq. (3-51) is applied at stack height, substituting  $h_s$  for  $z$  in order to calculate  $s$ .

#### **Bent-over stable, buoyant plume rising through irregular stability profile**

However, in certain cases it is evident from radiosonde profiles that a very strongly stable layer (typically a subsidence inversion) is present at some height,  $z_{lid}$ . A technique for the determining such layers is applied in the OML meteorological pre-processor (described by Olesen et al., (1992a)). In this case the plume is first assumed to rise through a layer having the constant stability parameter  $s$ , and then – if it reaches high enough – into a layer of another stability parameter,  $s_{zlid}$ . The appropriate formula for final plume rise is then no longer (3-47), but instead:

(stable, II)

$$\Delta h_f = \left( \frac{3F_B}{u \beta^2 s_{zlid}} + (z_{lid} - h_s)^3 \left(1 - \frac{s}{s_{zlid}}\right) \right)^{1/3} \quad (3-52)$$

where  $\beta = 0.4$  (Briggs, 1975).

Thus, either (3-47) or (3-52) is used to compute a “stable” value for final plume rise, which is compared to the “neutral” value (Eq. (3-46)). Under stable conditions, the lower of the two is the final buoyancy dependent candidate for plume rise (note, however, that there is also a momentum dependent candidate).

#### **Convective break-up, buoyant plume**

Termination of plume rise due to the *convective turbulence* is given by the “break-up model” of Briggs (1975, 1984):

(pure convective case)

$$\Delta h_f = 4.3 \left( \frac{F_B}{u} \right)^{3/5} H_*^{-2/5} \quad (3-53)$$

where

$$H_* = \frac{Hg}{T\rho c_p} \quad (3-54)$$

The constant of 4.3 in (3-53) corresponds to Briggs 1975, equation 8.86<sup>2</sup>.

#### Penetration case

Plume rise may, however, also be terminated or substantially reduced by the presence of an elevated inversion, and the plume may partially or totally penetrate into the elevated stable layer. We call this case for the “*penetration case*” and apply it for unstable conditions.

Briggs (1984) suggests the use of Eq. (3-47), which accounts for the “braking” effect of a stable layer, in order to calculate plume rise in the “penetration case”. The value of  $s$  in (3-47) should correspond to the lapse rate of the stable layer above. This is equivalent to assuming that the lapse rate throughout the mixing layer is the same as in the layer above. In fact, however, the temperature profile in the mixing layer is close to adiabatic, i.e.  $s \approx 0$ .

We use the more realistic approach of assuming a stability parameter of 0 below a certain height,  $z_{mx}$ , and a stability parameter  $s_i$  above it (the height  $z_{mx}$  usually is identical to the mixing height, although there are exceptions). Plume rise is then calculated using the equation for the rate of decrease of buoyancy:

$$\frac{dF_B'}{dz_1} = -su(\beta z_1)^2 \quad (3-55)$$

where  $F_B'$  is the buoyancy of the plume at height  $z_1$  relative to the stack top.  $\beta$  is the entrainment parameter ( $\beta \approx 0.4$ ).  $s$  is here the actual value of the stability parameter, and it is assumed to be zero in the layer below  $z_{mx}$ . The plume starts to lose its buoyancy when it enters the stable layer above  $z_{mx}$ , where the stability parameter  $s$  equals  $s_i$ . In general, only a fraction of the plume resides in the layer above  $z_{mx}$ , and only this fraction of the plume is subject to the loss of buoyancy. Simple geometric considerations (to be discussed in Section 3.7 on penetration) lead to an estimate for this fraction,  $\alpha$ , of the plume:

$$\alpha = 1.5 - \frac{z_{mx} - h_s}{z_1} \quad (3-56)$$

---

<sup>2</sup> In his 1984 paper, Briggs uses a value of 3.0 for this constant. This is due to a different assumption concerning the dissipation rate at plume breakup ( $\epsilon=0.25H^3$  in the 1984 paper, while in the 1975 paper  $\epsilon=0.1H^3$  (Briggs, 1975)). However, Weil and Brower (1982) state that the original value is more consistent with plume rise measurements and they suggest to retain it. Furthermore, Briggs (1984) states that his equation may be conservative. In the OML model the original constant of 4.3 from the 1975 paper has been retained.

Only this part of the plume is affected by the stable stratification, and accordingly the rate of decrease of buoyancy is:

$$\frac{dF_B'}{dz_1} = -s_i u (\beta z_1)^2 \left(1.5 - \frac{z_{mx} - h_s}{z_1}\right) \quad (3-57)$$

Eq. (3-57) can be integrated using the initial condition

$$F_B' = F_B \quad \text{when } z_1 = \frac{z_{mx} - h_s}{1.5} \quad (3-58)$$

The final rise is assumed to have occurred when  $F_B' = 0$ , i.e., when all the buoyancy has been lost. Integration of (3-57) results in:

(penetration case)

$$\Delta h_f^3 = \frac{2F_B}{u \beta^2 s_i} + \Delta h_f^2 (z_{mx} - h_s) - 0.5 \left( \frac{z_{mx} - h_s}{1.5} \right)^3 \quad (3-59)$$

Because (3-59) is cubic in  $\Delta h_f$ , it must be solved numerically using an iteration method.

#### Vertical temperature profile

A few words remain to be said about the values of  $z_{mx}$  and  $s_i$  used. This pair of values is obtained from the OML meteorological pre-processor. For each meteorological scenario, the meteorological pre-processor in fact supplies not only one, but possibly two or three pairs of such values. The three possible types of  $z_{mx}$ -values are:

- the convective boundary layer height  $z_i$  (essentially found by using an inversion rise model)
- the operational mixing height  $z_{mix}$  (which may be identical to  $z_i$ , or may be larger)
- the height  $z_{lid}$  of a clearly defined inversion evident from radio soundings.  $z_{lid}$  does only exist for certain meteorological scenarios.

To each  $z_{mx}$ -height corresponds a stability parameter  $s_i$  defined from the most recent radio sounding. The equation (3-59) could be solved for each pair of  $(z_{mx}, s_i)$ -values, and the lowest  $\Delta h_f$  value could be chosen as the "penetration case" final plume rise. However, as a short-cut, the values of the stability parameters corresponding to  $z_{mix}$  and  $z_i$  are compared in advance in order to obtain essentially the same result, but with less computational effort.

#### Final rise due to buoyancy in unstable conditions - recapitulation

We will now recapitulate the procedure for calculating final plume rise due to buoyancy under unstable conditions:

First, a "neutral" value for  $\Delta h_f$  is computed (Eq. (3-46)). Secondly, a "pure convective" value is computed (Eq. (3-53)), and finally, a "penetration

case" value is found from (3-59). The final plume rise is then chosen as the lower of the three.

### 3.6.8 Final rise due to momentum

We will now consider the second principal candidate for final plume rise: the one due to momentum. As it was the case for the principal candidate due to buoyancy, there are a number of different cases depending on stability. The various cases are as follows:

#### Neutral break-up due to momentum

A value of  $\Delta h_f$ , which is appropriate for plumes rising in a neutral atmosphere, and called here *the neutral break-up case due to momentum*, is calculated from the expression:

$$\Delta h_f = 0.93 \left( 0.4 + 1.2 \frac{u}{w_p} \right)^{-6/7} \left( \frac{F_M}{uu_*} \right)^{3/7} \left( \frac{h_s + \Delta h_f}{1 + \frac{3.7(h_s + \Delta h_f)}{L}} \right)^1 \quad (3-60)$$

The  $L$ -dependent term in the second denominator is included only for stable conditions. This expression corresponds to equation 8.99 in Briggs (1984). It has been derived in the same manner, but a stability correction has been added (the expression depends on the dissipation rate  $\epsilon$ , which we have taken from our equations (3-23) and (3-24). Eq. (3-60) is solved using an iterative procedure.

#### Bent-over, stable rise due to momentum

Another candidate for final rise due to momentum is computed for stable cases.

$$\Delta h_f = 1.1 \left( \frac{F_M}{u \left( 0.4 + 1.2 \frac{u}{w_s} \right)^2} \right)^{1/3} \frac{1}{s^{1/6}} \quad (3-61)$$

#### Convective break-up due to momentum

A third candidate for final rise due to momentum is computed during convective conditions, using the break-up model of Briggs. The pertinent equation is taken from Briggs (1984), equation 8.102. There is a misprint in the book with Briggs' paper; the correct equation is:

$$\Delta h_f = 1.3 \left( 0.4 + \frac{1.2u}{w_s} \right)^{-6/7} \left( \frac{F_M}{u} \right)^{3/7} H_*^{-1/7} \quad (3-62)$$

### 3.6.9 Summary of plume rise calculation

We can now summarize all the information on plume rise calculation which has been presented in the present section.

A primary candidate for *final plume rise due to buoyancy* is determined as the lowest of the following values:

- Neutral break-up, buoyant plume, Eq. (3-46);
- Bent-over stable, buoyant plume. Computed according to either Eq. (3-47) or to Eq. (3-52) (only for stable conditions);
- Convective, buoyant plume, Eq. (3-53) (only for unstable conditions);
- Penetration case, buoyant plume Eq. (3-59) (only for unstable conditions);

In a similar manner, a primary candidate for *final rise due to momentum* is determined as the lowest of the following:

- Neutral break-up, momentum-driven plume, Eq. (3-60);
- Bent-over stable, momentum-driven plume. Computed according to Eq. (3-61) (only for stable conditions);
- Convective, momentum-driven plume, Eq. (3-62) (only for unstable conditions);
- An upper bound: the distance from stack top to mixing height

Of the two principal candidates for final rise, the highest is chosen as *the final rise* (corresponding to the dominant mechanism for plume rise).

Subsequently, the height of the plume centre *at any given distance from the source* is determined using:

$$h_{ef} = h_s + \Delta h \quad (3-63)$$

where

$$\Delta h = \min(\Delta h_{mix}, \Delta h_f) \quad (3-64)$$

Note, however, that in case of penetration, the height given by (3-63) is not representative for that part of the plume, which remains in the boundary layer. This topic will be discussed in Section 3.7.

### 3.7 Penetration

In many plume models, it is assumed that when the effective plume height is predicted to be above the mixing layer height, the plume is decoupled from the ground, resulting in zero ground level concentrations. However, measurements show (e.g. Weil and Brower, 1982), that in just such situations the ground-level concentrations can often be very large. This is due to the fact that the plume might only *partially* penetrate the stable layer capping the mixing layer, while the remaining portion of the

plume is mixed down to the ground. In combination with low wind speeds, this can produce high ground-level concentrations.

Simple geometric considerations can be used to compute the fraction of the plume above the mixing layer. Let  $z_d$  be the depth of the layer between stack top and the top of the mixing layer, i.e.

$$z_d = z_{mix} - h_s \quad (3-65)$$

The width of a plume has been found to be approximately equal to the plume rise (Briggs, 1984). Thus the plume extends from a height of  $h_s+0.5\Delta h$  to  $h_s+1.5\Delta h$ . Therefore, the plume is completely trapped below the top of the mixing layer in the case when

$$\frac{z_d}{\Delta h} > 1.5 \quad (3-66)$$

On the other hand, the plume is entirely above the mixing layer top when:

$$\frac{z_d}{\Delta h} < 0.5 \quad (3-67)$$

For “in-between” cases, we may define a penetration factor  $P$  as the ratio of the part of the plume above the mixing layer to the total plume:

$$P = 1.5 - \frac{z_d}{\Delta h} \quad \text{for } 0.5 \leq \frac{z_d}{\Delta h} \leq 1.5 \quad (3-68)$$

This penetration factor is used for two purposes: the source strength is reduced to an “effective source strength”, and the plume height is reduced to an “effective plume height”. When computing  $P$ , the  $\Delta h$  value used is determined by the entire set of procedures leading to (3-64).

The *effective source strength*,  $Q'$ , is computed as:

$$Q' = Q (1 - P) \quad (3-69)$$

The *effective plume height*,  $h_{ef}$ , is the height representative for that part of the plume which remains in the mixing layer. Following Weil and Brower (1982),  $h_{ef}$  may be calculated as:

$$h_{ef} = h_s + (0.67 + 0.33P)z_d \quad (3-70)$$

In order to obtain continuity, the coefficients 0.67 and 0.33 are used here, while the original coefficients by Weil and Brower were 0.62 and 0.38, respectively.

When penetration occurs,  $h_{ef}$  calculated by (3-70) replaces the (larger) value found from (3-63).

### 3.8 Dispersion of buoyant plumes

As mentioned in Section 3.6, the plume buoyancy has not only the effect of increasing the effective plume height, but also influences the dispersion of the plume. Buoyant plumes that have significant vertical velocity with respect to the ambient air do not follow the ambient air trajectories. The result of this effect is that the turbulence level within the plume is smaller than that of the surrounding air. On the other hand, entrainment of ambient air into the rising plume acts as to increase the spread of the plume. The final result of these two opposing effects depends on the actual meteorological conditions and plume buoyancy.

#### 3.8.1 Modification of the turbulent dispersion parameters due to plume buoyancy

Several experiments performed with the OML-model indicates that in the case of convective, light wind conditions, the use of dispersion parameters derived in Sections 3.4 and 3.5 results in considerable overprediction of near stack ground level concentrations of buoyant plumes. The methods used for derivation of the dispersion parameters for non-buoyant plumes were based on the assumption that the elements of the plume follow the ambient air trajectories. Buoyant plumes, move, however, with respect to the ambient air, with the result that the spread of subsequent plume elements becomes less correlated than would be the case if they followed the air trajectories. Therefore, it is necessary to modify the dispersion parameters in the case of buoyant plumes.

The approach used in the present model is based upon the assumption that the decrease in the turbulent dispersion depends on the ratio of the vertical velocity of the plume to mean wind velocity. The vertical velocity of the plume at a given point during its initial rise – designated  $w_p$  – can be obtained by differentiating (3-44) for initial rise with respect to time:

$$w_p = \frac{2}{3} 1.6 \left( \frac{F}{x} \right)^{1/3} \approx \left( \frac{F}{x} \right)^{1/3} \quad (3-71)$$

Both the vertical and horizontal dispersion parameters are now computed using formulae presented in Sections 3.4 and 3.5, but with the travel distance  $x$  replaced by an effective distance  $x_{ef}$ ,

$$x \rightarrow x_{ef} = x \left( 1 - \exp\left(-0.15 \frac{\bar{u}}{w_p}\right) \right) \quad (3-72)$$

Note that (3-72) is used regardless of stability conditions.

Expression (3-72) is purely empirical. It acts so as to increase the distance to maximum ground-level concentrations. The effect is most significant for convective, light wind conditions.

As it will be shown in Section 3.8.2, the use of the method outlined here results in finite maximum ground level concentration even in the case of zero wind speed convective conditions.

### 3.8.2 Buoyancy-induced plume dispersion (internal turbulence)

Because buoyant plumes have a motion relative to the ambient air they are subject to entrainment processes. Entrainment of the clean, cold air acts as to dilute the plume and thus enhance its dispersion.

In the following we call this effect for *internal dispersion*, or buoyancy-induced dispersion, as it is usually connected with plumes with significant buoyancy. The effect on dispersion parameters is discussed in the present section. You may refer to Eq. ( 3-2 ) and Figure 2.1 for an overview of the components of dispersion parameters.

According to Briggs (1975, 1984) the physical width of a rising buoyant plume is, as previously mentioned, approximately equal to plume rise. Assuming a “top-hat” concentration distribution in the plume, the  $\sigma_{internal}$  of the plume becomes:

$$\sigma_{internal} = \frac{\Delta h}{\sqrt{2\pi}} \quad (3-73)$$

For stable conditions, internal (buoyancy-induced) dispersion can have a substantial influence on plume dispersion. Under these conditions, the “internal” part is often greater than the turbulent part, and neglecting it would lead to severe underestimation of ground-level concentrations.

In the OML model several modifications are made to the internal part of the dispersion parameters. All the modifications are introduced in order to account for some significant deviations of the real plume behaviour from the simple Gaussian plume model used here. The approaches differ for the vertical and horizontal dispersion, respectively.

In the initial stage of rise, a buoyant plume has its axis inclined with respect to the horizontal direction. Eq. (3-73) indicates the width of the plume perpendicular to the plume axis. As far as we are interested in the ground-level concentrations, an erroneous result would result if we directly used the value for  $\sigma_{internal}$  given by (3-73).

Instead of using Eq. (3-73) directly, we must estimate the contribution of buoyancy induced dispersion (internal dispersion) to the vertical dispersion, taking the inclination of the plume axis into account.

The vertical velocity of the plume at a given point of its path is  $w_p$ . The horizontal velocity is the same as wind speed,  $u$ . It is reasonable to assume that the average speed by which the particles move from plume axis, due to internal dispersion, is equal to plume rise velocity, i.e.  $w_p$ . According to this assumption, the velocity is perpendicular to the plume axis. Simple geometric considerations show that the vertical component of this velocity –  $w_p^v$  – is:

$$w_p^v = w_p u / (w_p^2 + u^2)^{1/2} \quad (3-74)$$

The effective  $\sigma_{internal}$  thus becomes

$$\sigma_{z\_internal} = \frac{1}{\sqrt{2\pi}} \int_0^t w_p^v(t') dt' \quad (3-75)$$

where  $t$  is the travel time. Expression (3-75) can be evaluated analytically, but it appears that a very good approximation is:

$$\sigma_{z\_internal} = \frac{1}{\sqrt{2\pi}} \Delta h \exp(-0.6 w_p / u) \quad (3-76)$$

where  $\Delta h$  is the actual plume rise.

The correction due to inclination of plume axis is only valid when the Gaussian formula is used for computation of ground-level concentrations. When OML is used for calculations of concentrations at elevated receptors, a simple linear interpolation is applied to (3-76) in such a way that (3-76) reduces to (3-73) for a receptor height equal to the height of plume center-line.

When the plume is partially above the mixing layer (penetration case), only the fraction  $(1-P)$  contributes to the ground-level concentrations. The internal part of  $\sigma_z$  is in this case also reduced by the factor  $(1-P)$ .

The internal part of the *horizontal* dispersion –  $\sigma_{y\_internal}$  – is basically computed using Eq. (3-73), but with one significant extension, which takes place when the plume is “bumping” or “lofting” an elevated inversion layer.

It is often observed that when the plume rise is terminated by the presence of an elevated stable layer the horizontal dispersion of the plume becomes much larger than else expected (e.g. Weil and Corio (1988)). One can say that the plume behaves in this case like a “hot-air balloon”. It becomes “splashed” when it hits the “loft”. In order to simulate this “lofting effect”, the following procedure is used in OML:

The value of  $\Delta h$  used to calculate  $\sigma_{y\_internal}$  is computed without including penetration, i.e. as if the inversion had not been encountered by the plume. On the other hand,  $\sigma_{z\_internal}$  is calculated using  $\Delta h$  computed in the normal way.

The reasoning behind this procedure is that, while the vertical dispersion of the plume is restricted by the inversion layer, the horizontal dispersion continues to increase due to remaining plume buoyancy. This effect has a significant influence on ground-level concentrations in the case of a low inversion base and light winds.

The use of the “lofting model”, together with the previously mentioned modifications of  $\sigma_{turb}$  has interesting consequences in the case of vanishing wind speed conditions.

Recalling the methods for calculation of the turbulent dispersion parameters, presented in Section 3.4.1, we can write the following expres-

sion for  $\sigma_z$  for a buoyant plume in the case of extremely convective conditions:

$$\sigma_z \approx 0.6 w_* \frac{x_{ef}}{u} \quad (3-77)$$

Inserting the zero-wind-speed limit of  $x_{ef}$  into (3-77), we obtain

$$\sigma_z \approx 0.1 \frac{x^{4/3}}{F^{1/3}} w_* \quad (3-78)$$

If the plume rise is terminated by the presence of an elevated inversion, we can also expect that the horizontal dispersion is dominated by  $\sigma_{internal}$ . In this case we have,

$$\sigma_y \approx 0.64 \frac{F^{1/3}}{u} x^{2/3} \quad (3-79)$$

As the effective plume height will be close to the height of inversion -  $z_i$ , we can expect that the maximum ground-level concentration will occur at such a distance for which,

$$\sigma_z \approx z_i \quad (3-80)$$

Substituting these expressions into the standard Gaussian formula we can obtain an approximate expression for maximum ground-level concentration,

$$c_{max} = 0.5 Q \left( \frac{w_*}{z_i^3 F} \right)^{1/2} \quad (3-81)$$

As it is seen from (3-81),  $c_{max}$  does not depend on the value of the wind speed.

### 3.8.3 Plume dispersion at the top of the convective boundary layer

The vertical turbulence associated with convective motion decreases at the top of the convective boundary layer (Caughy and Palmer, 1979). When the plume, due to buoyant rise, is brought up to the top of the convective boundary layer, the turbulent dispersion decreases. In the OML model, it is assumed that the growth of convective dispersion ( $\sigma_{zc}$ ) terminates when the effective plume height reaches  $0.9z_i$ , where  $z_i$  is the height of the convective boundary layer. The distance from the stack at which the effective plume height reaches  $0.9z_i$  is given by:

$$x_i = \frac{((0.9z_i - h_s) u)^{3/2}}{1.6^{3/2} F^{1/2}} \quad (3-82)$$

When the effective plume height exceeds  $0.9 z_i$ , the convective dispersion parameter is maintained at value  $\sigma_{zc}(x_i)$ . When the vertical dispersion is computed further downwind, only the mechanical turbulence ( $\sigma_{zm}$ ) increases. This procedure is clearly a crude simplification, but our under-

standing of plume dispersion at the top of a convective boundary layer is still too limited for a more sophisticated approach.

### 3.9 Stack tip downwash

Stack tip downwash is an effect caused by low pressure in the wake of a stack. Stack tip downwash does not occur if the efflux velocity  $w_s$  is high, but at low efflux velocities the plume is drawn down.

This effect is modelled by an empirical formula (Briggs, 1973). The height of the plume centerline is decreased by an amount of  $\Delta h_d$ :

$$\Delta h_d = 2D(1.5 - w_s / u) \quad (3-83)$$

when  $w_s < 1.5 u$ .

In the OML model, stack tip downwash is assumed to have the further effect of increasing the vertical dispersion,  $\sigma_z$ .

The downwash contribution is added to  $\sigma_z$  in the following manner:

$$\sigma_z^2 = \sigma_{zc}^2 + \sigma_{zm}^2 + \sigma_{z\_internal}^2 + \sigma_{z\_building}^2 + \Delta h_d^2 \quad (3-84)$$

### 3.10 Summary of dispersion parameterization

The present section gives an overview of the dispersion parameterisation in the current standard OML model.

The Gaussian dispersion parameters for non-buoyant plumes are derived in Sections 3.4 and 3.5. Both  $\sigma_z$  and  $\sigma_y$  are continuous functions of  $u^*$  and  $w^*$ . The horizontal dispersion parameter  $\sigma_y$  depends also on the systematic change in wind direction. For stable conditions, the lower limit for  $\sigma_y$  is  $0.5x / \bar{u}$ .

The vertical dispersion parameter  $\sigma_z$  is a function of source height. The height dependence of  $\sigma_z$  is governed by the height dependence of the convective component of the vertical velocity fluctuations and also by the vertical structure of the mechanical time scale. This time scale depends on the height above the ground, but in the case of stable stratification, the upper limit is determined by the value of the Monin-Obukhov length  $L$ .

For buoyant plumes, the dispersion parameters depend also on the buoyancy parameter  $F_B$  (Section 3.8). One effect of buoyancy is that it decreases the ability of a plume to respond to the ambient air turbulence, thus leading to a decrease of the turbulent part of the dispersion parameters compared to non-buoyant plumes. This effect is modelled by introducing an effective downwind distance which is smaller than the true downwind distance. The reduction of the dispersion parameters depends on the ratio between the rise velocity of the plume and the wind speed.

As another effect of buoyancy, buoyancy-induced internal dispersion is added to the turbulent dispersion. The internal dispersion is related to plume rise, i.e. the width of the plume is proportional to plume rise. The contribution of buoyancy-induced (internal) dispersion to the vertical dispersion parameter  $\sigma_z$  is reduced corresponding to the angle of the plume axis with respect to the horizontal axis (Eq. 3-76). This correction is significant under stable conditions when the internal dispersion dominates over the turbulent dispersion. The contribution of internal dispersion to the horizontal dispersion parameter  $\sigma_y$  is also proportional to plume rise, but when the rise is limited by an elevated inversion, the internal dispersion is computed as if the inversion were not present.

When, under stable conditions, the plume, due to rise, is brought to the top of the convective boundary layer, the further vertical plume dispersion takes place only due to the mechanical contribution.

### 3.10.1 Summary: Components of horizontal dispersion

$\sigma_y$  is composed *either* of  $\sigma_{yc}$ ,  $\sigma_{ym}$ ,  $\sigma_{y\_internal}$  and  $\sigma_{y\_building}$  added in the following way:

$$\sigma_y^2 = \sigma_{yc}^2 + \sigma_{ym}^2 + \sigma_{y\_internal}^2 + \sigma_{y\_building}^2 \quad (3-85)$$

*or* - in the case of large wind direction changes - with  $\sigma_{y\_shift}$  instead of the two first components:

$$\sigma_y^2 = \sigma_{y\_shift}^2 + \sigma_{y\_internal}^2 + \sigma_{y\_building}^2 \quad (3-86)$$

Here,  $\sigma_{y\_building}$  is a component due to building effect as described in Section 3.12.

	Components	Basic method of calculation	Remarks
$\sigma_y$	$\sigma_{yc}$ (convective)	From Deardorff, 1976 $\sigma_{yc} = \frac{0.5 w_* \frac{x}{u}}{\sqrt{1 + 0.9 w_* \frac{x}{z_i u}}}$ (3-36)	Reduced in case of buoyant plumes - especially in light wind conditions near the source. Implemented by using a dummy distance $x$ in the expression for $\sigma_{y\_turb}$ . For stable conditions, a minimum value of $u^*$ is imposed in the equation for $\sigma_{ym}$ : $u^* \geq 0.5$ m/s
	$\sigma_{ym}$ (mechanical)	$\sigma_{ym} = \frac{u^*}{u} x$ (3-37)	
	Alternatively: $\sigma_{y\_shift}$		$\sigma_{y\_shift}$ is an alternative to the contributions from ambient turbulence $\sigma_{yc}$ and $\sigma_{ym}$
	$\sigma_{y\_internal}$	$\sigma_{y\_internal}$ is essentially $\frac{\Delta h}{\sqrt{2\pi}}$ (3-73)	In order to account for a "lofting effect", $\Delta h$ used in the formula is allowed to grow even after the plume reaches the inversion (Sect. 3.8.2)
	$\sigma_{y\_building}$	$\sigma_{y\_building} = \sqrt{\frac{2}{\pi}} R_{0y}$ (3-100)	Contribution due to building effect; zero when the stack is higher than 1.2 building heights.

### 3.10.2 Summary: components of vertical dispersion

$\sigma_z$  is composed of three components which are discussed in previous sections:  $\sigma_{zc}$ ,  $\sigma_{zm}$  and  $\sigma_{z\_internal}$  plus contributions due to stack downwash ( $\Delta h_d$ ) and building effect (Section 3.12). The components are added in the following way:

$$\sigma_z^2 = \sigma_{zc}^2 + \sigma_{zm}^2 + \sigma_{z\_internal}^2 + \Delta h_d^2 + \sigma_{z\_building}^2 \quad (3-87)$$

	Components	Basic method of calculation	Remarks
$\sigma_z$	$\sigma_{zc}$	Eq. (3-12)-(3-15); Eq. (3-12) is the relevant for tall stacks: $\sigma_{zc}^2 = 0.33 w_*^2 t^2$ (3-12)	$\sigma_{zc}$ is reduced for <i>buoyant</i> plume - especially in light wind conditions near the source. Implemented by using a dummy distance $x$ in the expression for $\sigma_{z\_turb}$ . The growth of $\sigma_{zc}$ is stopped at $0.9z_i$ . (Section 3.8.3)
	$\sigma_{zm}$	Equations (3-30) and (33).	
	$\sigma_{z\_internal}$	$\sigma_{z\_internal}$ is essentially $\frac{\Delta h}{\sqrt{2\pi}}$ (3-73) (internal turbulence introduced by buoyancy)	Reduced because of penetration by a factor of $(1-P)$ . Reduced because we are interested in only the <i>vertical</i> component of $\sigma_z$ (( 3-74) and (3-75)). The final expression is (3-76).
	$\Delta h_d$	$\Delta h_d = 2D(1.5 - w_s / u)$ (3-83)	Maximum stack downwash is two stack diameters.
	$\sigma_{z\_building}$	$\sigma_{z\_building} = \sqrt{\frac{2}{\pi}} R_{0z}$ (3-100)	Contribution due to building effect; zero when the stack is higher than 3 building heights.

### 3.11 Wind speed

The wind speed plays several different roles in dispersion calculations. It appears as a parameter in the Gaussian plume formula (3-1) as well as through the time-distance dependence  $t = x / \bar{u}$  in the expressions for the dispersion parameters. Further, it is used for plume rise determination.

When using the Gaussian expression for evaluation of ground-level concentrations, it is considered an appropriate approximation to use a wind speed averaged over the layer between the ground and the effective plume height. On the other hand, for determination of plume rise, it is more relevant to use the wind speed at stack height.

Thus, the standard OML model uses two values for wind speed:

- $u_{hs}$  which is a wind speed at release height; it is used for plume rise determination and for computation of building effects.
- $u_{av}$  which is a vertically averaged wind speed used for several purposes (in the  $\sigma$  formulas, in the Gaussian expression and in deriving travel time  $t$ ).

The approach in the current standard OML model is crude in some respects, as noted in Chapters 4 and 5.

The details of the methods used are described below.

The variation of wind speed with height is computed using the well-known similarity functions (Monin and Obukhov, 1954).

$$u(z) = \frac{u_*}{\kappa} \left( \ln \left( \frac{z + z_0}{z_0} \right) - \psi_m \left( \frac{z}{L} \right) + \psi_m \left( \frac{z_0}{L} \right) \right) \quad (3-88)$$

where  $z_0$  is the roughness length and  $\psi_m$  are the universal similarity functions. For the similarity functions, the standard OML model uses the expressions derived by Businger et al. (1971). The explicit forms of the  $\psi_m$ -functions can be found in Paulsen (1970) and Barker and Baxter (1975).

Eq. (3-88) is only valid in the lower part of the boundary layer. In the upper part (above  $0.1z_i$ ), the wind is almost constant with height. In the OML model, the following procedure is used:

$$u(z) \begin{cases} \text{is computed by (3-88)} & \text{for } z \leq z_B \\ = u(z_B) & \text{for } z > z_B \end{cases} \quad (3-89)$$

where

$$z_B = \max(0.1z_i, \text{abs}(L))$$

Here, we also include the condition that the thickness of the layer where the wind still has a vertical gradient shall be at least equal to the numerical value of the Monin-Obukhov length  $L$ . This condition is well established in the case of unstable stratification, but might be dubious when the stratification is strongly stable. In the latter case, the wind profile depends not only on surface conditions but also on some large scale effects. These phenomena are not taken into account in the model.

Under strongly unstable conditions, when the mean wind speed is very low, the transport and dispersion of a plume are governed by the large convective eddies. Because these eddies have an average speed of about  $0.6 w_*$ , the lowest value for the effective wind speed used in the model is  $0.6 w_*$ . This should be considered only as a practical approach, because it is known that a stationary Gauss-plume model is not very appropriate for light wind conditions.

### 3.12 Influence of nearby buildings

If a building or another large obstacle is situated close to a stack, plume dispersion can be disturbed. The influence of buildings on plume dispersion can be very complicated, as it depends on the orientation of the building with respect to the stack, the wind direction and the shape of the building.

According to the OML building downwash algorithm, building influence has two main effects: it increases the initial dilution of the plume, and it decreases the plume rise. Most often, both effects contribute towards an increase of ground level concentrations. The total effect can be considerable.

The basis for the current standard OML model is an empirical procedure developed by Schulman and Scire (1980). The effects of a building on a dispersing plume are modelled by assuming that the plume has an initial

dilution radius,  $R_0$ . The radius  $R_0$  is used to calculate the initial enhanced diffusion parameters ( $\sigma_y$  and  $\sigma_z$ ), and to reduce the plume rise.

In the next subsections we will go into more details, while Chapter 6 presents further discussions on building effects. Here, it will first be shown how the initial dilution of a plume lowers plume rise for buoyant plumes. Next, the empirical formula used in the model for calculation of the initial dilution radius  $R_0$  will be presented in general terms. Finally, the practical implementation of the  $R_0$ -algorithm will be discussed.

### 3.12.1 Decrease of plume rise due to initial dilution.

The rise of buoyant plumes can be derived using the momentum conservation equations (Briggs, 1984):

$$wr^2u = F_B t \quad (3-90)$$

$$w = \frac{dz}{dt} \quad (3-91)$$

$$r = \beta z' \quad (3-92)$$

Here,  $w$  is the vertical velocity of the plume,  $r$  is the radius of the plume,  $u$  the horizontal wind velocity,  $F_B$  the buoyancy flux, and  $t$  the travel time. The height of the plume centerline above the stack top is denoted  $z'$ . Eq. (3-92) is the closure assumption which relates the plume radius to plume rise. The proportionality coefficient  $\beta$  (the entrainment rate) is assumed to be 0.6.

Solving Eqs. (3-90) to (3-92) with the initial condition  $z'=0$  at  $t=0$ , we obtain:

$$z = \left( \frac{3}{2\beta^2} \right)^{1/3} \left( \frac{F_B}{u} \right)^{1/3} t^{2/3} \quad (3-93)$$

When we substitute the expressions  $\beta = 0.6$  and  $t = x/u$ , we obtain

$$z = 1.6 \frac{F_B^{1/3}}{u} x^{2/3} \quad (3-94)$$

Eq. (3-94) is the well known formula for the initial plume rise (Briggs, 1984).

The initial dilution of the plume is taken into account by modifying Eq. (3-92)

$$r = \beta z' + R_0 \quad (3-95)$$

where  $R_0$  is the initial plume radius.

Solving Eqs. (3-90), (3-91) and (3-92), we obtain

$$z' = \left[ \left( \frac{3}{2\beta^2} \right) \frac{F_B t^2}{u} + \left( \frac{R_0}{\beta} \right)^{1/3} \right]^{1/3} - \frac{R_0}{\beta} \quad (3-96)$$

If we compare Eqs. (3-96) and (3-93), we can conclude that the effect of initial dilution on plume rise can be expressed as follows

$$\Delta h = \left[ \Delta h_0^3 + \left( \frac{R_0}{\beta} \right)^3 \right]^{1/3} - \frac{R_0}{\beta} \quad (3-97)$$

Here,  $\Delta h$  is the rise when taking initial dilution into account, while  $\Delta h_0$  is the rise of a source free of initial dilution.

In the OML model, Eq. (3-97) expressing the modification due to building effects is used for both the initial and the final plume rise.

In order to apply (3-97),  $R_0$  must be known. The next section deals with this problem.

### 3.12.2 Determination of initial plume dilution radius, $R_0$

The initial plume dilution radius is determined by an empirical method suggested by Schulman and Scire (1980). The procedure is as follows:

- i) The effective plume height due to momentum and thermal rise is computed at a position two building heights downstream of the source. As a first approximation, neglecting building effects, we have:

$$h_{ef} = h_s + \Delta h_0 \quad (3-98)$$

where  $h_s$  is the stack height and

$$\Delta h_0 = \left[ \frac{3F_m \frac{x_B}{((0.4 + 1.2 \frac{u}{v_s})u)^2} + 4.17F_B \frac{x_B^2}{u^3}} \right]^{1/3} \quad (3-99)$$

Here,  $F_M$  is the momentum flux and  $F_B$  the buoyancy flux. The distance  $x_B$  is the distance from the stack to the point  $P$ , where the plume height is evaluated. Presently, we assume  $x_B$  to be equal to  $2h_B$ , where  $h_B$  is the building height; some modifications follow later. The remaining parameters in (3-99) are wind velocity  $u$  and stack exit velocity  $v_s$ . With  $h_{ef}$  computed from (3-98), the ratio  $h_{ef}/h_B$  can be calculated; this ratio is used next.

- ii) The initial dilution radii,  $R_{0y}$  and  $R_{0z}$ , are determined as a function of the ratio  $h_{ef}/h_B$ . If the ratio is greater than 3, no enhancement of dispersion is assumed, i.e.  $R_{0y} = R_{0z} = 0$ . If  $h_{ef}/h_B < 1$ , then  $R_{0z} = h_B$  and

$R_{0y}=1/2h_B$ . The enhancement of the horizontal radius  $R_{0y}$  is furthermore assumed to be zero if  $h_{ef}/h_B>1.2$ . When the ratio  $h_{ef}/h_B$  is between these extreme values, a linear interpolation is performed (Figure 3.4).

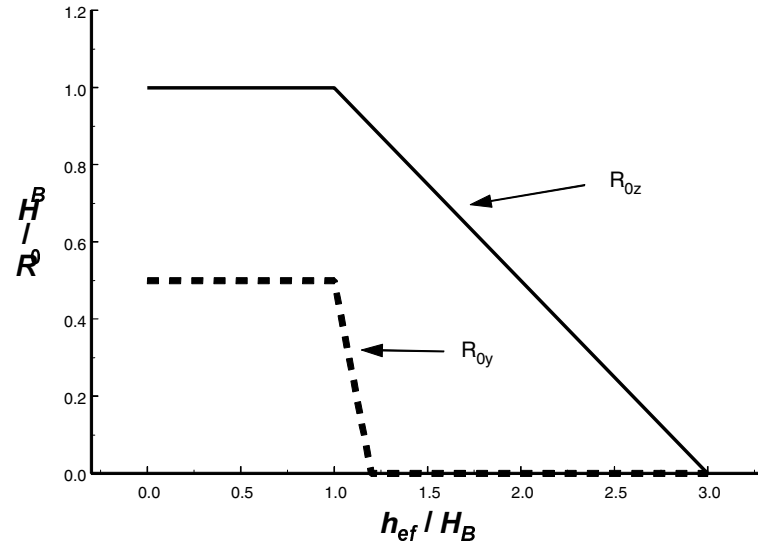


**Figure 3.4** Dilution radii  $R_{0z}$  and  $R_{0y}$ .

Only the vertical  $R_0$  ( $R_{0z}$ ) is used for plume rise calculations. Thus, the plume rise after modification due to building effects is determined from (3-97), where it is assumed that  $R_0=R_{0z}$ .

Both  $R_{0z}$  and  $R_{0y}$  are used for calculation of the enhancement of the dispersion parameters. These contributions to the dispersion parameters,  $\sigma_{y\_building}$  and  $\sigma_{z\_building}$ , are computed assuming a 'top-hat' distribution of the concentrations in the plume:

$$\begin{aligned}\sigma_{y\_building} &= \sqrt{2/\pi} R_{0y} \\ \sigma_{z\_building} &= \sqrt{2/\pi} R_{0z}\end{aligned}\tag{3-100}$$

### 3.12.3 Implementation of the $R_0$ -algorithm in the operational model.

First, let us explain the notion of a so-called "computational building height",  $h_B$ , which is used in the OML model. For "wide" buildings (i.e. buildings with a width larger than their height),  $h_B$  is identical to the physical height  $h_{phys}$ . For narrower buildings, the following formula applies:

$$h_B = \frac{h_{phys} + 2L}{3}\tag{3-101}$$

$L$  is the width of a building, or more precisely, the width of the projection of the building along the wind direction. An example is shown below:

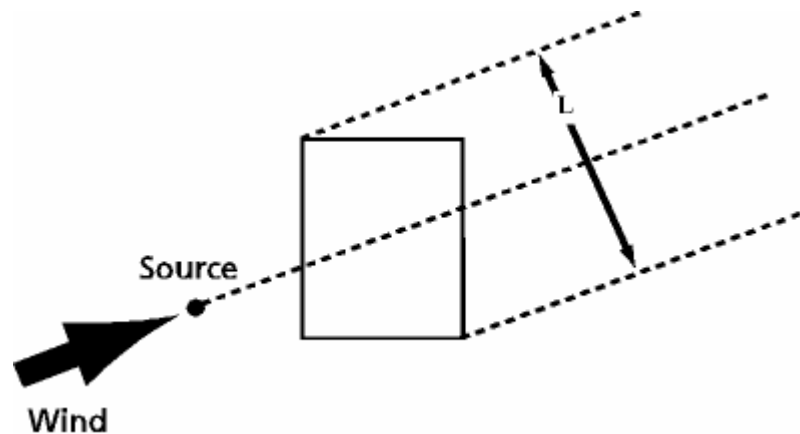
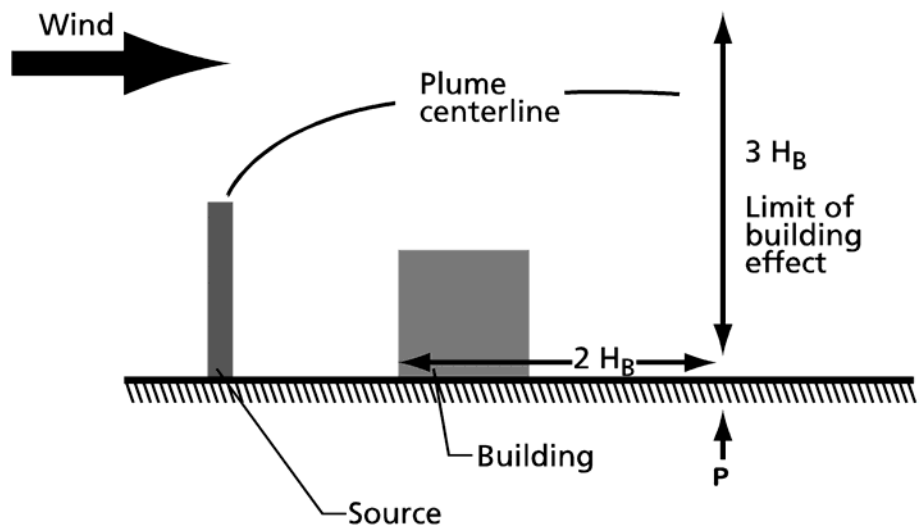


Figure 3.5 Building width  $L$

When the effect of buildings is to be evaluated in the OML model, the underlying assumption is that a building of (computational) height  $h_B$  creates a domain of influence, which extends  $2 h_B$  downstream of the building. If a stack is placed within this domain, dispersion from the stack may be affected by the building. If, on the other hand, the stack is placed outside of the influence domain, the plume remains unaffected.

In the model, the height of the plume centerline above a certain point  $P$  is evaluated. There is such a point  $P$  for each wind direction; once the geometry of the buildings surrounding the stack has been defined, the positions of all points  $P$  can be determined. As a main rule  $P$  is the point at the downwind edge of the influence domain (i.e. at a distance of  $2 h_B$  from the building); if, however, the stack is downstream of the building,  $P$  is defined as being  $2 h_B$  from the stack.

Plume height above the point  $P$  is evaluated in order to determine the amount of building influence. If the plume height at that point is greater than  $3h_B$ , building effects will be ignored. If, on the other hand, it is lesser, modifications are imposed upon the plume rise and the dispersion coefficients through the parameter  $R_0$  discussed in the previous section. Fig 3 illustrates the criteria used for deciding whether the plume is disturbed or not.



**Figure 3.6** Criteria to decide whether the plume is disturbed by a building

As accounted for earlier,  $R_0$  is determined from the ratio  $h_{ef}/h_B$ . Here,  $h_{ef}$  is evaluated at the point  $P$  (implying that  $x_B$  in Eq. (3-99) is equal to  $2 h_B$  except for a configuration, where the stack is upstream of a building).

Thus, for each meteorological scenario, the parameters  $R_{0z}$  and  $R_{0y}$  are determined. These parameters are used to modify the dispersion parameters. Furthermore, based upon the value of  $R_{0z}$ , a modified plume height according to Eq. (3-97) is calculated for each receptor along the path of the plume.

It can be added that when several buildings are present at the same time, it is not *a priori* given which of the buildings possesses the dominating influence. The OML model handles this situation by considering - for each meteorological scenario - separately the effect of each building; the building causing the greatest initial dilution radius  $R_0$  is chosen and used for the subsequent computations.

The procedure outlined here for handling of building effects is based on simple semi-empirical methods, whereas in reality, aerodynamics in the wake of a building is an extremely complex matter. The primary intention of the building effect algorithm used in the OML model is to provide concentration estimates applicable for distances beyond, say, ten building heights downwind. Concentration estimates close to buildings should not be considered reliable.

### 3.13 Terrain effects

The OML model is not designed for use in complex terrain. However, some simple procedures are included for handling dispersion in the case of small terrain elevations. The procedure is restricted to correction of the effective plume height in (3-1). No correction of the dispersion coefficients, wind speed or wind direction is performed.

The procedure for correction of effective plume height is based on results from potential flow theory. In the case of stable conditions, the suppression of the flow due to buoyancy forces is also taken into account. Here, results are used from experiments in the early eighties leading to the

concept of dividing streamline height (Strimaitis et al., 1985). As implemented in OML, there are, however, certain simplifications.

### **3.14 Area sources**

The treatment of area sources is discussed in Appendix A. The algorithm for area sources was revised in year 2000. Appendix A is a note describing the version used prior to 2000, as well as the version applied afterwards.

## 4 Problems identified

During the review of the OML model in 2005-6 certain weaknesses of the existing model were identified. Based on numerous experimental results it was studied how the problems could be resolved by changes in the model parameterisation. The present chapter gives a brief overview of the various problems, while the subsequent chapter presents new formulations of certain model components. One problem - the one of building effects - is so complex that the current study has not yet resulted in a new formulation of the OML algorithms. An entire chapter (Chapter 6) is devoted to a discussion of building effects, as they are observed in experimental studies and as the models OML, AERMOD and MISKAM simulate them.

### 4.1 Overview of problems

The following problems are addressed by changes in the OML algorithms, resulting in the "Research Version" of OML. Details on the problems and the solution to them are found in the subsequent chapters.

#### **Wind profile: Discontinuity stable/unstable**

In the current standard OML model, in the case of *stable* conditions, the effective wind speed is calculated as an average value between the ground and the plume height. For *unstable* conditions, the effective wind speed is set equal to the value at the plume height. This can lead to a discontinuity when the stability conditions changes from unstable to stable.

#### **Assessing an effective wind speed for plume transport**

In the current standard OML model, the effective wind speed is constant regardless of the distance from the source (as long as there is no plume rise). However, it is quite a crude assumption that effective wind speed does not change during plume transport - in particular for sources close to the ground, where the wind changes rapidly with height, while the plume increases its vertical extent during transport.

A further issue - mainly relevant for very low sources - is that a minimum value is set for the height at which wind speed is calculated, namely 10 times  $z_0$ .

#### **Von Karman constant**

In the current standard OML model, wind velocity profiles are calculated using Businger's similarity functions with von Karman constant  $\kappa=0.35$ . The value of the von Karman constant has been debated for many years. It is most likely that the "true" value of the von Karman constant is 0.4 and that the empirical coefficients used in the similarity functions should be somewhat different from those given by Businger. This issue is of limited significance.

**Very large horizontal dispersion in stable conditions; discontinuity in  $\sigma_y$** 

In the standard OML model, in the case of stable conditions the horizontal dispersion ( $\sigma_y$ ) is calculated as

$$\sigma_y = u_* \times T_{eff} \quad (4-1)$$

When  $u_* < 0.5\text{m/s}$ , expression (4-1) is replaced by

$$\sigma_y = 0.5 \times T_{eff} \quad (4-2)$$

This parameterisation results in a discontinuity when the stability conditions change from unstable to stable. Furthermore, the current standard model assumes a large horizontal dispersion for small values of  $u_*$ . This seems unrealistic in view of the experimental data that are now available. They warrant a revised parameterisation of  $\sigma_y$ .

**Tendency to predict maximum too close to the source**

Comparisons of model results with available measurements have revealed a tendency for OML to predict the maximum ground level concentrations too close to the source in unstable conditions. This trend has become more obvious in new, additional model evaluation studies.

With modern computers it is now feasible to implement a model structure where the vertical dispersion does not follow a simple Gaussian distribution. A Gaussian distribution has long been known to be an oversimplification of reality when it comes to vertical dispersion in convective conditions. A new model formulation allows for a "vertical meandering" of the plume, combined with a Gaussian shape of the basic plume. This formulation is capable of curing the problem with overprediction close to the source.

**Reflection term in Gaussian equation**

In the OML model concentrations are calculated using a standard Gaussian plume formula with multiple reflections at the ground and the top of the mixing layer. Due to a coding error in the current standard OML version, the term that describes reflection from the top of the mixing layer is always neglected in the case when  $\sigma_z < (h_s - z_r)/4$ . This has the result that concentrations at the top of the mixing layer are only half of what they should have been. The consequences of this mistake for ground level concentrations are normally marginal.

**Plume rise – loss of plume buoyancy**

In the current standard version of OML the formulas used for calculation of plume rise in the case of multiple layers with varying temperature gradient are simplified. The final plume rise is calculated taking into account only the loss of plume buoyancy in the layer with the *largest* temperature gradient. A more precise formulation is applied in the new Research Version.

**Plume rise – effective wind speed**

In the current standard OML model, the value of wind speed used for calculation of plume rise is always determined at the stack height. For low level sources this can lead to an underprediction of the effective plume transport velocity, and consequently overprediction of the plume

rise. In the Research Version of OML, an iterative procedure is used to calculate the effective wind speed, thus taking into account the increase of wind speed with increasing height of the plume.

#### **Minor issues**

A minor issue concerns certain default values used in OML when there is insufficient available data to determine mixing height. In such cases, the OML meteorological pre-processor makes an estimate of mixing height (based on wind speed), and the OML model assumes a default value for the vertical temperature gradient above the mixing layer.

The default value for the gradient is currently set very low. Expressed in terms of the parameter and units used in the OML meteorological input file, namely the Brunt-Vaisälä frequency squared in the unit  $1000/s^2$ , it is set to 0.001. A more suitable default value would be a value close to the median, such as 0.15. This corresponds to a potential temperature gradient of 4 K/km.

This issue only matters when there is insufficient meteorological data, so it affects some meteorological data sets more than others. In the case of e.g. Kastrup 1976, less than 1% of the data are affected.

The current implementation of the default value will imply a tendency for buoyant plumes to obtain too large plume rise - thus, resulting in too low ground-level concentrations for such plumes in the hours affected.

#### **Building effects**

It is a recognised problem that the current standard OML model treats building effects in a very simplified manner. One of the consequences is unrealistic changes in concentrations, when a building is moved from the domain where it has an influence to a location immediately outside this domain. However, the problem of building effects is so complex that the current study has not yet resulted in a new formulation of the OML algorithms. Many investigations have been performed in the framework of the current project, and Chapter 6 reports on these.

## 5 Revisions to model formulation

In the present chapter new formulations of certain model components are described. The new formulations are implemented in the Research Version of OML in order to resolve the problems listed in Chapter 4.

The chapter includes some model evaluation results, documenting improvements obtained by the changes. Detailed information on validation studies can be found in the supplementary report "OML: Model Validation" (Olesen et al., 2007). The new formulations are discussed in the following order:

- Section 5.1 deals with the formulation of effective wind speed. This addresses the problems listed in Chapter 4 under the headings *Wind profile: Discontinuity stable/unstable*, *Assessing an effective wind speed for plume transport* and *Von Karman constant*.
- Section 5.2 describes the revised formulation for horizontal dispersion, resolving the problem of very large horizontal dispersion in stable conditions.
- Section 5.3 describes the revised formulation for vertical dispersion. This refers to the problem that OML has a tendency to predict the maximum too close to the source.
- Section 5.4 provides evaluation results pertaining to non-buoyant sources. Results are shown for the standard OML model and for the Research Version. The results reflect the effect of the modifications introduced in the Research Version.
- Section 5.5 describes a reformulation of the algorithms for plume rise. These algorithms are relevant for buoyant plumes and plumes with significant momentum. Further, this section presents a revised parameterisation of dispersion due to internal turbulence - which is relevant in the case of plume rise.
- Section 5.6 presents corresponding evaluation results for buoyant plume dispersion.

### 5.1 New formulation of the effective wind speed ( $U_{\text{eff}}$ )

#### 5.1.1 Background

In the current standard OML model, the effective wind speed is constant regardless of the distance from the source (as long as there is no plume rise). However, it is quite a crude assumption that effective wind speed does not change during plume transport - in particular for sources close to the ground, where the wind changes rapidly with height, while the plume increases its vertical extent during transport.

As a further issue relevant for very low sources, there is a defined a minimum height at which the wind speed is calculated, namely 10 times  $z_0$ .

An additional problem is that the effective wind speed is calculated in slightly different ways, depending on whether stability conditions are stable or unstable. This leads to a discontinuity which should preferably avoided. Historically, this was a simplification intended to speed up calculations. The power of modern computers allows a more detailed treatment of wind speed. Effective wind speed is now computed using an iterative procedure, where the wind speed is integrated over the vertical extent of the plume. The details are explained in the subsequent section.

The consequence is mainly a more realistic treatment for low sources. For instance, for the Prairie Grass experiment where releases took place at a height of 0.46 m, it is very important whether the transport wind is computed based on the wind profile from the ground to a height of 0.46 m, or on the wind profile extending through a layer several meters deep.

### 5.1.2 Details of the new formulation

The previously used value of the von Karman constant,  $\kappa=0.35$  is now replaced by

$$\kappa=0.4$$

Previously, Businger's expressions for the similarity functions were used. They are now replaced by new formulations as recommended by Högström (1996). The difference concerns values of the empirical coefficients. Högström's formulations are consistent with a  $\kappa$  value of 0.4.

The effective wind speed is calculated using an iterative procedure.

$U_{\text{stack}}$  is calculated as the wind speed at the release height. The lowest height used for calculation of  $U_{\text{stack}}$  is set to  $z_0$ .

A height averaged wind speed ( $U_{\text{av}}$ ) is calculated at the actual distance from the source.

$$U_{\text{av}} = \frac{1}{z_2 - z_1} \int_{z_1}^{z_2} U(z) dz \quad (5-1)$$

where  $z_1 = \max(0, h_s - 2.15\sigma_z)$  and  $z_2 = \min(Z_{\text{mix}}, h_s + 2.15\sigma_z)$ .  $h_s$  is the source height, but for buoyant plumes this height is replaced by the actual height of the plume's centreline taking into account the effect of plume rise.  $Z_{\text{mix}}$  is the mixing height.

The integration in (5-1) is done in an exact manner using analytical expressions valid for the actual stability conditions. Thereby, the discontinuity at the transition from stable to unstable conditions is removed.

The effective wind speed is calculated as

$$U_{eff} = (U_{stack} * h_s + U_{av} * \sigma_z) / (h_s + \sigma_z) \quad (5-2)$$

Expression (5-2) ensures that at large distances from the source the effective wind speed becomes practically independent of the release height.

Because  $\sigma_z$  depends on  $U_{eff}$ , expressions (5-1) and (5-2) are calculated in a loop, where the new value of  $\sigma_z$  is calculated using the new value of  $U_{eff}$ . In the first iteration step the value of  $\sigma_z$  is calculated with  $U_{eff}=U_{stack}$ .

The concept of the effective wind speed is closely connected to the concept of the effective transport time  $T_{eff}$ . The effective transport time is calculated as

$$T_{eff} = \frac{x}{U_{eff}}$$

where  $x$  is the distance from the source. The effective transport time is used for calculation of the dispersion parameters – although with a modification in the case of plumes affected by plume rise (see Section 5.5.4)

## 5.2 New formulation of horizontal dispersion ( $\sigma_y$ )

### 5.2.1 Background

When the original OML model was developed, the parameterisation of horizontal dispersion was based partly on studies in literature, reporting that there was substantial dispersion under stable conditions with light winds.

Since then, evidence has shown that the effect was exaggerated, and that the parameterisation chosen leads to unrealistically large horizontal dispersion.

Furthermore, in a situation with low wind speed, when stability changes from unstable to stable, the current standard model will predict a very large jump in the value of  $\sigma_y$ . Both of these observations are confirmed by inspecting the plots based on wind tunnel studies, presented later in Section 5.4.4.

For such reasons, the parameterisation of horizontal dispersion has been reconsidered.

Now, ample measurements of horizontal wind velocity fluctuations are available. Figure 5.1 and Figure 5.2 show measurements of  $\sigma_v$  from two Danish locations. They were performed with sonic anemometer.

Also shown on the figure is a green line that indicates the implication of the parameterisation in OML for stable conditions. A similar line cannot

be drawn for unstable conditions, because  $\sigma_v$  is not only a function of  $u^*$ , but also of stability.

It appears that there is a need to change parameterisation. This has been done in the Research Version of OML. The subsequent section describes the details. For some situations, the change has a profound effect on model results (see Section 5.4.4 for examples)

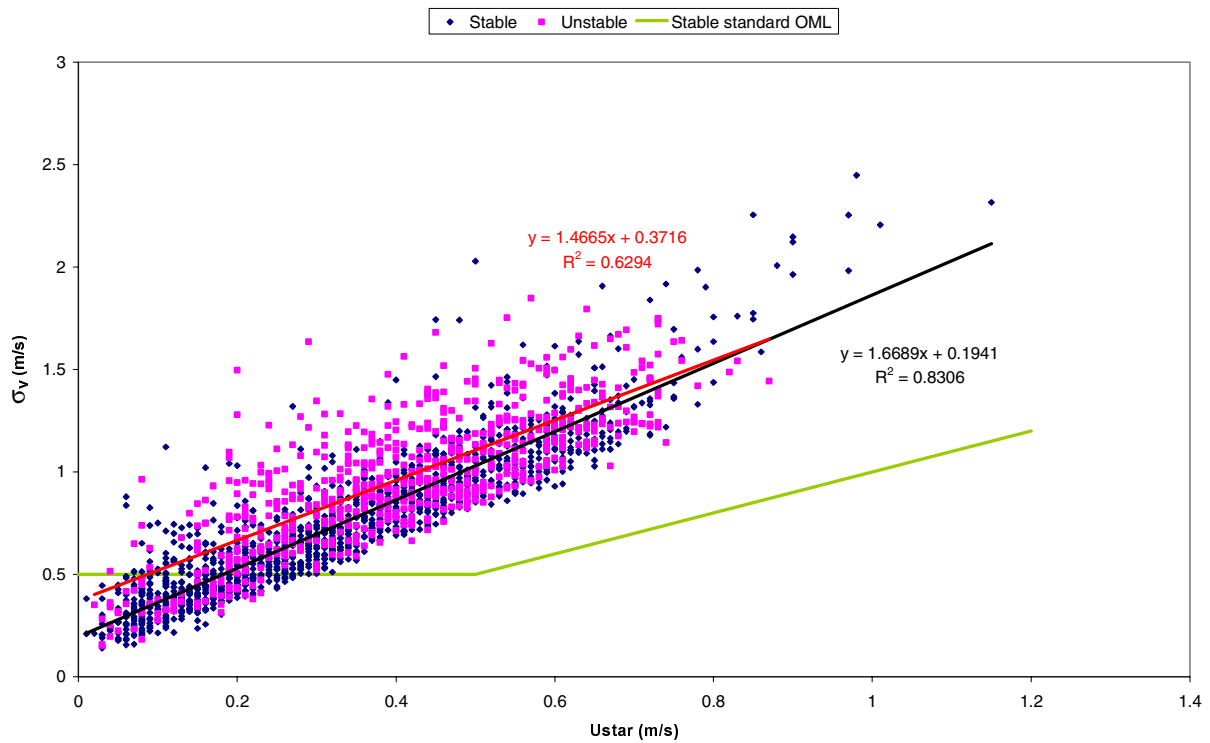


**Figure 5.1** Measurements of  $\sigma_v$  from a mast at the Køge Bugt highway. Red symbols for unstable conditions, black for stable. Measuring height 8m. Period: September-December 2003. Hourly averages.

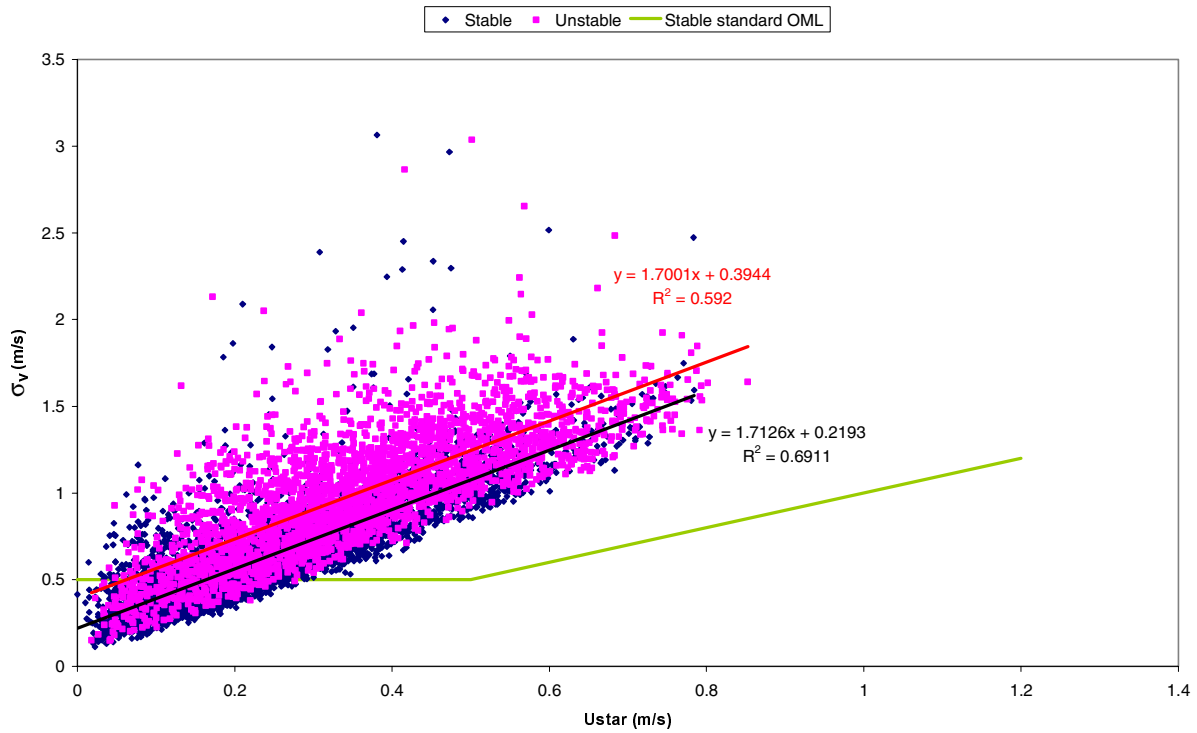


**Figure 5.2** Measurements of  $\sigma_v$  from a mast in Ringsted for the year 2005. Red symbols for unstable conditions, black for stable. Measuring height 7.5 m. Hourly averages.

### 5.2.2 Details of the new formulation

The horizontal dispersion is assumed to be composed of three contributions (assuming no plume rise, no obstacles):

1. wind friction driven dispersion (mechanical contribution)
2. thermally generated dispersion (convective contribution)
3. large scale processes (meander)

In accordance with the turbulence measurements available now, the neutral limit of the lateral velocity fluctuation in the surface layer is modelled as:

$$\sigma_v = 1.6 \times u_* \quad (5-3)$$

Field and especially wind-tunnel observations indicate that  $\sigma_v$  decreases with height, dropping down to about 50% of the surface value at the top of the mixing layer.

The horizontal dispersion is known to increase linearly with the distance from the source (or travel time) but only as long as the travel time ( $T_{eff}$ ) is much smaller than the Lagrangian time scale. When the travel time becomes much larger than the Lagrangian time scale, the time dependence of the horizontal dispersion attains the long-time limit given by the square root of travel time.

The Lagrangian time scale is modelled assuming that it is determined by the size of the most effective turbulent eddies that act on the plume (the parameter  $Z_m$ ) and by the characteristic velocity scale of these eddies. In the case of mechanically generated (wind friction driven) turbulence, the Lagrangian time scale is determined by the height above the ground and the friction velocity.

The *wind friction driven part* of the horizontal dispersion is thus modelled as

$$\sigma_{ymech} = \frac{\sigma_v T_{eff} \times \sqrt{1 - 0.8 \cdot h_s / Z_{mix}}}{\sqrt{1 + T_{eff} \times u_* / Z_m}} \quad (5-4)$$

Here, the Lagrangian time scale is assumed to be determined by

$$T_L = \frac{Z_m}{u_*}$$

where,  $Z_m$  is given by:

$$Z_m = \min(h_s + 2.15\sigma_z, Z_{lim})$$

where

$$Z_{lim} = \min(\max(\text{ABS}(L), 0.1 \times Z_{mix}), Z_{mix})$$

The source height  $h_s$  is replaced by the plume height in the case of buoyant sources.

The *thermally generated* horizontal dispersion is given by:

$$\sigma_{yconv} = \frac{0.5 \times w_* T_{eff}}{\sqrt{1 + 0.9 \times T_{eff} \times w_* / Z_i}} \quad (5-5)$$

In the case of the convective (thermally generated) turbulence the Lagrangian time scale is thus assumed to be determined by the height of the convective boundary layer  $Z_i$  and the convective velocity scale  $w_*$ .

The *large-scale contribution* to the horizontal dispersion is not well defined but the new turbulence data indicate that the value of  $\sigma_v$  is about 0.2m/s when  $u_*$  approaches zero. Therefore:

$$\sigma_{ymeand} = \sigma_{vmin} \times T_{eff} \quad (5-6)$$

where

$$\sigma_{vmin} = 0.2m/s$$

Finally, the horizontal plume dispersion is calculated as:

$$\sigma_y^2 = \sigma_{ymech}^2 + \sigma_{yconv}^2 + \sigma_{ymeand}^2 \quad (5-7)$$

The convective contribution is zero in the case of stable conditions. When simulating wind tunnel experiments (e.g. in Section 5.4) the contribution from the large scale processes (meandering) is assumed to be zero.

The effect of systematic changes in wind direction over time as described in Section 3.5.2 is retained.

## 5.3 New formulation of vertical dispersion

### 5.3.1 Background

Comparison of the model results with available measurements in unstable conditions have revealed a tendency for OML to predict the maximum ground level concentrations closer to the source than it actually occurs. This trend has become more obvious in new, additional model evaluation studies.

With modern computers it is now feasible to implement a model structure where the vertical dispersion does not follow a simple Gaussian distribution. A Gaussian distribution has long been known to be an oversimplification of reality when it comes to vertical dispersion in convective conditions. A new model formulation allows for a "vertical meandering" of the plume, combined with a Gaussian shape of the basic plume. This formulation is capable of curing the problem with overprediction too close to the source.

### 5.3.2 Details of the new formulation

The main innovation of the new approach is the different treatment of the mechanically and thermally generated turbulence. The small-scale mechanical eddies are still assumed to be responsible for vertical expansion of the plume, and the Gaussian plume formulation is retained here. However, the much larger convective eddies are not expected to lead to a Gaussian-type expansion of the plume, but rather to a kind of vertical meander, which results in a non-Gaussian vertical concentration distribution.

The mechanically generated vertical plume dispersion parameter ( $\sigma_z$ ) is calculated as:

$$\sigma_z^2 = \frac{0.7 \times (u_* T_{eff})^2 \times \exp(-0.7A) \times (1 - 0.8 \cdot h_s / Z_{mix})}{(1 + u_* T_{eff} / L)} \quad (5-8)$$

Where

$$A = \min(1, u_* T_{eff} / h_s)$$

The "stability correction" in the denominator of (5-8) is only applied in the case of stable conditions (Monin-Obukhov length  $L > 0$ ).

Formula ( 5-8 ) is similar to the original expression used in the current version of OML (Section 3.4.2) but with slightly different values of the empirical constants. The only major modification is the introduction of the height dependence term, which is identical to the one used for the horizontal dispersion parameter ( 5-4 )

However, for convective conditions,  $\sigma_z$  is not used directly in a Gaussian plume equation. Instead, a new procedure is used. The main innovation is that the effect of the convective eddies is not modelled as an increase of  $\sigma_z$  but as a vertical “meander” of the plume. The plume is assumed to be moved up or down by the convective eddies with a speed and a probability depending on the release height and stability. The concentrations at any receptor height are calculated as weighted average values of the upward and downward displaced plume. The speed with which the plume is displaced in upward or downward direction is given by

$$w(z) \propto u_* \sqrt{\frac{z}{-L}} \quad (5-9)$$

The vertical displacement of the plume is calculated by solving the following differential equation

$$\frac{dSigZ}{dt} = w(SigZ) \quad (5-10)$$

$SigZ$  denotes here the vertical displacement of the plume by the convective eddies.

This formulation of the growth rate of the vertical dispersion of a plume in convective conditions is in agreement with the findings by Venkatram (1992) that the vertical plume extension in the case of a surface release exhibits a  $x^2$  dependence on distance from the source, in contradiction to the  $x^{3/2}$  dependence predicted by the “free convection” theory. The last was used as the background for the formulation of the vertical dispersion in the current standard version of OML.

Eq. (5-10) is solved with the additional constraint that

$$w(z \geq 0.1Z_{mix}) = w(z = 0.1Z_i)$$

The upper and lower limits for  $SigZ$  are  $Z_i$  and 0, respectively.

The Gaussian plume formula with  $\sigma_z$  given by (5-8) is numerically integrated, and average concentrations of updrafts and downdrafts events are calculated.

$$C_{up}(x, z) = \frac{1}{SigZ_p} \int_{h_s}^{h_s + SigZ_p} C(h', x, z) dh' \quad (5-11)$$

And

$$C_{down}(x, z) = \frac{1}{SigZ_m} \int_{h_s - SigZ_m}^{h_s} C(h', x, z) dh' \quad (5-12)$$

$SigZ_p$  and  $SigZ_m$  are here the upward and downward plume displacements calculated as solutions to Eq. ( 5-10 ) for the particular distance  $x$  from the source. The expression under the integral sign is the concentration in a Gaussian plume (with  $\sigma_y$  and  $\sigma_z$  given by ( 5-7 ) and ( 5-8 )) but with the plume centreline “displaced” to height  $h'$ .

Finally, the weighted average concentration at distance  $x$  from the source and height  $z$  from the ground is calculated as:

$$C(x, z) = (A_{up}C_{up}(x, z) + A_{down}C_{down}(x, z)) / (A_{up} + A_{down}) \quad (5-13)$$

Here,  $A_{up}$  and  $A_{down}$  are weight factors, related to probabilities for updrafts and downdrafts, respectively. These factors are determined empirically. The following expressions are used in the Research Version of OML:

$$A_{up} = 1 - h_s / Z_i \quad (5-14)$$

$$A_{down} = \min\left(1, A_s \frac{-h_s \times L}{Z_i^2}\right) \quad (5-15)$$

where  $A_s=1500$  (dimensionless parameter). The value of  $A_s$  has been assessed based on experiments from Borex and Prairie Grass (see Section 5.4).

Figure 5.3 illustrates the behaviour of the weighting factor for updraft  $A_{up}$  (relative to the sum of  $A_{up}$  and  $A_{down}$ ). E.g., it is seen that for very low stacks, for unstable conditions, updrafts are most probable.

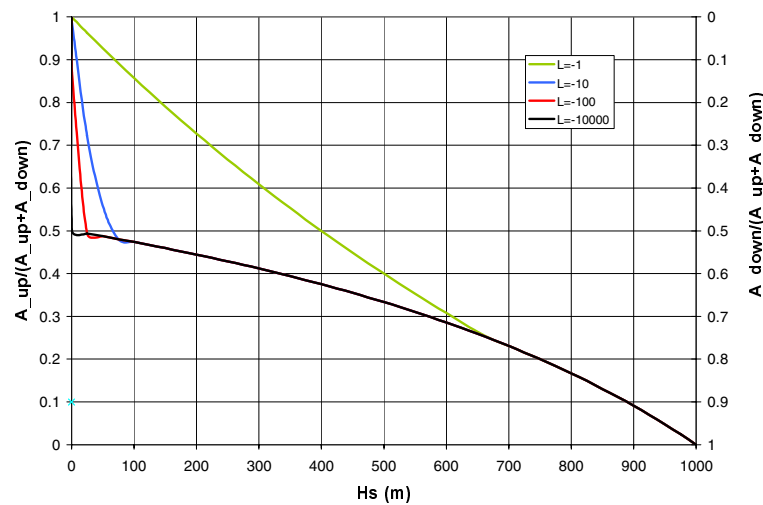


**Figure 5.3** The relative probability of updrafts according to the parameterisations in Eqs. (5-14) and (5-15).  $Z_i$  is 1000 m

## 5.4 Model performance for non-buoyant plumes

As a result of the new formulations described in the previous sections, model performance has improved. The present section shows results of model runs with the new Research Version of OML. For comparison, also results obtained with the standard version of OML and with the US AERMOD model are shown.

Results are presented for the following experiments:

- Prairie Grass (source at 46 cm height only, passive release)
- Borex 1992, 1994 and 1995 (mostly release at approximately 20 m, passive source)
- Copenhagen (Gladsaxe) experiment (release at 115 m, passive release)
- Roger Thompson's wind tunnel data.

The presentation of results here is intended as a summary. A further discussion with details on the data sets, data problems and on the processing of data can be found in the supplementary report "OML: Model Validation" (Olesen et al., 2007).

### 5.4.1 Prairie Grass

The classical Prairie Grass experiment (Barad, 1958) was conducted during the summer 1956 in very flat terrain, near the town O'Neill, Nebraska, USA. The tracer gas SO<sub>2</sub> was released from a source almost at ground level ( $h_s=46\text{cm}$ ). Ten-minute averages of concentration values were measured by a net of samplers located on five concentric arcs with the distance from the release point ranging from 50m to 800m. The arcs covered an entire 180° sector, ensuring plume capture for southerly winds. The spacing of samplers was 2° for the four inner arcs and 1° for the 800m arc. Due to the short sampling time (10 min only), only the results for the crosswind integrated concentrations are presented here (Figure 5.4). This makes it possible to evaluate the model performance with regard to the vertical dispersion, without considering the problems related to the horizontal dispersion.

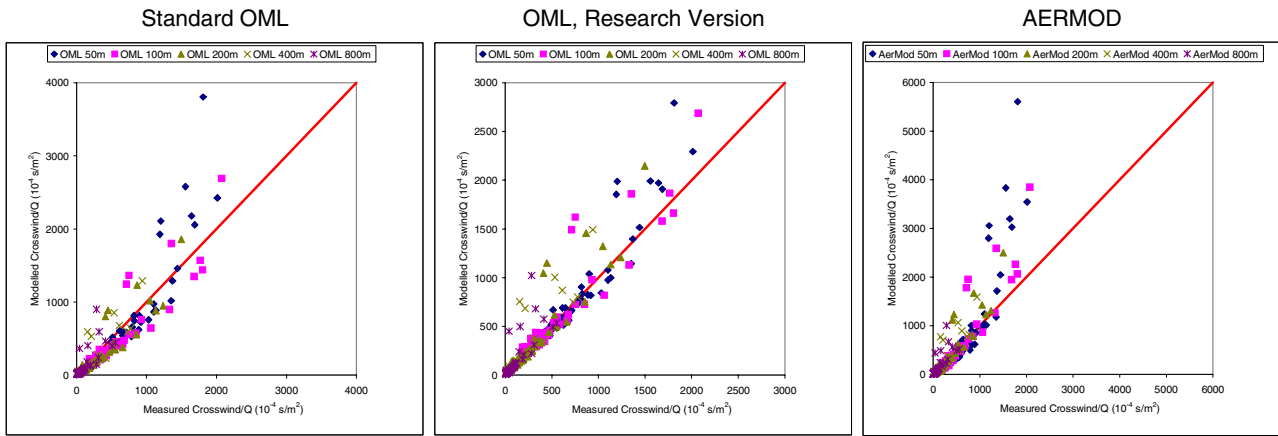


**Figure 5.4** Results of OML and AERMOD calculations for Prairie Grass experiments (1956). Crosswind integrated concentrations. Ground level release ( $H_s=0.46\text{m}$ ). Very broad range of stability conditions. Smooth terrain ( $Z_o=0.006\text{m}$ ). Note that the axes in the three panels are scaled differently.

When inspecting Figure 5.4 pay attention to the scale. No observed concentrations are larger than 2000. The scale in the three panels vary: The scale for the standard OML model goes to 4000 in order to include all predictions; the scale of the Research Version goes to 3000 only, while the scale for AERMOD has to be extended to 6000. The figure shows a systematic difference between using the Standard Version of OML compared to the Research version. With the Research version, many observations are brought close to the one-to-one line. However, for some experiments a tendency to overpredict still exists.

The AERMOD model results in substantial overprediction for stable cases. These overpredictions are not revealed in some presentations of AERMOD performance, which are based on a subset of Prairie Grass data only (See Olesen et al., 2007).

Figure 5.4 does not clearly reveal model behaviour at large distances from the source (800 m), because concentrations are so low that the dots melt together. However, model performance for the Research version of OML is superior to the other models (see the supplementary report, (Olesen et al., 2007)).

With the new parameterisation of the vertical dispersion introduced in the Research Version, the model predictions are improved compared to the current, standard version of OML. The results are also better compared with AERMOD. The main improvement is achieved for unstable conditions and larger distances from the release point. This is discussed in more details in the supplementary report.

#### 5.4.2 Borex

The Borex experiments took place at the heath at Borris in 1992, 1994 and 1995. During these experiments, monitors ( $\text{SF}_6$  sampling bags) were placed along several arcs at different distances from the release point. Up to 3 arcs had a sufficient dense coverage with samplers to catch the plume. For some experiments, there were additional samplers placed away from the densely populated arcs. Such isolated measurements are not used here.

During the Borex experiments in 1994 and 1995, monitors were placed at *concentric arcs at fixed distances from the source*. However, for the first experiment in Borex 1992, the location of the arcs was variable, covering *different distances from the source*. Therefore, for the 1992 data shown in Figure 5.5, we only refer to the different arcs as Arc 1, Arc 2 and Arc 3. The figure shows results from the Standard OML model, the Research Version of OML, and AERMOD. The upper three panels show arcwise maxima as scatter plots, while the lower panels present arcwise maxima (modelled and measured) as a function of distance. This set of plots reveal that both the standard version of OML and AERMOD have a tendency to overpredict close to the source: The red (modelled) points are distinctly higher than the black (measured).

The Research Version of OML does a much better job of reproducing the variation of concentrations with distance.

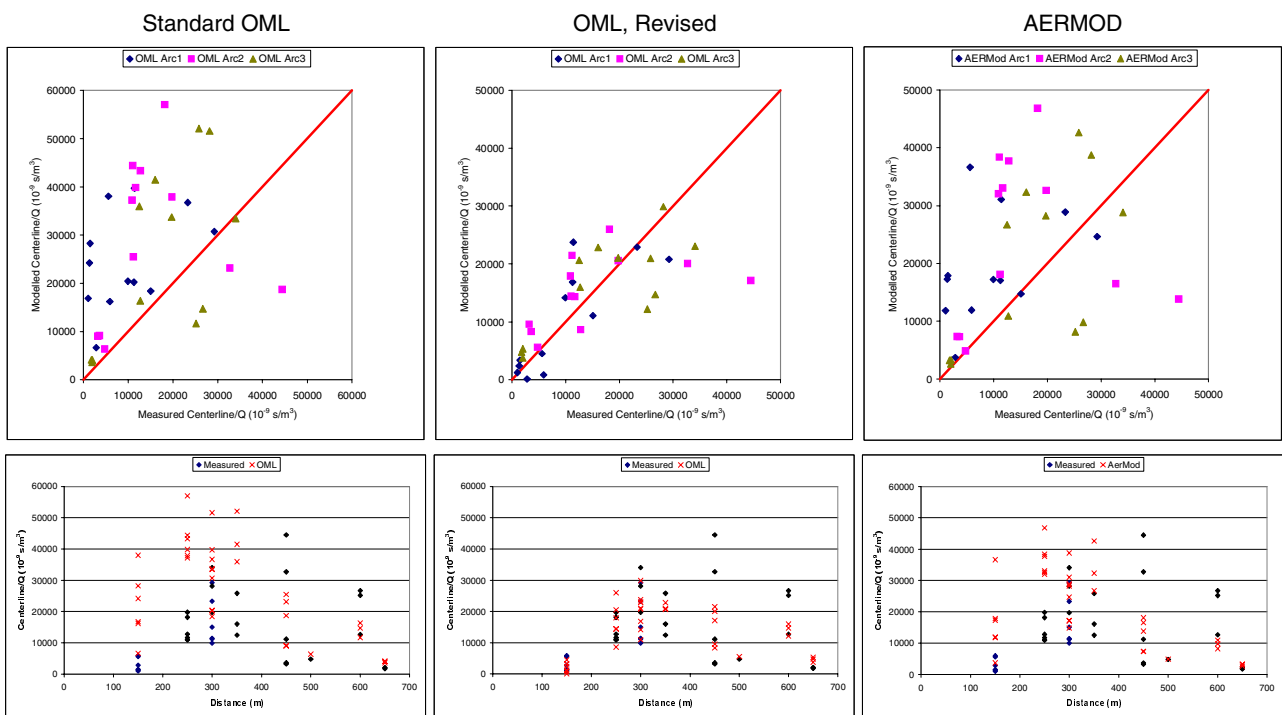


Figure 5.5 Borex 1992,  $H_s = 22$  m, centreline

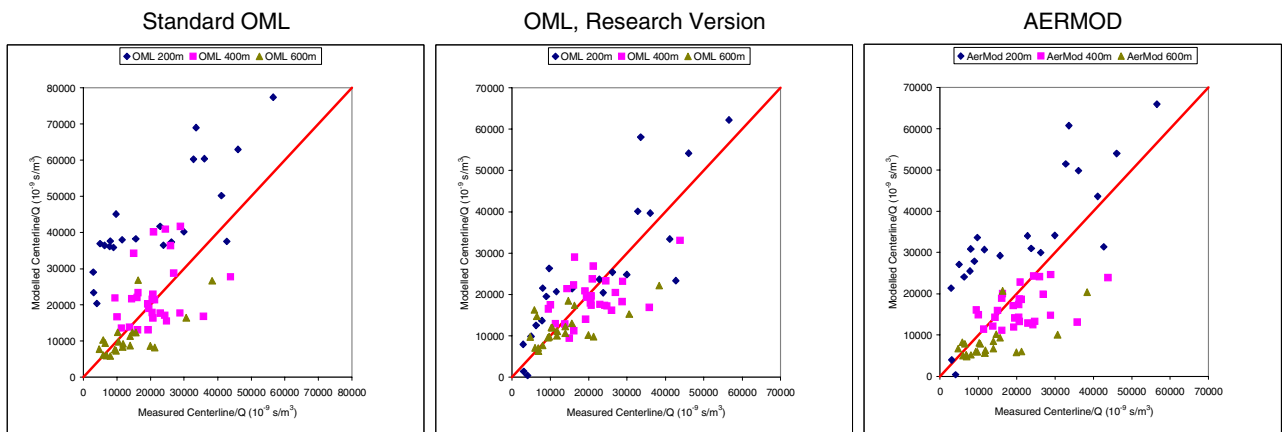


Figure 5.6 Borex 1994,  $H_s = 24$  m, centreline

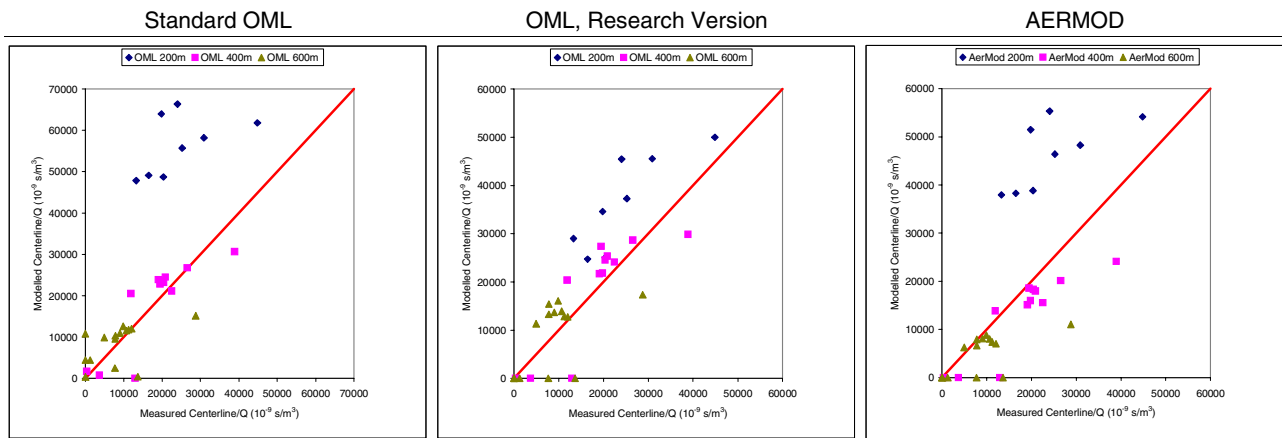


Figure 5.7 Borex 1995, Hs=21 m, centreline

In 1994 and 1995, there were measurements at fixed distances, as indicated in the legends to Figure 5.6 and Figure 5.7. For these two years arc-wise maxima are shown as scatter plots with different symbols indicating the distances. More details can be found in the supplementary report "OML: Model Validation" (Olesen et al., 2007).

### 5.4.3 Copenhagen

The experiments were carried out in September-November 1978 and April-July 1979 in the Northern part of Copenhagen. A passive tracer ( $\text{SF}_6$ ) was released from a TV tower at Gladsaxe at a height of 115 m (Gryning and Lyck, 1984). Samplers were positioned on up to three arcs, East of the release point, at distances of approximately 2 km, 4 km and 6 km. The downwind area was predominantly residential to heavily built-up.

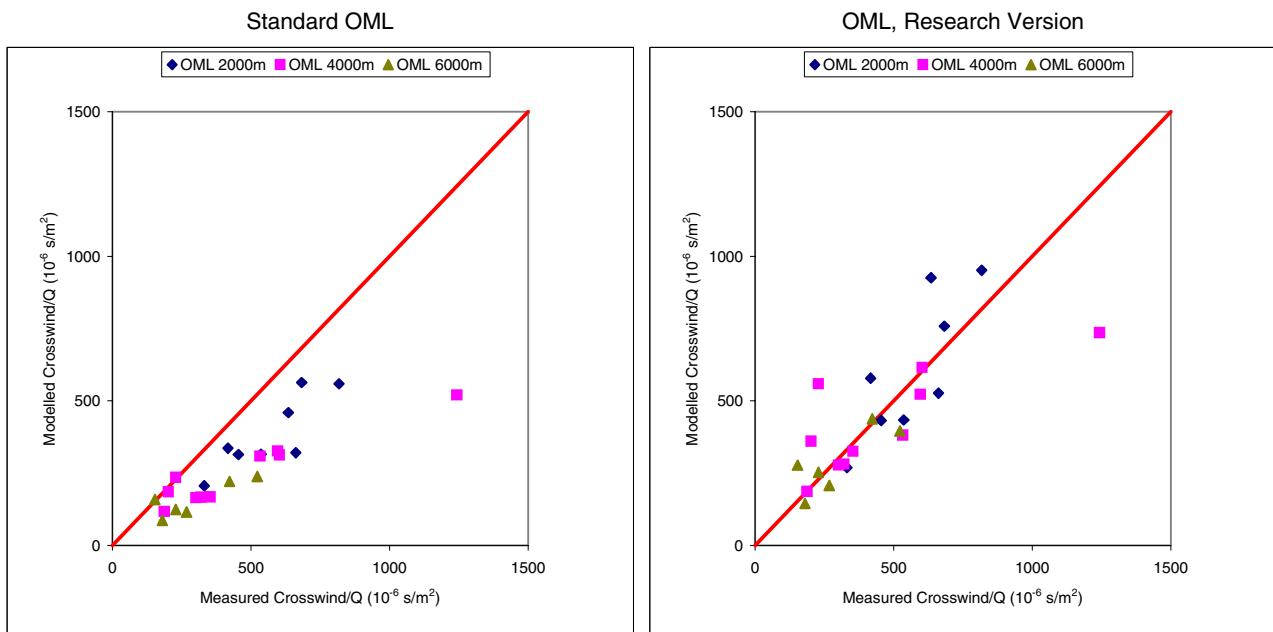


Figure 5.8 Copenhagen, Hs=115 m, crosswind integrated concentrations.

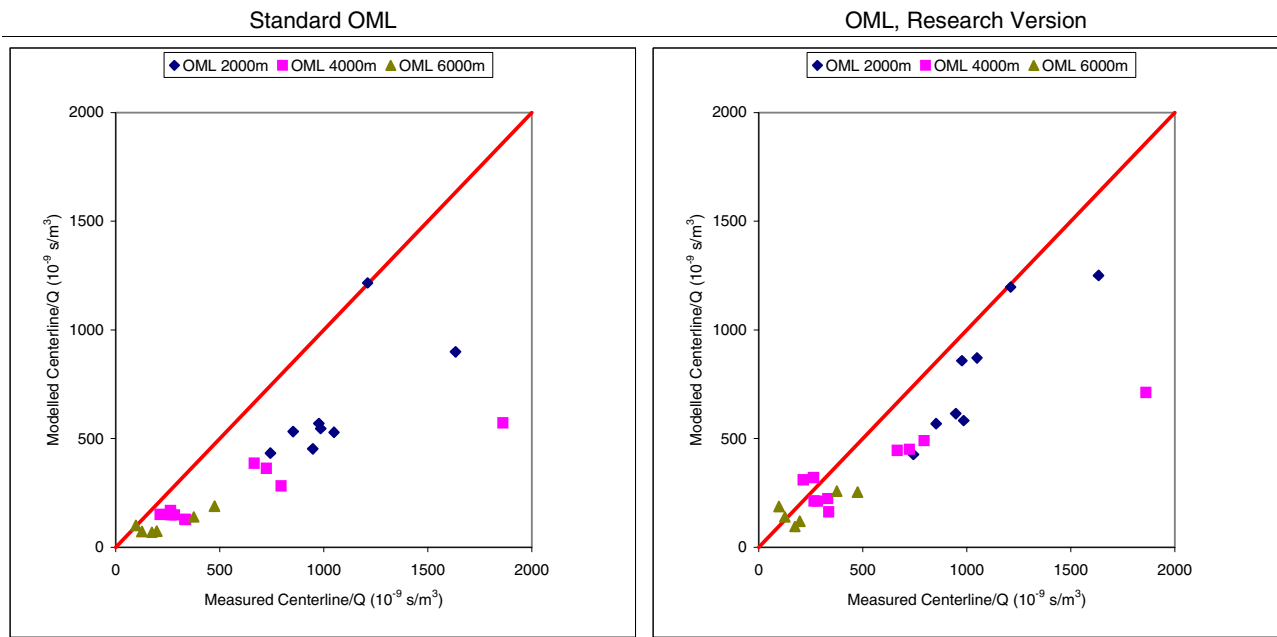


Figure 5.9 Copenhagen, Hs=115 m, arc-wise maximum concentration values.

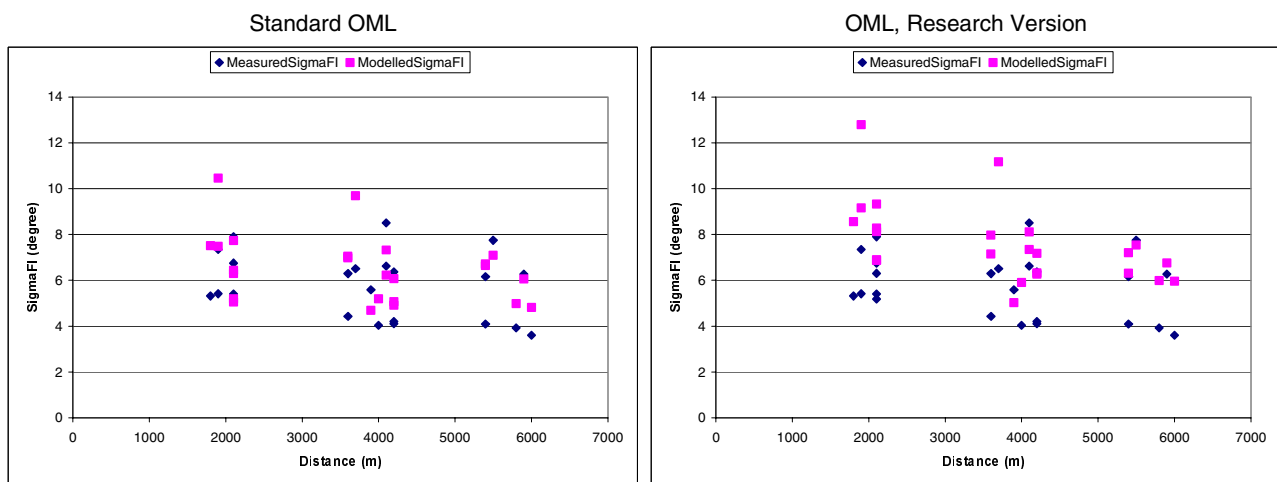


Figure 5.10 Copenhagen, Hs=115 m. Variation of the plume's opening angle ( $\sigma_y$ /distance) with the distance from the source.

The experiments were carried out during September-November 1978 and April-July 1979. The conditions were predominantly neutral to slightly unstable with relatively high wind speeds. A total of 10 hourly release experiments are available for analyses. The hourly sampling data were made up of three consecutive 20 min samplings. A quite dense net of sampling positions (about 2° separation) makes it possible to make a reasonable precise determination of both the arcwise maxima and the crosswind integrated concentrations.

The results of model calculations with both the current Standard Version of OML and the new Research Version for the crosswind integrated concentrations are shown in Figure 5.8, while results for the arcwise maxima are shown in Figure 5.9. A considerable improvement of the results with the new parameterisation is evident both in the case of the arcwise maxima and the crosswind integrated concentrations. Good agreement is evident for the crosswind integrated concentrations, while the arcwise maxima are still underpredicted by the model. This indicates

good model performance with respect to the vertical dispersion, but some overprediction of the horizontal dispersion. This conclusion is substantiated by the results shown in Figure 5.10. This figure shows the variation of the measured and modelled plume's opening angle with the distance from the source. The opening angle, given here in degrees, is defined as  $\sigma_y/distance$  and the modelled results are shown both for the old and the new version of the model. Even though this parameter seems better represented by the Standard version of OML, the improved skill in predicting vertical dispersion is sufficient to ensure that the overall results are better in the new version.

#### 5.4.4 Wind-tunnel experiments

In 1991, a set of wind tunnel experiments were conducted by Roger Thompson of the EPA wind tunnel in North Carolina (Thompson, 1993). The data contains measurements of ground-level concentrations from stacks of different height and with different distances to a building. These data have been used in the present study, where they are further discussed in Chapter 6, as well as in the supplementary report "OML: Model Validation".

Already in a previous study by Olesen and Genikhovich (2000) the OML model was evaluated with Thompson's data in the presence of buildings. From that study it appears that the OML model significantly underestimates the ground-level concentrations for all stack heights and for all distances from a building. This was the case even when the influence of the building should be negligible.

Within the present study the reasons for this discrepancy were explored.

Thompson's data set not only contains measurements of concentrations *with* buildings, but also a series of measurements *without* building. A number of OML simulations were performed for such simple cases. Results for four different stack heights are shown in Figure 5.11.

The concentrations measured in the wind tunnel and the corresponding model results are through out this report shown in a non-dimensional form using the following formula.

$$C_{non-dim} = C \frac{U_{ref} \times H^2}{Q} \quad (5-16)$$

Where:

$U_{ref}$  is the free wind velocity in the tunnel. In the case of the Thompson's experiments shown here,  $U_{ref}=4m/s$ .

H is a length scaling height and in the case of the Thompson's experiments shown here,  $H=150mm$ , which corresponds to the height of the building models used in the experiments. This scaling is also used for experiments without buildings.

Q is the tracer emission rate.

The left column in Figure 5.11 shows results of standard OML computations similar to those conducted by Olesen and Genikhovich (2000). Wind tunnel measurements normally represent neutral stability, so the

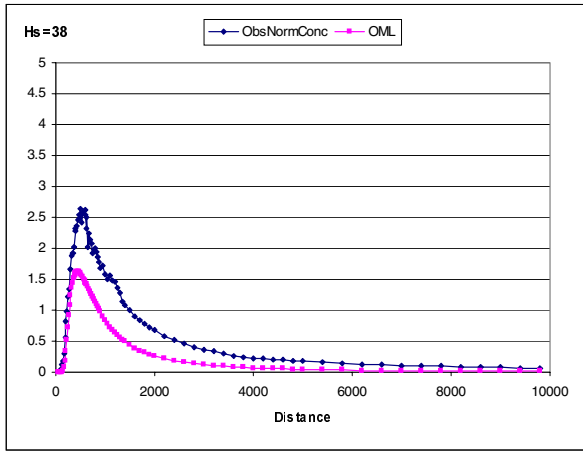
model runs were conducted with a heat flux of practically zero - but very slightly to the *stable* side. With the standard OML model, parameterisation of horizontal dispersion takes place according to Eq. ( 3-39 ).  $u^*$  for all the wind tunnel experiments was only 0.17m/s. Because  $u^*$  is below a threshold of 0.5 m/s it is (within the model) replaced by the assumed minimum value for stable conditions, i.a. e. 0.5 m/s.

The figures in the right column show corresponding results for slightly *unstable* conditions (heat flux = 1.2 W/m<sup>2</sup>). In this case the horizontal dispersion, according to the current procedure (Eq. ( 3-39 )), is modelled with the value of  $u^*=0.17$ m/s. This, roughly speaking, results in horizontal dispersion being 3 times smaller than in the case of slightly stable conditions.

In both columns of figures the black line represents the observed data, the same observed data are plotted in the left and right panels.

The two sets of graphs reveal striking differences. According to standard OML, the maximum concentrations are roughly 3 times higher for slightly unstable than for slightly stable conditions.

Almost neutral, but slightly stable



Almost neutral, but slightly unstable

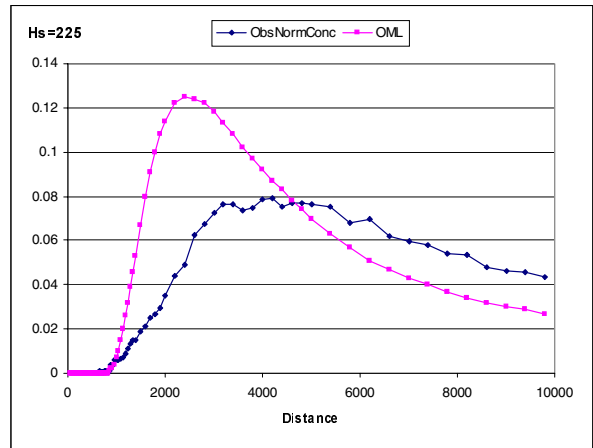
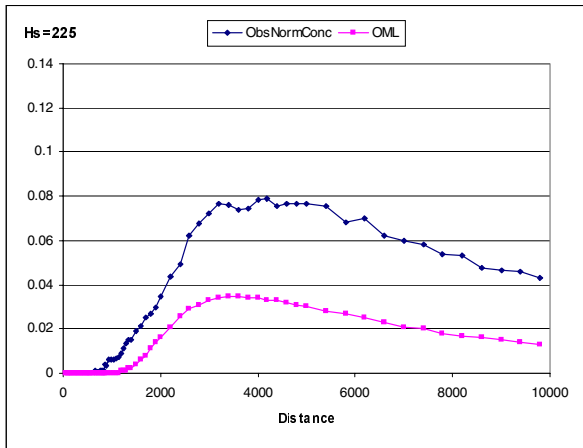
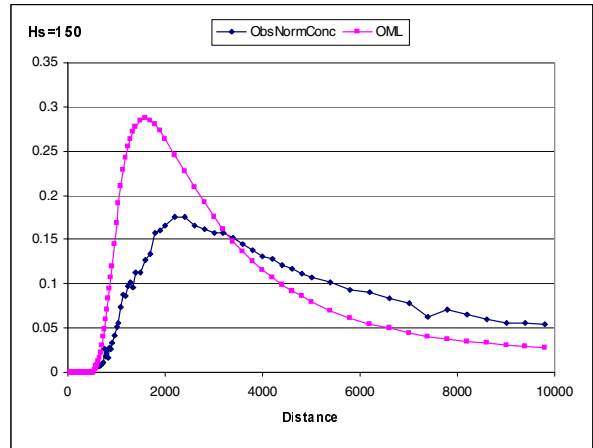
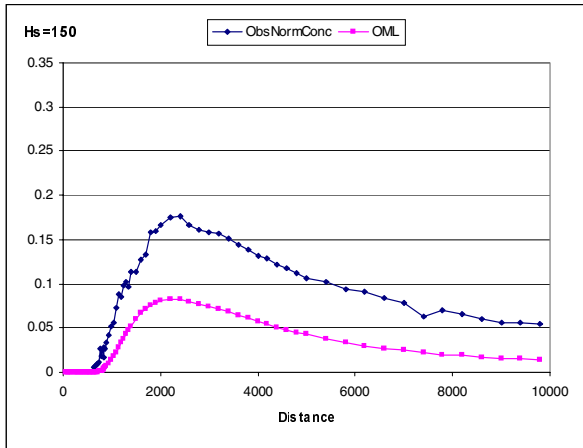
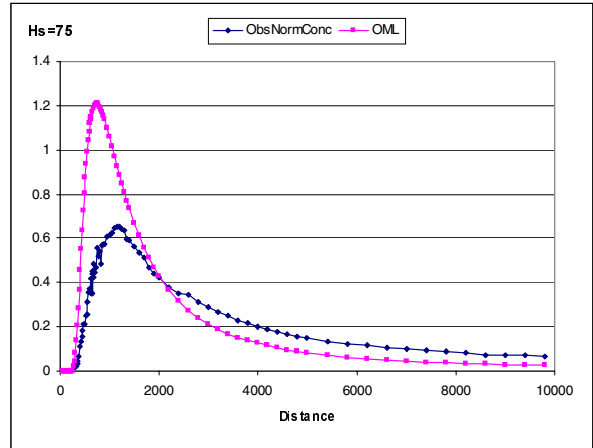
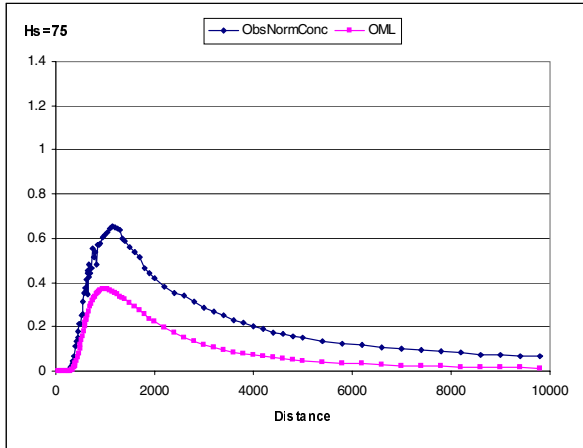
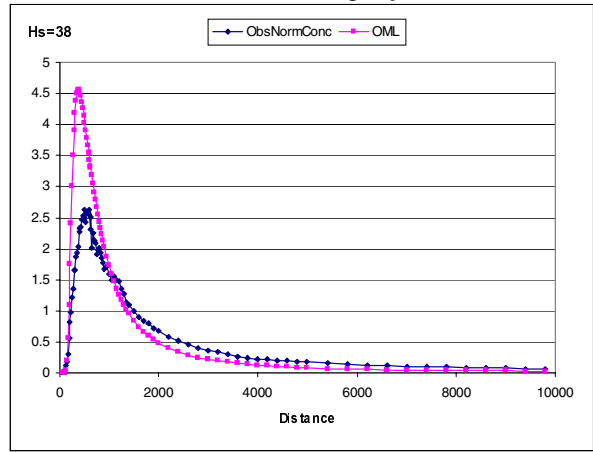


**Figure 5.11** Results of calculations using the *standard OML model* for wind-tunnel experiments. Left: assuming slightly stable conditions (heat flux practically 0 but on the stable side). Right: assuming slightly unstable conditions, corresponding to the observed turbulence profile (heat flux=1.2 W/m<sup>2</sup>). The black line represents the observed data, which are the same in the left and right panels.

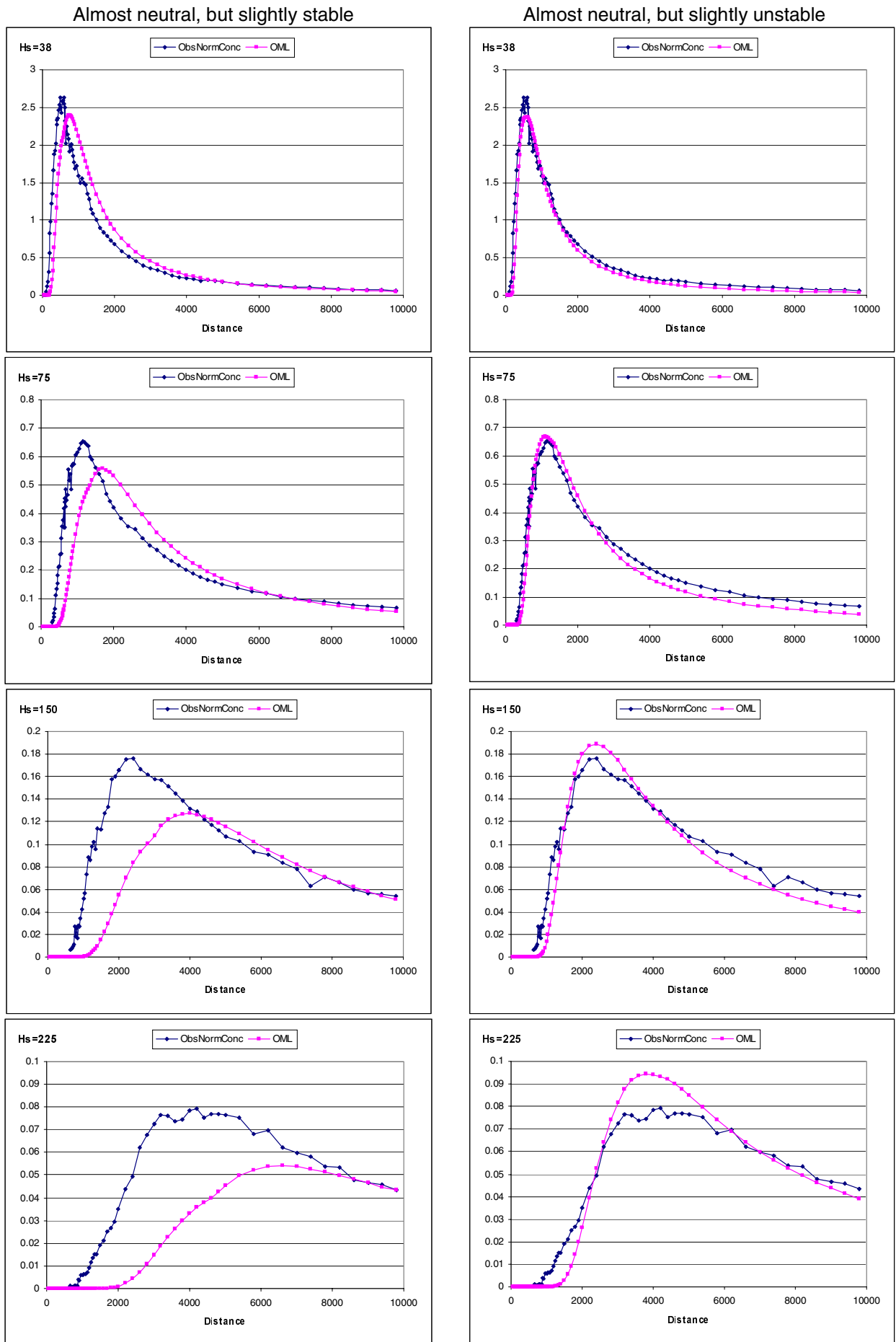


**Figure 5.12** Results of calculations using the *Research Version of OML* for wind-tunnel experiments. Left: assuming perfectly neutral conditions (heat flux=0). Right: assuming slightly unstable conditions (heat flux=1.2 W/m<sup>2</sup>). The black line represent the observed data, which are the same in the left and right panels

It can be justified that there is a difference between model results in slightly stable and slightly unstable conditions, because convective eddies act only during unstable conditions. Further, wind tunnel simulations cannot account for large-scale meandering in stable conditions such as observed in nature, and this can justify a larger horizontal dispersion in OML (implying smaller concentrations) than in a wind tunnel. However, the results indicate also that the observed underestimation of the ground-level concentrations far away from the buildings, as reported by Olesen and Genikhovich (2000), was primarily due to the deficiencies in parameterisation of the horizontal dispersion and not as much related to the shortcomings in modelling of the building effects.

As explained in Section 5.2 the parameterisation of the horizontal dispersion  $\sigma_y$  has been revised in the Research Version of OML. Figure 5.12 show results computed with the Research Version of OML. While computing the results, the large-scale contribution to horizontal dispersion (Eq. 5-6) has been "switched off" in order to simulate wind tunnel conditions. It appears that the change of parameterisation has the consequence that model results fit the wind tunnel data very well, when slightly unstable conditions are assumed (right column).

When interpreting wind tunnel data results it is an obvious question to ask whether the scenarios studied represent slightly stable or slightly unstable conditions. Our examination of the vertical turbulence profiles from the wind tunnel reveals they have such a structure that the data can be assumed to represent *slightly unstable* conditions. We ascribe this to the fact that the turbulence structure was generated with large fans, which generate large eddies similar to those of a convective boundary layer. This is discussed in more details in the supplementary report "OML: Model Validation" (Olesen et al., 2007).

For the Research Version of OML (Figure 5.12) the difference between model results for slightly stable and slightly unstable conditions is much smaller than for Standard OML. Mathematically, in the model code of the Research Version, there is a continuous transition between stable and unstable conditions - but with a rapid evolution when the conditions move away from neutral. As noted above, it can be justified that model results are different in slightly stable, respectively slightly unstable conditions.

## 5.5 Reformulation of plume rise

### 5.5.1 Background

In the current standard OML model, parameterisation of plume rise is simplified in certain regards - implying that for certain cases inaccurate results are to be expected. It is possible to avoid certain of the simplifications with slight revisions of the code. The issues concerned include the following:

- Wind speed: In the Research Version, the wind speed used for computation of plume rise is an effective wind speed (vertically averaged), and not simply the wind speed at stack height.

- The entrainment coefficient  $\beta$  appears in Briggs' equations in two contexts with different values. This results in some inconsistencies in the Standard version of OML, which have now been resolved.
- A more accurate computation of the fate of the plume as it moves up through layers with different stabilities.
- Changes in parameterisation of dispersion due to internal turbulence, motivated e.g. by a more accurate description of vertical plume velocity.
- The height at which dispersion parameters are calculated: The Research Version uses an average effective height depending on plume history, instead of the simple plume centreline height.

### 5.5.2 Initial Plume Rise

Initial plume rise is calculated taking into account both the momentum and buoyancy fluxes. The following formula is used

$$DH_{init} = \left[ \frac{3F_m}{(\beta_m + 1.2u_{pr} / w_s)^2} \frac{X}{u_{pr}^2} + \frac{3F_b}{2\beta_b^2} \frac{X^2}{u_{pr}^3} \right]^{1/3} \quad (5-17)$$

The first term on the right hand side of (5-17) refers to the contribution from momentum flux while the second refers to the buoyancy part (Briggs, 1984).

X	is the distance from the source
$w_s$	is the (vertical) plume exhaust velocity
$F_m$ and $F_b$	are momentum and buoyancy fluxes of the plume (Eqs. ( 3-42 ) and ( 3-43 ))
$\beta_m$ and $\beta_b$	are entrainment coefficients of momentum and buoyant rise, respectively (see the definition below)
$u_{pr}$	is the effective wind speed used for calculation of plume rise (see the definition below)

The entrainment coefficients  $\beta_m$  and  $\beta_b$  are related to the rate of increase of the plume cross-section radius R due to entrainment of the ambient air.

$$\beta = \frac{dR}{dz} \quad (5-18)$$

where z is the height of the plume centreline above the stack top.

Briggs (1984) recommends different values for the entrainment rate of momentum rise and buoyant rise.

$$\begin{aligned}\beta_m &= 0.4 \\ \beta_b &= 0.6\end{aligned}\tag{5-19}$$

Furthermore, an empirical correction dependent on  $u_{pr}/w_s$  is recommended (Briggs, 1984) for the effective entrainment rate for momentum rise (see Eq. 5-17).

Eq. (5-17) is derived using principles of conservation of the plume's vertical momentum and buoyancy (Davidson, 1989).

$$\begin{aligned}\frac{d}{dt}(w_p R^2 u_{pr}) &= F_b \\ w_p &= \frac{dz}{dt}; \quad R = R_0 + \beta \cdot z\end{aligned}\tag{5-20}$$

The second line of Eq. (5-20) provides expressions for the plume rise velocity  $w_p$  and the expanding plume's radius. The formula (5-17) corresponds to a solution of (5-20) but with an assumption of zero initial plume radius  $R_0$ . This is a reasonable assumption for simple point sources but might need a modification for sources with significant horizontal dimensions, like e.g. cooling towers. Additionally, Eq. (5-20) assumes that expansion of a plume is entirely related to the entrainment of fresh air due to the plume movement with respect to the surrounding air (with entrainment rate  $\beta$ ). Also this assumption needs to be modified in the case the plume is subject to extra dilution by interaction with a nearby building.

The effective wind speed,  $u_{pr}$ , used in calculations of plume rise is determined as the average wind speed in the layer between stack top and the final rise (see the next section for description of the methods used to calculate the final rise).  $u_{pr}$  is calculated in a similar way as the average transport wind speed (Eq. 5-1) but with the integration limits given by the stack height and the final rise height. Because the final rise depends also on the wind speed, the calculations are done using an iterative loop.

This procedure described here differs from the one used in the standard version of OML, where the wind speed used in calculation of plume rise was always determined at the height of the stack top. This difference will have the largest implications for low sources, in which case significant vertical gradients of wind speed can be expected. Use of the wind speed at the release height for calculation of plume rise can result in significant overestimation of plume rise.

### 5.5.3 Final rise

The final plume rise is calculated assuming that there are 3 different processes that can result in stopping the plume rise:

- Dissipation of the plume's internal turbulence until it has reached a level equal to the dissipation rate of the mechanical turbulence in the surrounding air.

- Dissipation of the plume's internal turbulence until it has reached a level equal to dissipation rate of the convective turbulence in the surrounding air (relevant only for unstable conditions).
- The plume buoyancy is consumed due to rise through a positive vertical temperature gradient.

We consider first the processes involving dissipation, then the process involving the vertical temperature gradient.

#### Plume rise limited by dissipation

According to Briggs (1984), plume rise can be terminated when dissipation of the turbulent energy within the plume drops below the ambient value.

$$\eta \frac{w_p^3}{z} = \epsilon_a \quad (5-21)$$

Here,  $w_p$  is the actual plume rise velocity,  $\eta$  is an empirical constant ( $\approx 1.5$  according to Briggs, 1984) and  $z$  is the height above the stack top (the final rise height) at which the in-plume dissipation rate equals the ambient dissipation rate  $\epsilon_a$ .

The ambient dissipation rate is determined taking separately into account the two different turbulent energy production mechanisms: the mechanically generated turbulence (due to wind shear) and the thermally generated turbulence (due to unstable atmospheric stratification).

The mechanical dissipation rate is given by

$$\epsilon = \frac{u_*^3}{\kappa} \left( \frac{1}{h_s + z} + 5.3/L \right) \quad (5-22)$$

while the dissipation rate of the thermally produced turbulence (convective turbulence) is given by

$$\epsilon = \eta_c \frac{w_*^3}{z_i} \quad (5-23)$$

For the proportionality coefficient  $\eta_c$  a value of 0.25 is recommended by Briggs (1984).

The stability correction given in (5-22) by the term  $5.3/L$  is applied only for stable conditions. The thermally generated turbulence is applied only for unstable conditions. The final expressions are practically the same as in the standard current version of OML (Eqs. (3-46) and (3-52)) and are not repeated here.

The final plume rise as calculated by Eqs. (5-22) and (5-23) is only used when it is smaller than the height determined due to rise through a temperature gradient.

A similar set of equations is applied to momentum rise. The procedure is practically unmodified compared to the standard version of OML. The final plume rise is taken as the largest calculated for buoyancy and momentum.

**Plume rise limited by vertical temperature gradient**

The vertical temperature gradient of the atmosphere is expressed through a number of stability parameters,  $S_i$ . The definition of the different  $S_i$  parameters is the following:

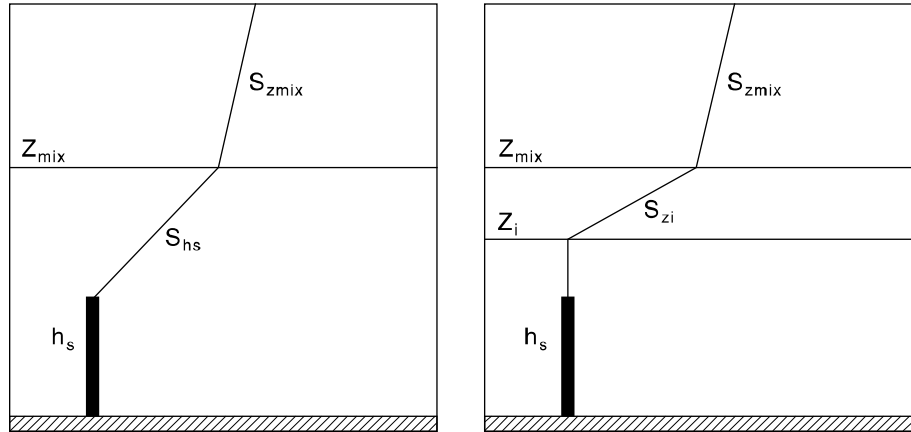


**Figure 5.13** Temperature structure used in connection with calculation of the final plume rise. The curve shows potential temperature  $\theta$  as a function of height  $z$ . Left: stable conditions; right: unstable conditions. The definition of the different  $S_k$  parameters is given below.

$$S_k = \frac{g}{T} \frac{d\theta}{dz} \Big|_{z = z_k} \tag{5-24}$$

Where  $z_k$  is the height at which the potential temperature gradient,  $d\theta/dz$ , is evaluated.

For stable conditions only two temperature gradient regimes are considered: temperature gradient at the stack height ( $S_{hs}$ ) and the temperature gradient above the stable boundary layer height ( $S_{zmix}$ ). The temperature gradient at the stack height is calculated using the similarity profiles for temperature (Högström, 1996)

$$S_{hs} = \left( \frac{u_*}{\kappa L} \right)^2 \left( \frac{L}{h_s + z_o} + 8 \right) \tag{5-25}$$

$S_{zmix}$  is calculated using the temperature gradient above  $Z_{mix}$ . This gradient is estimated from the radio soundings.

In the case of unstable conditions, three different layers can exist. If the stack top is within the convective mixing layer ( $h_s < Z_i$ ), then it is assumed that the potential temperature within this layer is constant, i.e.  $S_{hs}=0$ . Temperature gradients above  $Z_i$  and  $Z_{mix}$  (elevated inversions) are estimated from radio soundings. Note that  $Z_{mix} \geq Z_i$ .

The basic equation used for determination of the final plume rise due to loss of buoyancy is:

$$\frac{dF_{zb}}{dz} = -u_{pr}(\beta z)^2 \cdot \sum_k \alpha_k S_k \quad (5-26)$$

where  $F_{zb}$  is the actual plume buoyancy at the height  $z$  above the stack top.  $S_k$  refers to the corresponding value of  $S$  in the  $k$ -th layer through which the plume is rising.  $\alpha_k$  is the fraction of the plume contained in the  $k$ -th layer. In the case of interaction of the plume with a nearby building, the decrease of buoyancy due to entrainment of fresh air in the building wake, must also be taken into account.

Eq. (5-26) is solved analytically and the final rise is determined as the height at which all buoyancy flux is lost, i.e. when  $-\Delta F = F_b$ . The actual plume fraction contained in a particular layer is calculated using simple geometrical principles, as illustrated in Figure 5.14 for a situation corresponding to an unstable stratification. In this case parts of the plume can be contained in up to three different layers simultaneously. A top-hat (uniform) concentration distribution is assumed within the plume, with the vertical extent of the plume equal to the actual plume rise ( $DH$ ). The top of the plume starts thus to penetrate into a layer  $k$  when,

$$1.5 \cdot DH = Z_k - h_s \quad (5-27)$$

and is entirely contained in the layer when

$$0.5 \cdot DH = Z_k - h_s \quad (5-28)$$

Eqs. (5-27) and (5-28) are used to calculate the plume fraction ( $\alpha_k$ ) in the  $k$ -th layer.

The procedure described here differs from the one used in the current standard version of OML only in the case of unstable conditions. In the standard version of OML the penetration of the plume into the layers above  $Z_i$  and  $Z_{mix}$  is calculated independently of each other. The loss of buoyancy in the layer between  $Z_i$  and  $Z_{mix}$  is not taken explicitly into account. The final rise is determined as the smallest of the two penetration cases. This will in general result in a somewhat larger plume rise than when using the new procedure.

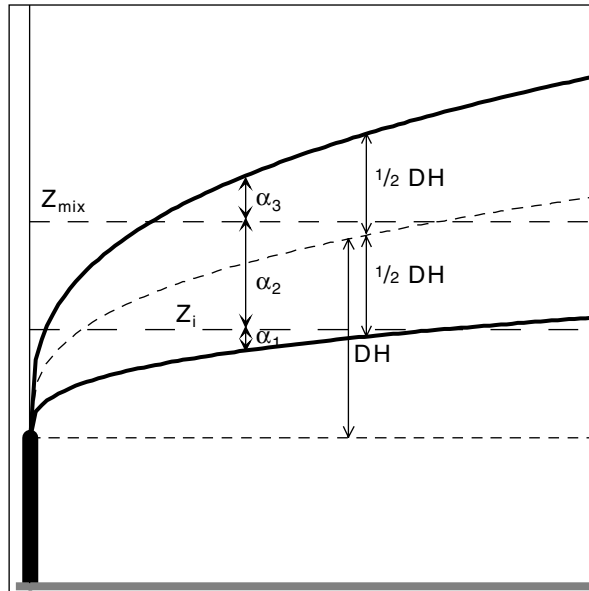


**Figure 5.14** Illustration of the layering principle of a rising plume. In the example shown here, which depicts a situation corresponding to unstable atmospheric conditions, the plume can partially be contained in up to three different layers simultaneously.

#### 5.5.4 Dispersion of rising plumes

Plume rise has not only the effect of increasing the effective plume height, but also influences the dispersion of the plume. Rising plumes with significant vertical velocity with respect to the ambient air do not follow the ambient air trajectories; this results in diminishing of the turbulent dispersion. At the same time, entrainment of ambient air into the rising plume acts as to increase the spread of the plume. The final result of these two opposing effects depends on the actual meteorological conditions and the stage of the plume rise.

According to Briggs (1984) the physical width of a rising plume is, as previously mentioned, approximately equal to plume rise. Assuming a “top-hat” concentration distribution in the plume, the  $\sigma_{\text{internal}}$  of the plume becomes:

$$\sigma_{\text{internal}} = \frac{\Delta h}{\sqrt{2\pi}} \quad (5-29)$$

Eq. (5-29) insures that the plume centreline concentration calculated, while assuming either a top-hat distribution or a Gaussian distribution, will be the same. However, the real concentration distribution in a rising plume is neither exactly top-hat nor Gaussian. Therefore, the contribution of the plume dispersion caused by plume rise to the Gaussian dispersion parameters must be determined empirically. The procedure used in the revised version of the model differs slightly from the one used in the standard version. The procedure is as follows:

$$\begin{aligned} \sigma_{y\text{internal}} &= \Delta h_{\text{max}} / 3.5 \\ \sigma_{z\text{internal}} &= (\Delta h / 3.5) \cdot f_{\text{mit}} \end{aligned} \quad (5-30)$$

A factor 3.5 is used instead of  $\sqrt{2\pi}$  (~2.5), because 3.5 is more consistent with the general practise in many other models. This change has only a

slight effect on the performance of the model on available experimental data (Kincaid).

Several issues have been considered by the revision of the model, including

- vertical velocity of the plume during its rise
- The height at which dispersion parameters are calculated (plume centreline or an average effective travel height?).

The enhancement of the horizontal dispersion coefficient is calculated using a value of plume-rise ( $\Delta h_{\max}$ ) estimated without taking into account termination of the rise due to penetration into elevated inversion layers. This should simulate “splashing” of the plume (i.e. enhancement of its horizontal extension) when rising through an elevated inversion.

For the vertical dispersion, an additional empirical correction is applied in order to account for the inclination of the plume in the initial stage of the rise (before it reaches its final rise). The correction factor  $f_{\text{init}}$  is defined as

$$f_{\text{init}} = u_{pr} / \sqrt{u_{pr}^2 + w_p^2} \quad (5-31)$$

The factor  $f_{\text{init}}$  is actually the ratio between the horizontal velocity of the plume and the corresponding velocity along its centre-line trajectory. Thus,  $\Delta h f_{\text{init}}$  is the projection of plume’s cross-section on the vertical axis z.

$w_p'$  is the vertical plume velocity computed in the following way: Let  $w_p$  be the vertical plume velocity as calculated from the equation for initial rise, Eq. (5-17):

$$w_p = \frac{dz}{dt}; \text{ where } z \text{ is the plume rise height given by Eq. (5-17)} \quad (5-32)$$

Now,  $w_p'$  is computed as a modification of  $w_p$ , where it is assumed that  $w_p$  becomes zero when the plume reaches its final height:

$$\begin{aligned} w_p' &= w_p \cdot (1 - x / X_{\text{final}}) \quad \text{for } x < X_{\text{final}} \\ w_p' &= 0 \quad \text{for } x \geq X_{\text{final}} \end{aligned} \quad (5-33)$$

$X_{\text{final}}$  is the distance from the source where the plume attains its final height. This distance is calculated by solving Eq. (5-17) for x with the condition  $DH_{\text{init}}=DH_{\text{final}}$ . Expression (5-33) insures a smooth transition of the vertical plume rise velocity towards the value of zero that applies when  $x>X_{\text{final}}$ . This procedure is new compared to the previous (standard) version of the model, where the vertical plume velocity is always calculated as if it were in the stage of initial rise (i.e.  $w_p' = w_p$ ). Another difference is that in the standard version of the model, the vertical rise velocity is calculated taking only the buoyancy effect into account. The

momentum rise is neglected. This will in general result in underestimation of the rise velocity for non-buoyant sources that have significant exhaust momentum

The contribution to dispersion parameters from internal dispersion ( $\sigma_{internal}$ ) is added to the remaining turbulent dispersion parameters to obtain the effective  $\sigma$ -parameters for use in the Gaussian plume formula,

$$\begin{aligned}\sigma_{y\,eff}^2 &= \sigma_y^2 + \sigma_{y\_internal}^2 \\ \sigma_{z\,eff}^2 &= \sigma_z^2 + \sigma_{z\_internal}^2\end{aligned}\quad (5-34)$$

It is important to note that the enhancement of the vertical dispersion due to plume rise is only applied to the mechanically created turbulence. The vertical dispersion under unstable conditions is calculated using the new method described in the section 5.3.

An empirically derived expression is used in order to take into account the reduction of turbulent dispersion of rising plumes. The reduction of the turbulent dispersion is simulated by introduction of an effective travel distance,  $X_{ef}$ , which is defined as

$$X_{ef} = X \cdot (1 - \exp(-0.2u / w_p')) \quad (5-35)$$

where  $X$  is the actual travel distance,  $u$  is the travel velocity (a plume average travel velocity, Eq. (5-2) and  $w_p'$  is the modified vertical plume velocity as defined in (5-33). The turbulent dispersion parameters are subsequently calculated using the modified distance  $X_{ef}$ . This procedure corresponds to Eq. (3-72) that is applied in the Standard OML model.

The expressions used for calculation of the turbulent dispersion parameters all depend on the source height. For passive plumes (without plume-rise) this height is constant, while this is not the case for sources with plume-rise. In the current standard version of the model the height used for calculation of the dispersion parameters (at any distance from the source) is assumed to be the actual *height of the plume-centreline* (i.e.  $h_s + \Delta h$ ). Here we introduce an *effective calculation height*, which is based on plume history and estimated as a distance weighted average height of the plume-centreline,

$$h_{eff} = h_s + \frac{1}{X} \left[ \int_0^X \Delta h(x) dx \right] \quad (5-36)$$

The integral in (5-36) is calculated using expression (5-17) for  $x < X_{final}$  and the value of the final plume-rise for  $x \geq X_{final}$ . As a simplification, the integral of (5-17) is calculated separately for the momentum and buoyancy parts. Note that the actual plume-centreline height is still used in the Gaussian plume concentration formula.

## 5.6 Model performance with revised formulation – buoyant plumes

Model performance in the case of buoyant plumes has been evaluated using experimental data from the Kincaid dataset. Further details on the data and on the evaluation are presented in the supplementary report "OML: Model Validation" (Olesen et al., 2007). A summary of the evaluation results is given here.

It should be clearly understood that for the Kincaid data set there is a very large stochastic variability in the pattern of measured concentrations. As a consequence, results from individual hours at Kincaid cannot be used to derive firm conclusions on model behaviour. Conclusions will have to be supported by observations from many hours.

We have mainly used data as provided in the Model Validation Kit (Olesen, 2005). However, the meteorological input parameters were re-evaluated using the meteorological pre-processor of OML with corrected value of  $\kappa$  and new formulation of the similarity functions. Mixing heights were estimated by manual inspection of the available radio sonde data.

The Kincaid Power Plant has one 187m stack with highly buoyant exhaust. The Kincaid dataset contains tracer measurements ( $\text{SF}_6$ ) from several concentric arcs placed at distances ranging from 500 m to 50 km from the stack. For the purpose of evaluation, the highest measured concentration for each arc is compared to the modelled centre-line concentration at the corresponding distance.

Model calculations were performed with the standard version of OML, with the Research Version and with AERMOD. The same meteorological data were used as input to all these models. The results presented here refer to the subset of data that were assigned a quality index of 3 - e.g., the observed arcwise maxima were relatively well-defined. This selection restricts the dataset to 128 hours but with measurements at several distances for each hour.

Figure 5.15 show results of comparison between measured and modelled arc-maximum concentrations. Results are shown for the Standard Version of OML, for the new Research Version, and for the AERMOD model.

Figure 5.16 shows another type of comparison. Here, the data for each arc-distance are *averaged over all hourly data* available for the particular arc. The number of available hours is different for different arcs. Only 1 observation is available for the 40 km arc. Both the old standard and the new Research Version of OML reproduce reasonably well the variation of average concentration with distance from the source. AERMOD significantly underestimates the measured concentrations for distances larger than 3 km from the source. However, both the standard version of OML and AERMOD overpredict the maximum measured distance averaged concentration, predicting a sharp maximum at the 2km distance. This observation is also evident when inspecting results for individual hours, plotted in the same fashion as in Figure 5.16.

Figure 5.17 shows comparison of maximum measured and maximum modelled concentrations, but regardless of the distance from the stack. Thus, there is one pair of data values for each hour (108 data values, as opposed to 338 in Figure 5.15). Thus, here the data are paired in time, but not in space. The overall behaviour of the Standard Version and the Research Version of OML is quite similar. AERMOD again shows a tendency to underpredict the maximum concentrations.

Figure 5.18 shows rank sorted arc-wise maximum concentrations using all the available observations with quality 3 index. The underlying data are the same as in Figure 5.15, but in the graph the data are neither paired in time nor in space, but just sorted according to size. The difference between the new and the standard versions of OML is small. AERMOD underpredicts the concentrations in the lower range but is better with respect to reproducing the behaviour in the upper range.

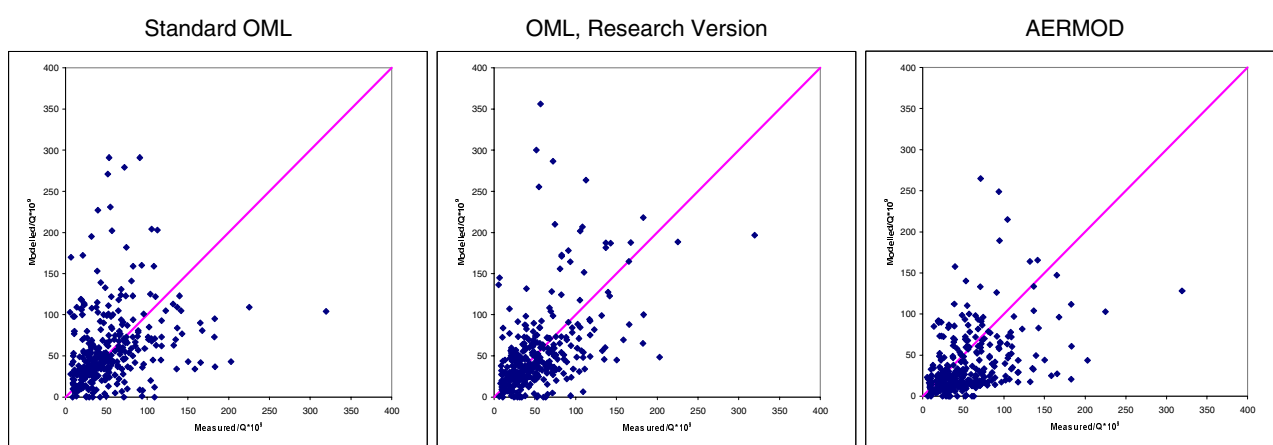


Figure 5.15 Comparison of measured and modelled arc-maximum concentrations for the Kincaid tracer data.

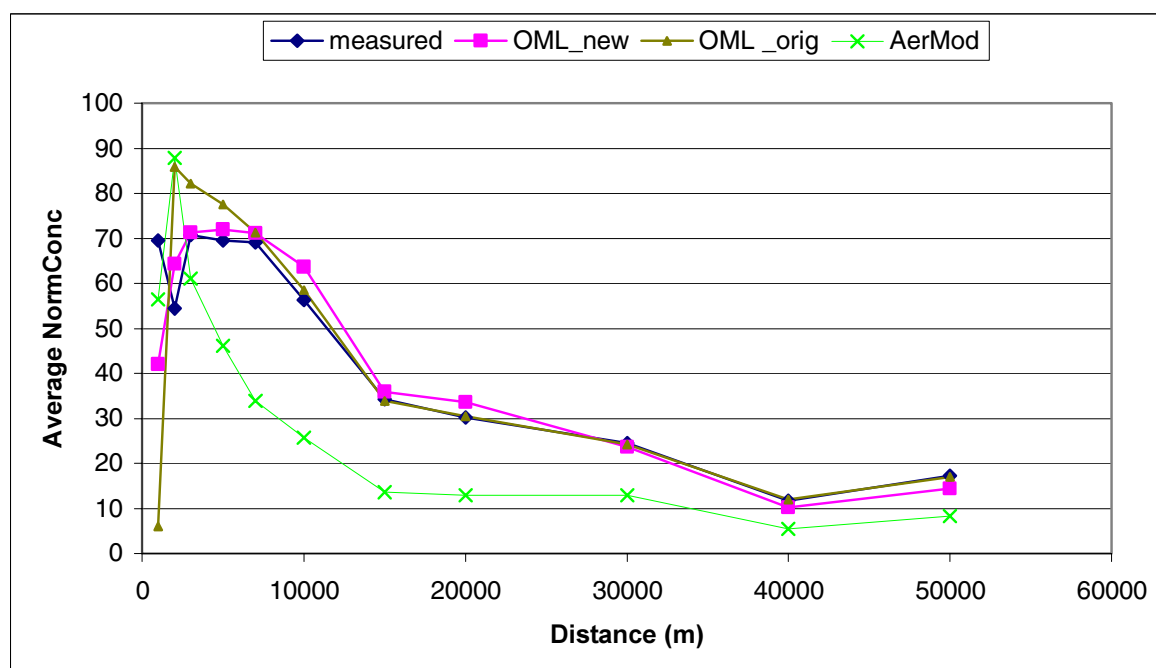
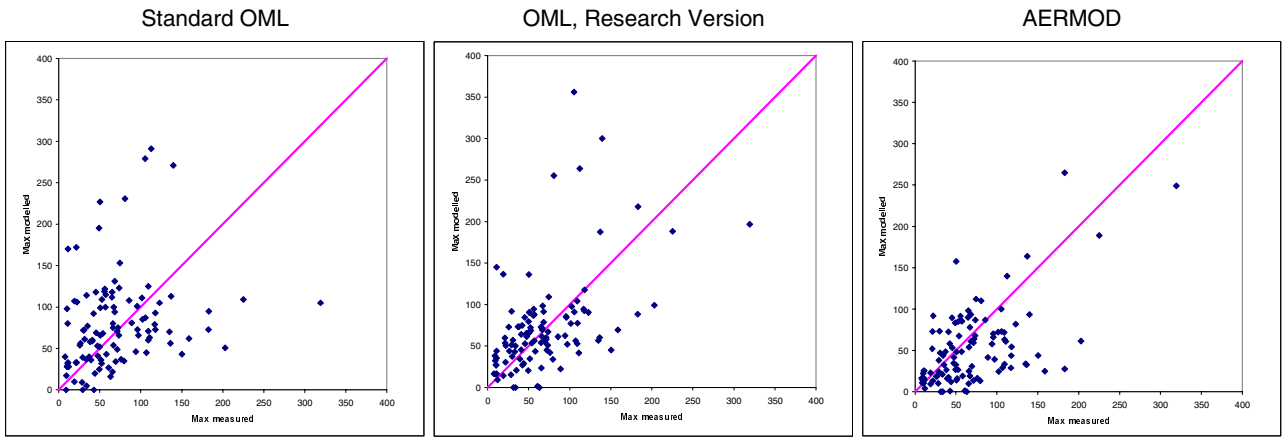
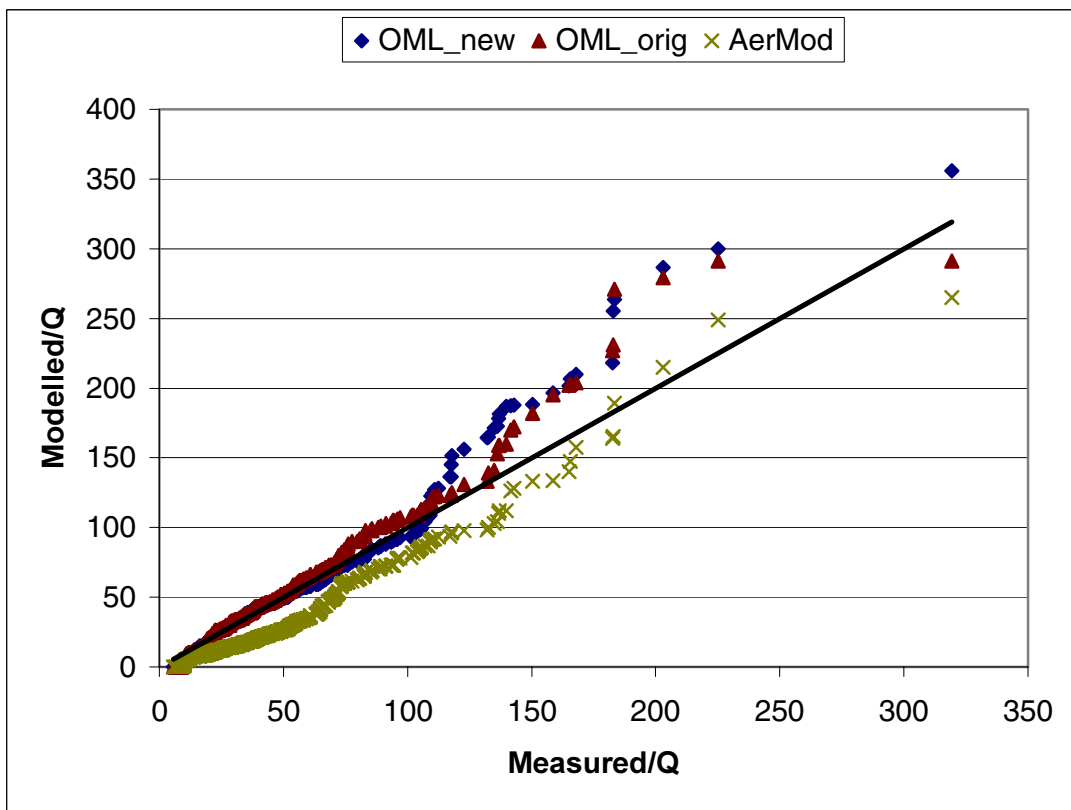


Figure 5.16 Comparison of measured and modelled distance averaged concentrations for Kincaid. For each arc distance the concentrations are averaged over all hourly data available for the particular arc. The number of available hours is different for different arcs. Only 1 observation is available for the 40km arc.



**Figure 5.17** Kincaid. Comparison of measured and modelled maximum concentrations for each of the observation hours regardless of the position of the maximum.



**Figure 5.18** Comparison of rank sorted concentrations. Based on arc-wise maximum concentrations as presented in Figure 5.15. The data are neither paired in time nor in space.

## 6 Studies on building effects

### 6.1 Introduction

It is a recognised problem that the current standard OML model treats building effects in a very simplified manner. One of the consequences is unrealistic changes in concentrations, when a building is moved from the domain where it has an influence to a location immediately outside of this domain.

This problem and a couple of others are, e.g., described in the report by (Olesen et al., 2005), and summarised again here in Section 6.5.

Within the current project, a substantial effort has been devoted to the study of building effects. A main element within the studies has been investigations based on a comprehensive – but surprisingly little known – data set by Thompson, simulating dispersion around buildings in a wind tunnel. Another element within the studies has been investigations of the behaviour of the building algorithm of the US EPA AERMOD model.

The current chapter reports on this work. The chapter includes the following sections:

- Physical description of the problem
- The models
- Investigations based on Thompson's wind tunnel data
- Discussion of building effects, and the implications for OML development.

### 6.2 Physical description

If a building or another large obstacle is situated close to a stack, plume dispersion can be disturbed. This can have a substantial effect on the resulting ground-level concentrations.

When the airflow meets a building, it is forced up and over and around the building. This not only modifies the streamlines of the airflow, but also has an effect on the speed and turbulence of the air.

On the lee side of the building, the flow can separate, thus forming a closed re-circulation zone – see Figure 6.1. This is the *Near Wake recirculation zone* (or *Cavity zone*). In this zone the wind speed is significantly reduced, but due to intensive turbulence the mixing is very rapid. If a plume becomes caught in the cavity, very high concentrations can result, with the highest values close to the leeward face of the building.

Further downwind, there is a zone with intensified turbulence (compared to the situation without building). The region where this effect is significant is usually called the *Far Wake zone* (or the *Turbulent Wake zone*)

On the upwind side of the building, an *Upwind Recirculation zone* (or upwind cavity) exists.

Over the roof the approaching flow separates, thus forming a *Roof cavity*. The flow may reattach to the roof, depending on geometry.

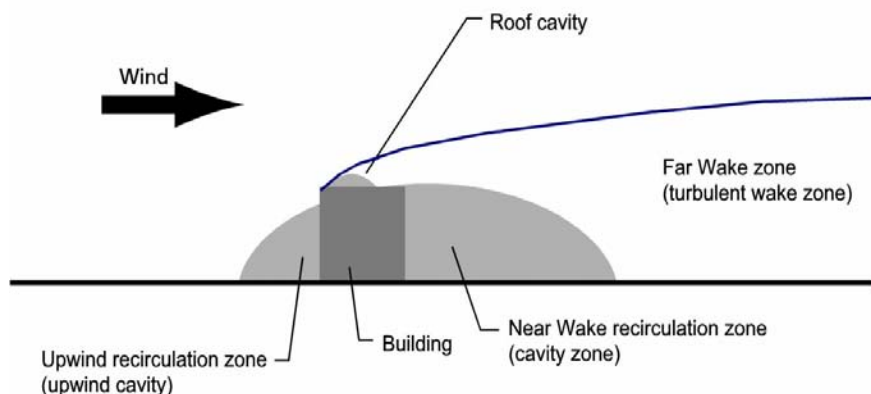


**Figure 6.1** Schematic illustration of the effect of a building on the airflow.

If a plume enters the Far Wake zone, its trajectory will more or less follow the streamlines of the airflow in the zone. Close to the building, in the air above the building (i.e. in the Far Wake zone) the streamlines will have an upward slope and thereby the plume in this area will be lifted up. At some distance from the building the streamlines will have a downward slope and this will bring the plume closer to the ground. Increased turbulence in the wake will result in an increased dispersion and dilution of the plume material, and the final effect on the ground level concentrations will depend on the combined effect of the increased dispersion and reduced plume height.

The impact of buildings on transport and dispersion thus depends on the building characteristics, on the location of the source with respect to the building, and last but not least, on the source characteristics itself.

Often a plume from an outlet is subject to plume rise. Plume rise can take place because the plume is warmer than the ambient air, and/or because the plume has a vertical exit velocity. Plume rise acts to increase the effective release height and can thereby contribute to a substantial reduction of the maximum ground level concentrations. Plume rise can also have significant influence on how a plume will interact with the nearby buildings. Sufficiently large plume rise can effectively bring the plume out of the building's influence zone, or it can reduce the portion of the plume that is captured in the zone. However, the interaction between plume rise and the building effects is twofold. The increased turbulence and thereby dispersion in the building's influence zone will generally result in a reduction of the plume rise. This will tend to give increased maximum ground-level concentrations, but the final result will depend on the combined effect of the reduction of the plume height and the increased dispersion of the plume material.

## **6.3 The models**

### **6.3.1 Standard OML**

As indicated in the preceding section it is a recognised problem that the current standard OML model treats building effects in a very simplified manner.

The effect of buildings on plume dispersion is very complex, and a precise description in the framework of a simple Gaussian model is almost impossible. The pragmatic solution is to extend the Gaussian plume approach with some empirical algorithms, which simulate the different aspects of plume interaction with buildings. Such an approach is used in the standard version of OML. This approach is extremely simplified and suffers from several major shortcomings. The current standard procedure is described in Section 3.12. A further discussion can be found in Olesen and Genikhovich (2000).

### **6.3.2 AERMOD Prime**

A new approach for modelling building effects was introduced in the model PRIME (Schulman et al., 2000). PRIME is a separate model, but it has been combined with the US EPA regulatory model AERMOD. PRIME is used for calculation of plume rise and dispersion in the case of plumes influenced by buildings. Thus, the combined model AERMOD/PRIME uses PRIME close to the source, while there is a transition to AERMOD at greater distances from the source.

The PRIME model has been considered a candidate to be combined with OML, and therefore the behaviour of AERMOD/PRIME has been investigated. In the following, it is simply referred to as AERMOD. For the present work version 04300 of the model has been applied.

### **6.3.3 MISKAM**

Another reference model used here is the comprehensive CFD model MISKAM (Eichhorn, 1996). MISKAM is a 3D Eulerian wind flow and dispersion model and the results on flow modifications by buildings can be used as guidance when parameterising simpler building algorithms in models like OML. For the present work version 5.01 (January 2005) of MISKAM has been applied.

### **6.3.4 Research Version of OML**

The Research Version of OML is not yet equipped with a building algorithm. It was the aim of the investigations reported here to create a basis, so such an algorithm could be developed.

One option which was considered promising at the outset of the current project was to adopt the PRIME algorithm and code, and implement it in OML. However, investigations revealed that this is by no means simple, because the structures of the models are very different.

Another option that has been considered is to revise the simple parameterisations in OML with a more refined approach using similar concepts as PRIME.

As a third option it is possible to revise OML's original formulation by a set of relatively simple modifications.

A substantial number of investigations have been conducted within the frame of the current project in order to map challenges and explore the potential of possible approaches. Especially the second option – that of adopting an approach based on PRIME – has received attention.

#### 6.4 Investigations based on Thompson's wind tunnel data

In order to improve the present parameterisation of building effects in OML a detailed investigation of experimental data, as well as of methods implemented in other similar models has been performed.

In Chapter 5, we have referred to the wind tunnel measurements by Thompson (1993). In section 5.4.4, results for the case *without buildings* were presented. However, the emphasis of Thompson's data is on cases *with building effects*.

The experimental database of Thompson consists of measurements of ground-level centreline concentration distributions for several different combinations of building shapes, stack heights, and stack location relative to the building. Measurements of concentration distributions along building facades are also available, but they are not used here.

Four building geometries were considered by Thompson, as shown in Figure 6.2.

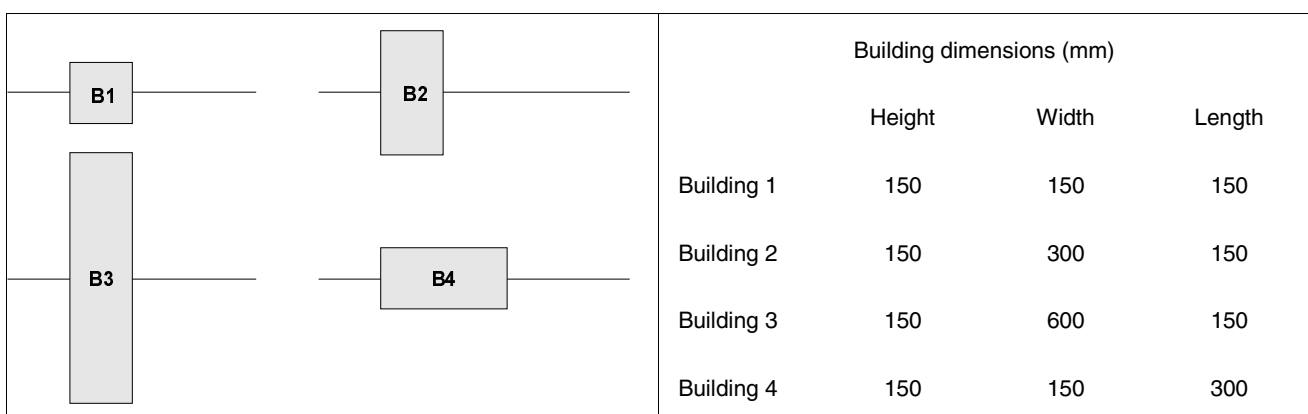


**Figure 6.2** Top view of the buildings in Thompson's experiment. The wind blows from the left along the indicated line. Measurements were performed along this line. All buildings have the same height (150 mm). B1 is a cube, while the remaining buildings have a footprint which is twice or four times the size of B1 (Thompson, 1993).

As mentioned in Section 5.4.4, the wind tunnel data measurements refer to several different release heights. In the present Chapter, results for only two release heights are presented:  $H_s=150$  mm and  $H_s=225$  mm. This corresponds to the stack/building height ratios of 1 and 1.5, respectively. For easy reference, results from the case *without building*, but for the same two stack heights, are shown in Figure 6.3. This figure shows measured concentration values and results for four models: Standard

OML (OML\_old), Research Version of OML (OML\_new), AERMOD with PRIME (AERMOD), and MISKAM. Model results for both flavours of OML have already been presented and discussed in Section 5.4.4. The two panels in Figure 6.3 show results for stack heights of 150 mm, respectively 225 mm. The concentration values are normalised. The meteorological conditions used for modelling with OML and AERMOD represent slightly unstable conditions (see the discussion in Section 5.4.4). MISKAM does not contain an option for unstable conditions, so only neutral stratification was simulated. The results are sensitive to the choice of meteorology, so conclusions from the figure should be drawn with caution. For details on the data used, please refer to the supplementary report "OML: Model Validation" (Olesen et al., 2007).

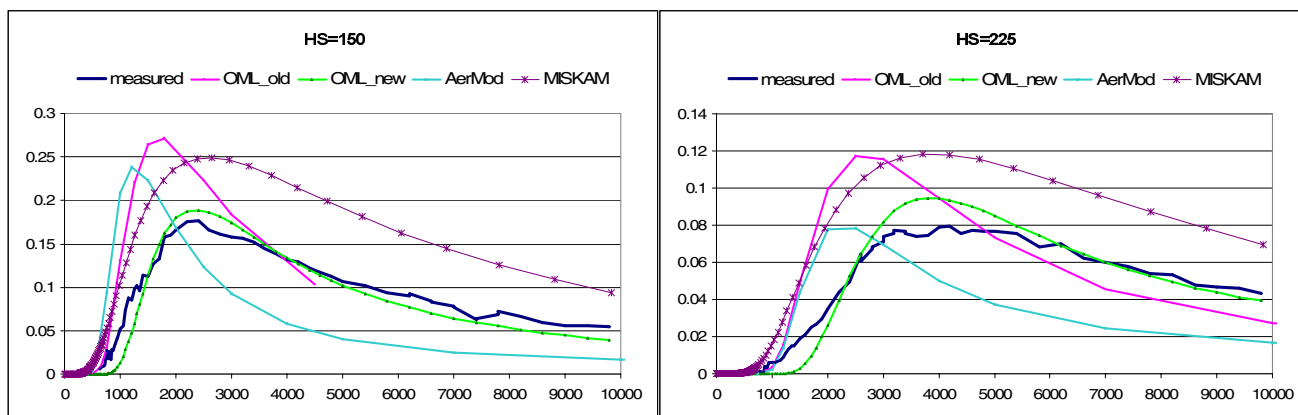


**Figure 6.3** Comparison of measured and modelled concentrations of wind-tunnel data in the case of simulations without buildings. Model results are shown for the present version of OML (OML\_old), the Research Version of OML (OML\_new), AERMOD and MISKAM. The left panel shows results for a stack height of 150 mm, while the right panel refers to a stack height of 225 mm.

In Figure 6.3 it is noteworthy that AERMOD results show a tendency to predict the location of maximum too close to the source, and to under-predict the concentrations at larger distances from the source. This behaviour is similar to that of the Standard version of OML. MISKAM is much more successful in predicting of the location of maximum ground-level concentrations, but the modelled concentrations are in general higher than the measured. The Research Version of OML fits observations very well.

#### 6.4.1 OML and AERMOD studies

Figure 6.5 and Figure 6.6 present results of simulations of Thompson's wind tunnel experiments *with buildings* using OML (standard version only) and AERMOD. The figures require some explanation.

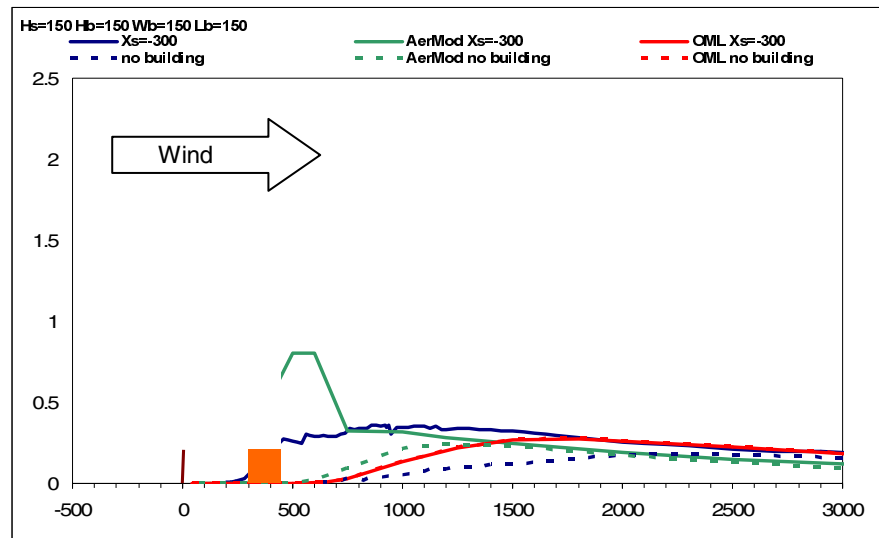


**Figure 6.4** Example of one of the panels in Figure 6.5. Measured and modelled concentrations for one of Thompson's experiments. See text.

One of the panels in Figure 6.5 is shown in large size as Figure 6.4.

The panel shows both the geometry of the simulation and the results in terms of concentrations. Like all panels of Figure 6.5, the graph shows results from AERMOD and the standard OML model, with and without building. Furthermore, measurements are displayed as the black, irregular curve. In the example shown, for OML the two (red) curves with and without building are identical.

The wind blows from the left to the right. The stack and the building are drawn on the figure. The stack is located at  $x = 0$ , and the  $x$  axis indicates distance from the stack.

The scale on the  $y$  axis shows normalised concentrations.

The physical dimensions in the wind tunnel and on the graph are in mm. The building height is 150 mm, and the boundary layer in the wind tunnel has a height of 700 mm. One may interpret the result as having a different scale. For instance, with a scaling factor of 1000 the building height would be 150 m and the distance from the stack shown on the  $x$ -axis would be in meters. When results are scaled, all length scales are adjusted, whereas the wind speed remains the same.

Superposed on the figure, there is a drawing of stack and building. The scale corresponds to the scale of the  $x$  axis, so a 150 mm cube building appears as a square with side lengths of 150.

The first line of the legend on top indicates stack height ( $H_s$ ) and building dimensions (height  $H_b$ , width  $W_b$ , length  $L_b$ ).

In the second line the statement  $X_s = -300$  refers to the position of the building relative to the stack.  $X_s$  is measured from the building's upwind face to the stack, and counted positive along the  $x$  axis.

A large number of graphs, similar to Figure 6.4, are presented in Figure 6.5 and Figure 6.6. Measurements and model results are shown for all four building geometries (as defined in Figure 6.2), but only for a few se-

lected combinations of the stack location with respect to the studied buildings. Results for  $H_s/H_b=1$  are presented in Figure 6.5 while results for  $H_s/H_b=1.5$  are presented in Figure 6.6.

Figure 6.5 extends over four pages. For all panels in the figure, the relative stack height  $H_s/H_b = 1$ , implying that the release takes place at roof level. Panels corresponding to the same location of the stack are shown in the same row of the figures. The different rows represent different stack locations.

For the first page of the figure, the panels are arranged in a tabular format, where the two columns represent buildings 1 and 2, while the rows represent various positions of stack relative to the building

The next page show corresponding results for buildings 3 and 4. The third and fourth pages of the figure have a similar layout, but refer to three additional stack positions.

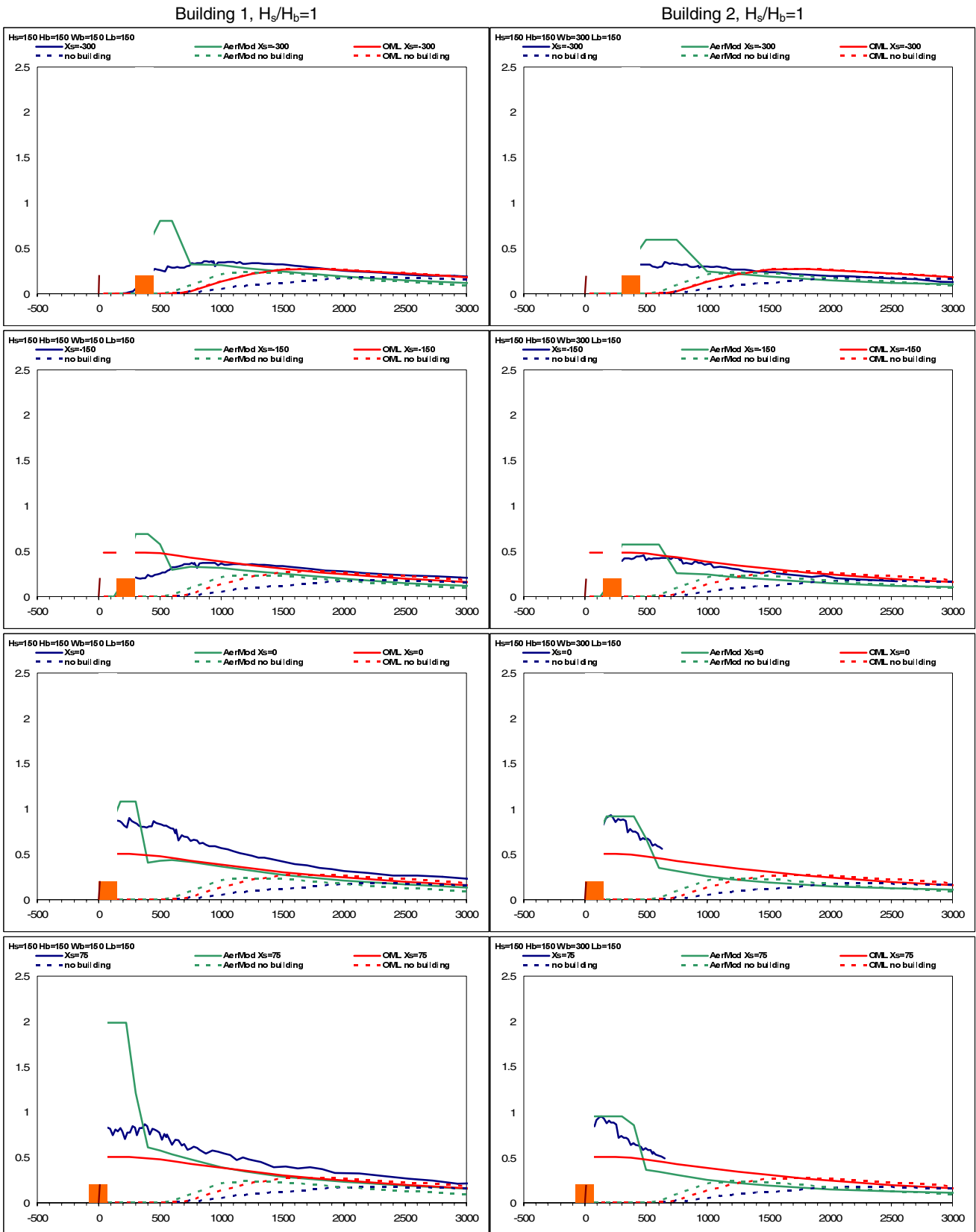


**Figure 6.5** rows 1-4. The panels on this page refer to Building 1 (cubic) and 2 (wide), and to four building positions: downwind of the stack and centred on stack.

Measured and modelled centreline concentrations for Thompson's wind tunnel experiments with  $H_s/H_b=1$ . Model results are shown for the (old) standard version of OML and AERMOD/PRIME. For comparison, the measured and modelled concentrations for the case without building, but for the same stack height and position, are also shown.

The  $X_s$  value in the legend refers to the position of the building relative to the stack.  $X_s$  is measured from the building's upwind face to the stack.

Building 3,  $H_g/H_b=1$

Building 4,  $H_g/H_b=1$

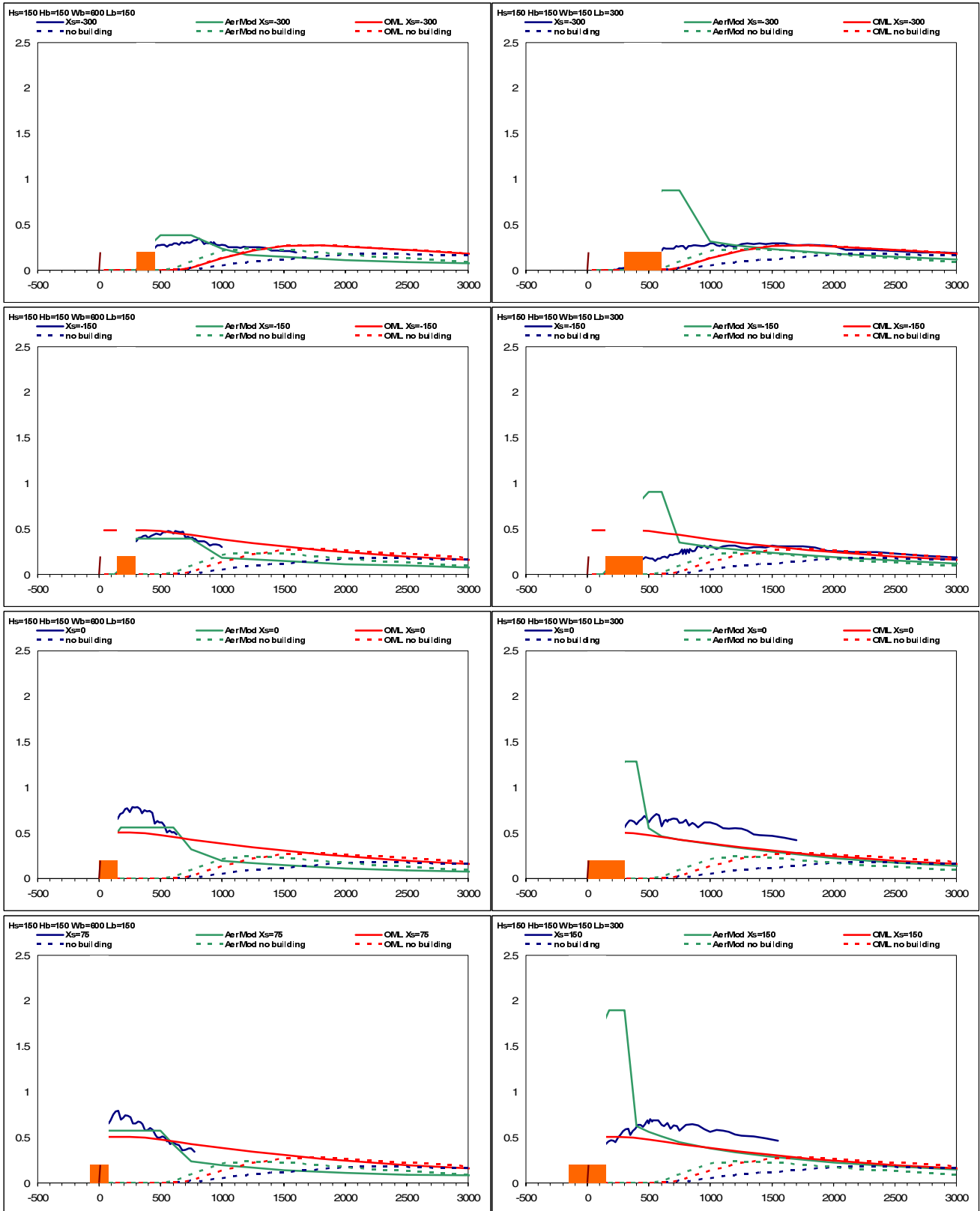
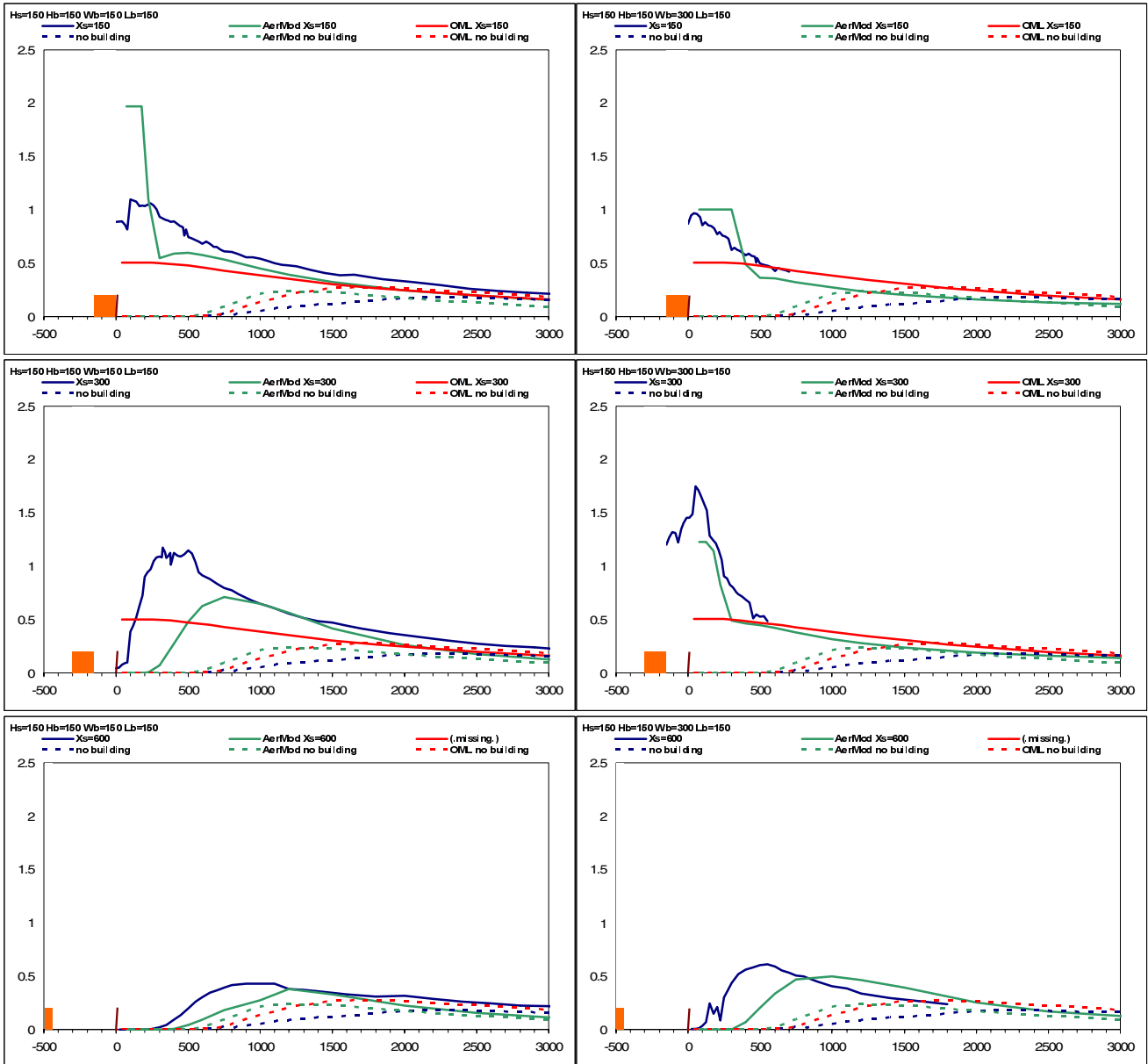


Figure 6.5, rows 1-4 (continued). The panels on this page refer to Building 3 (very wide) and 4 (long), and to four building positions: downwind of the stack and centred on stack.

Building 1,  $H_g/H_b=1$

Building 2,  $H_g/H_b=1$



**Figure 6.5** (continued) Rows 5-7. The panels on this page refer to Building 1 and 2, and to three building positions: building up-wind of the stack. The cases in Row 5 of the figure are discussed in Section 6.5.

Building 3,  $H_g/H_b=1$

Building 4,  $H_g/H_b=1$

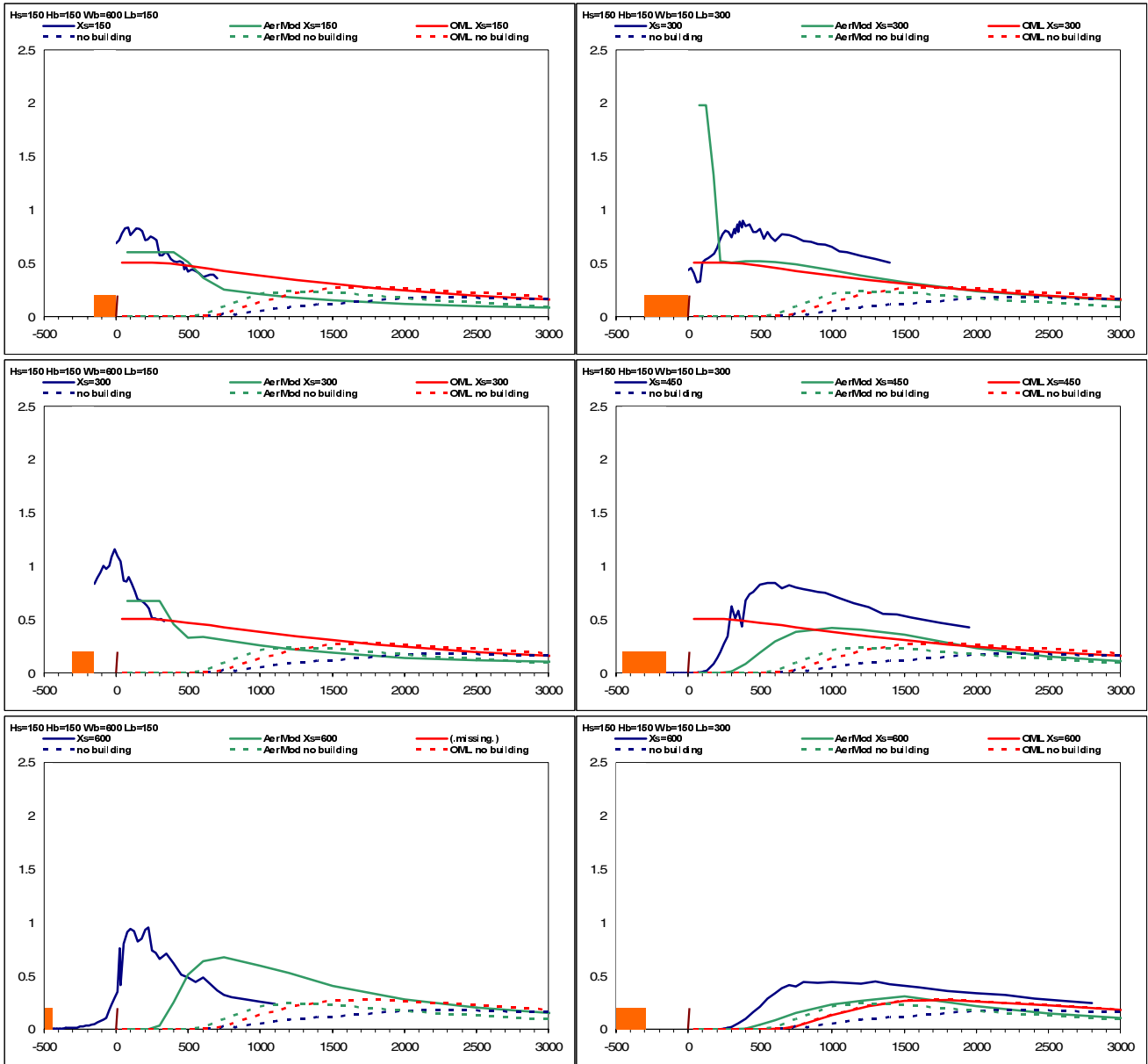
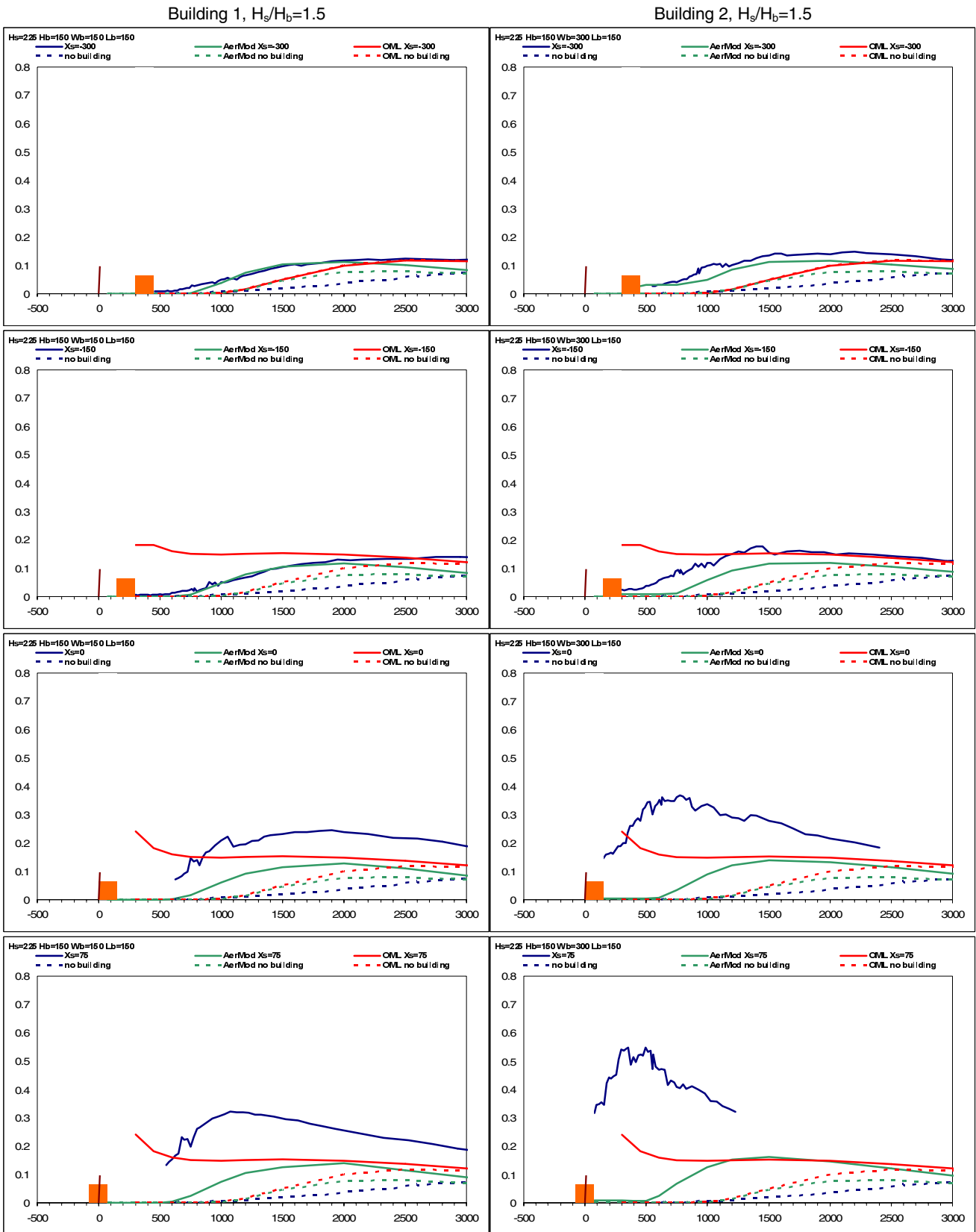


Figure 6.5 (continued), rows 5-7. The panels on this page refer to Building 3 and 4, and to three building positions: building up-wind of the stack. The cases in Row 5 of the figure are discussed in Section 6.5.



**Figure 6.6**, rows 1-4. The panels on this page refer to Building 1 (cubic) and 2 (wide), and to four building positions: downwind of the stack and centred on stack.

Measured and modelled centreline concentrations for Thompson’s wind tunnel experiments with  $H_s/H_b=1.5$ . Model results are shown for the (old) standard version of OML and AERMOD/PRIME. For comparison, the measured and modelled concentrations for the case without building, but the same stack height, are also shown.

The  $X_s$  value in the legend refers to the position of the building relative to the stack.  $X_s$  is measured from the building’s upwind face to the stack.

Building 3,  $H_s/H_b=1.5$

Building 4,  $H_s/H_b=1.5$

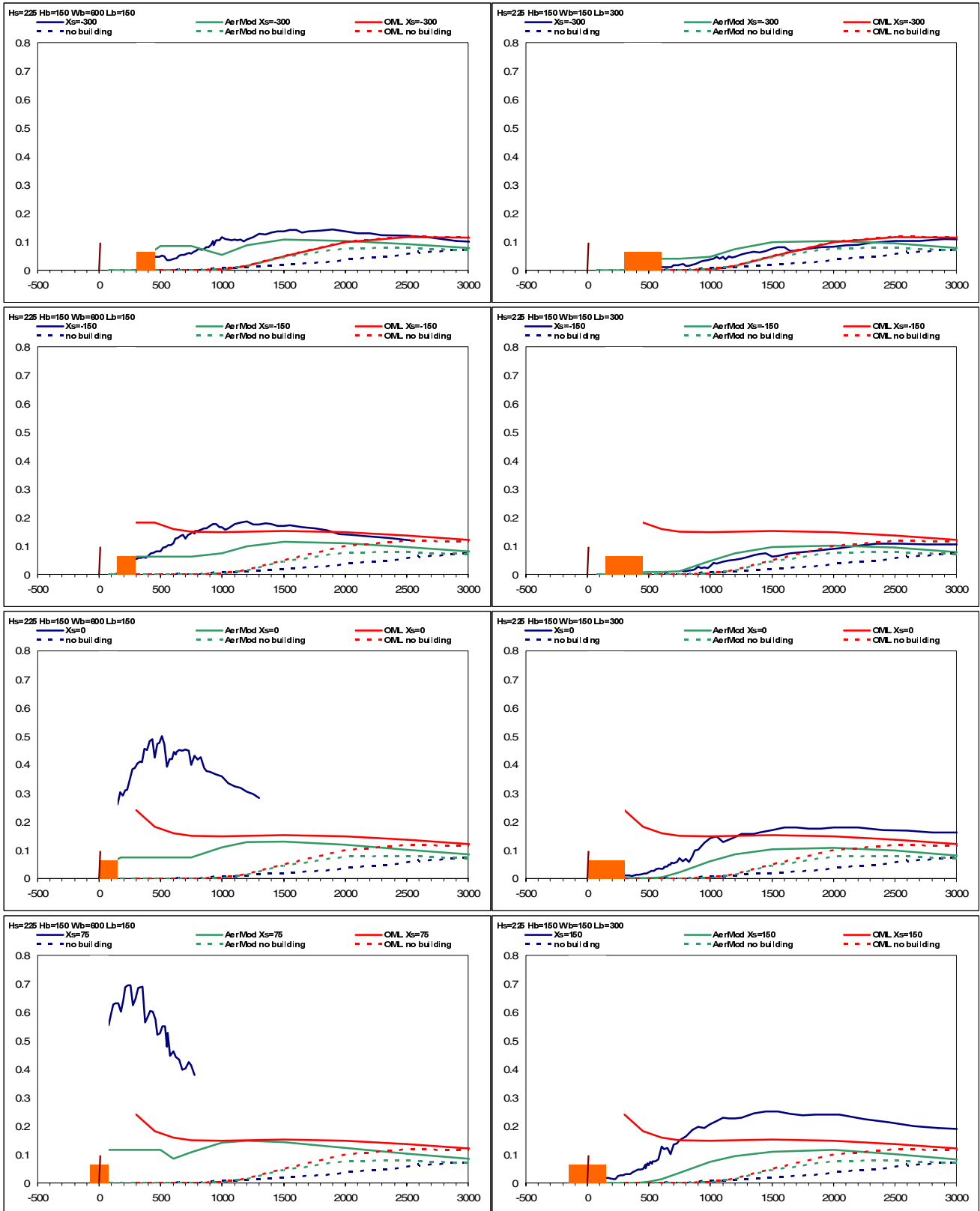


Figure 6.6, rows 1-4 (continued). The panels on this page refer to Building 3 (very wide) and 4 (long), and to four building positions: downwind of the stack and centred on stack.

Building 1,  $H_s/H_b=1.5$

Building 2,  $H_s/H_b=1.5$

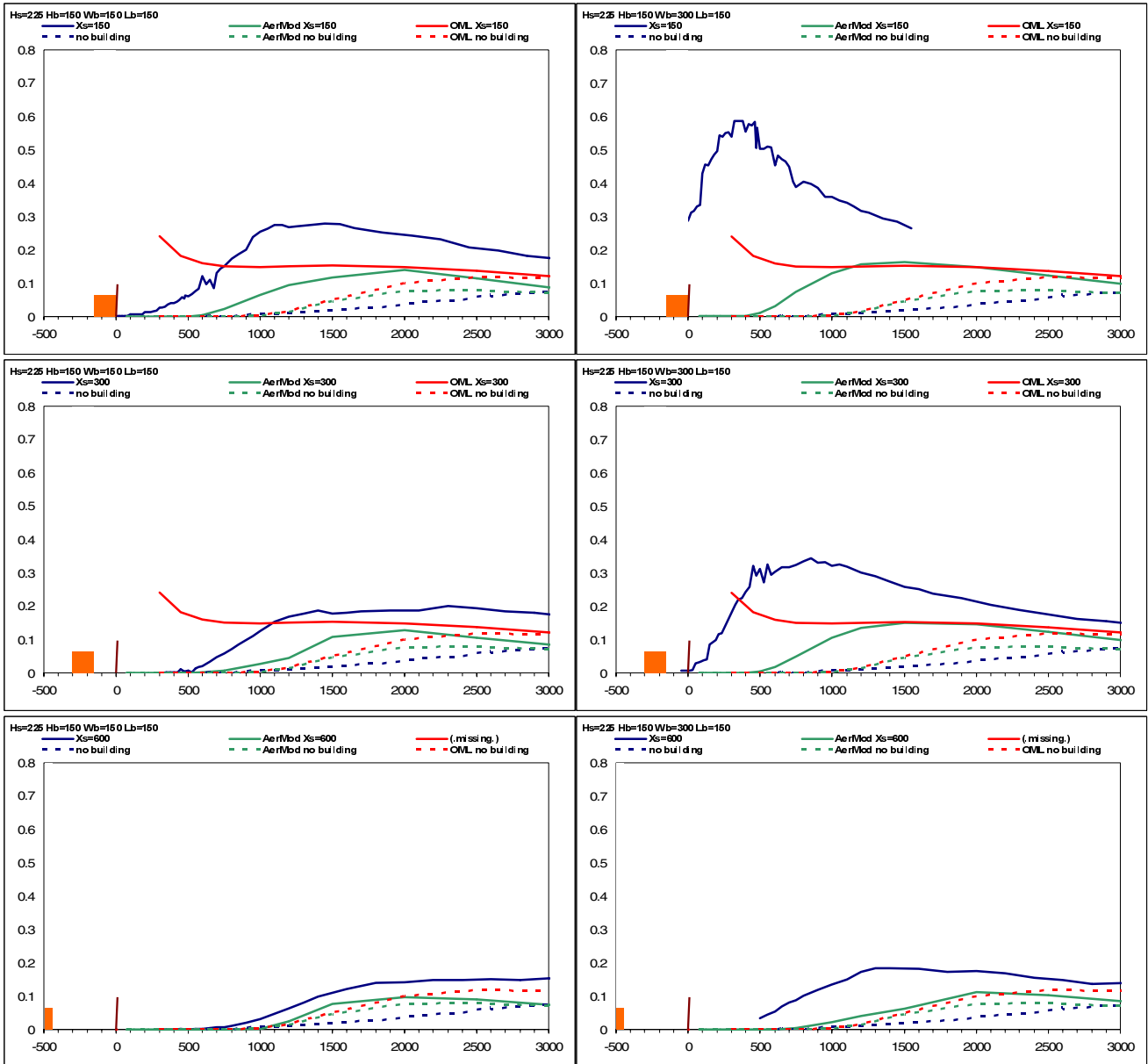


Figure 6.6 (continued). Rows 5-7. The panels on this page refer to Building 1 and 2, and to three building positions: building upwind of the stack. The cases in Row 5 of the figure are discussed in Section 6.5.

Building 3,  $H_s/H_b=1.5$

Building 4,  $H_s/H_b=1.5$

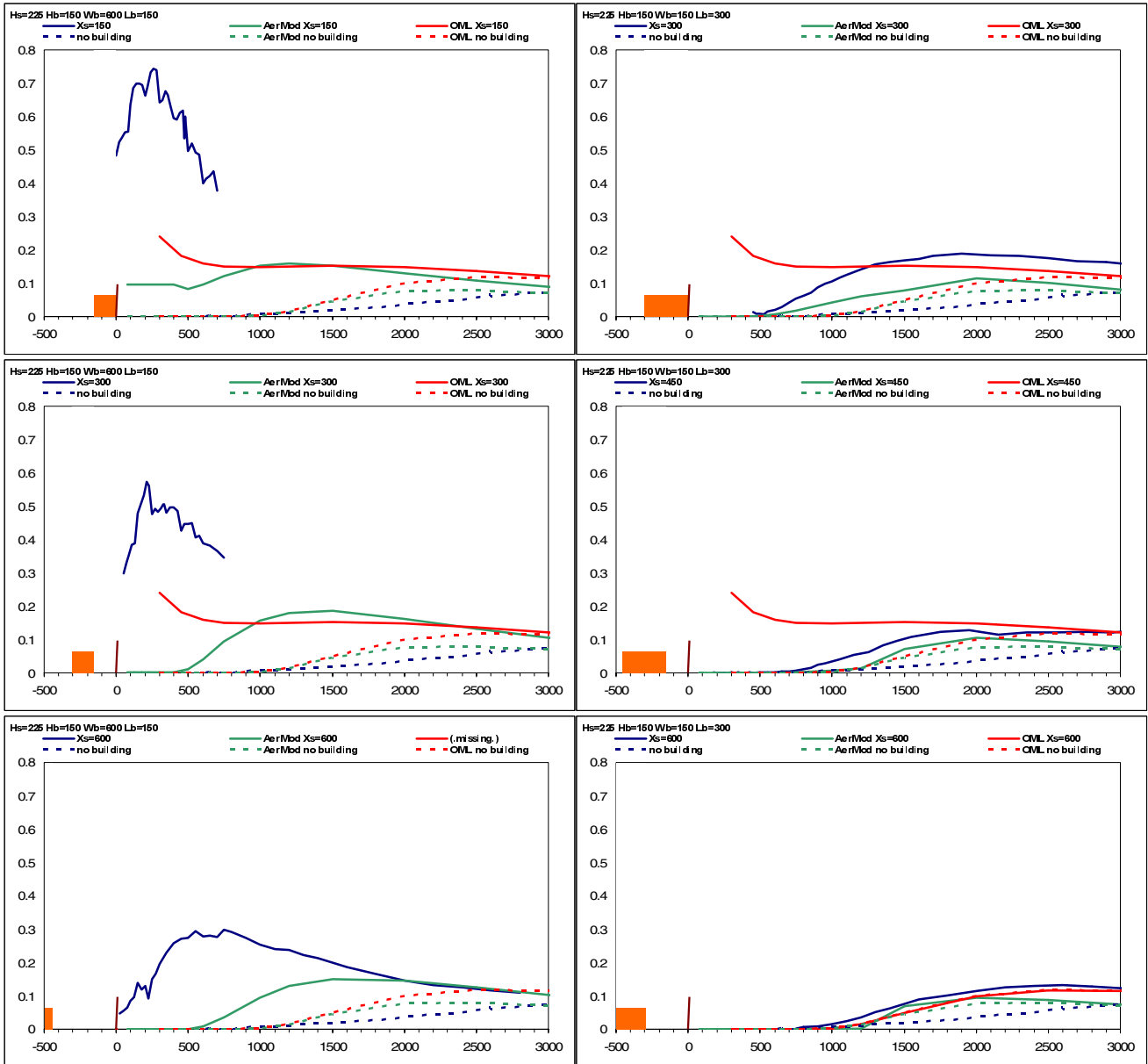
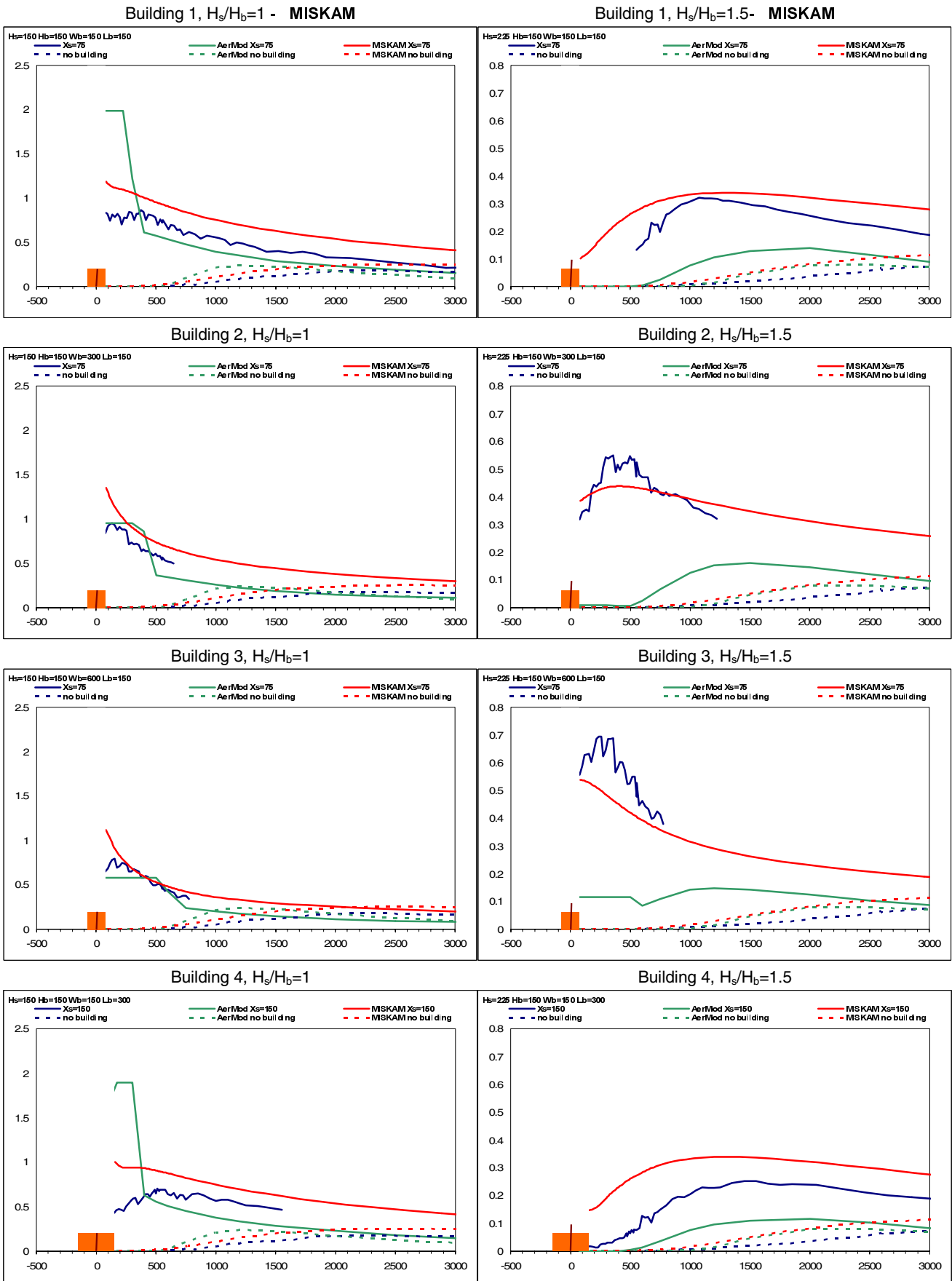
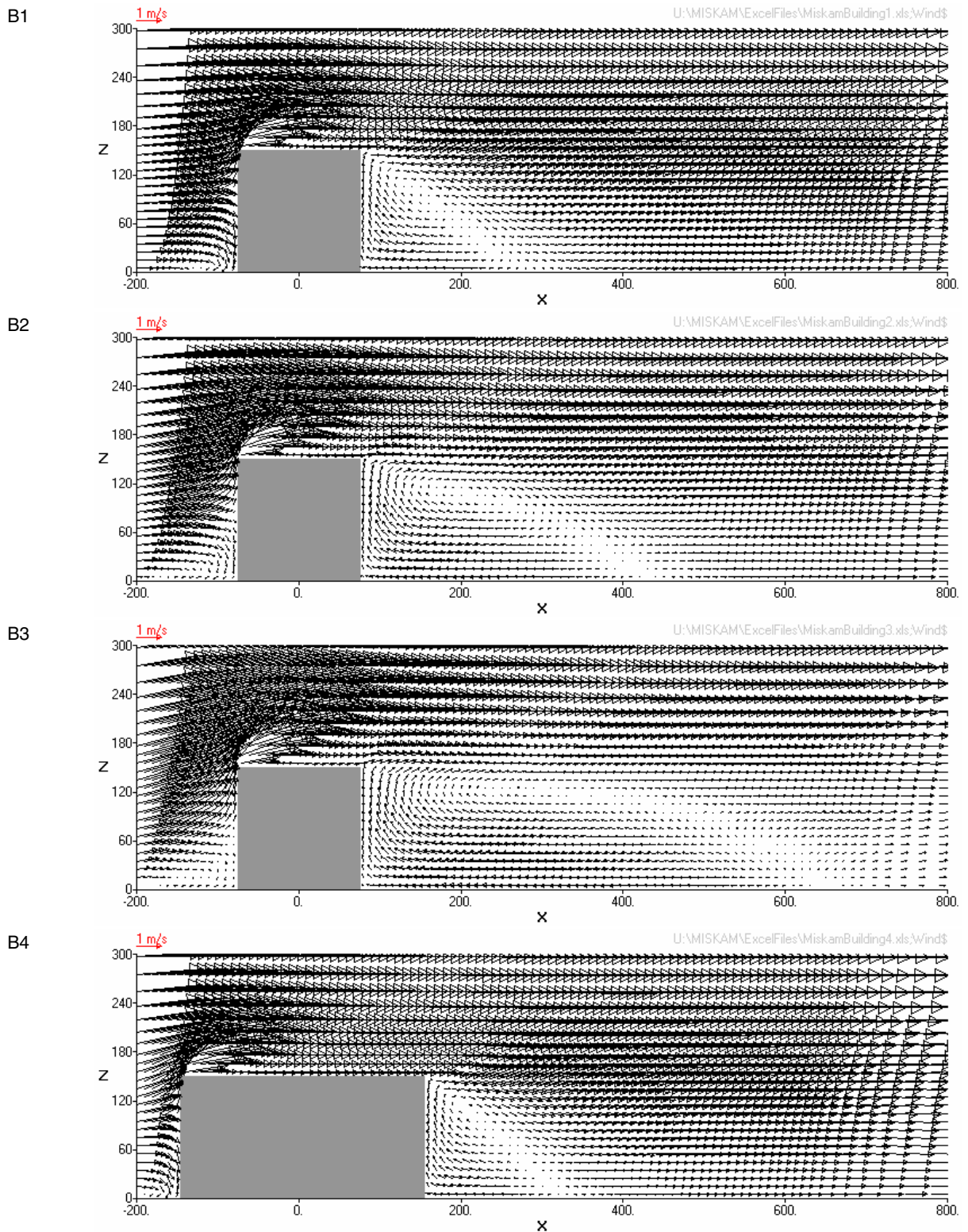


Figure 6.6 (continued). Rows 5-7. The panels on this page refer to Building 3 and 4, and to three building positions: building upwind of the stack. The cases in Row 5 of the figure are discussed in Section 6.5.



**Figure 6.7** Comparison of model results from MISKAM with wind-tunnel measurements. For comparison, the model predictions by AERMOD are also shown. Note that the panels are arranged in a different manner compared to the previous figures. Here, results for the four buildings (rows) and two source heights (columns) are shown. Only one  $X_s$  value (source position) is considered: the stack is placed in the centre of the building.



**Figure 6.8** Wind flow around the four buildings as calculated by MISKAM in the x-z plane in the centre of the building.

Commonly, when results are presented in literature, they are aggregated and shown in summarised form. Here, we have chosen to present a large number of graphs showing detailed observations and model results, because aggregation conceals information. Facts and problems can easily be overlooked.

The results shown are discussed in Section 6.5.

#### 6.4.2 Miskam simulations

In addition to computations with OML and AERMOD, the CFD model MISKAM has also been used to simulate Thompson's data. Results of model simulation with MISKAM are shown in Figure 6.7. Results are shown for all the four building configurations, but only for one stack location - a stack centred on the buildings. For comparison, the corresponding results from AERMOD are also included in the figure. MISKAM results are considerably better than AERMOD's.

Underlying the dispersion results from MISKAM is a detailed flow simulation. It is of interest to study the wind field and turbulence structure predicted by MISKAM, because it drives dispersion.

The wind field as modelled by MISKAM is shown in Figure 6.8. For all four building configurations (B1 to B4) wind vectors are shown for a vertical cross-section in the centre plane of the building.

Above the building, the flow field is essentially horizontal, although there is a small lift at the front (windward) edge. However, a recirculation zone (cavity) is evident on the leeward side of the building. The extent of this recirculation zone clearly depends on *the width* of the building. The larger the width (from B1 to B3), the longer is the recirculation zone. The wind field predicted for building B1 (cube) is very similar to the one predicted for building B4 (long building). Thus, *the length* of the building does not have any large influence on the flow structure.

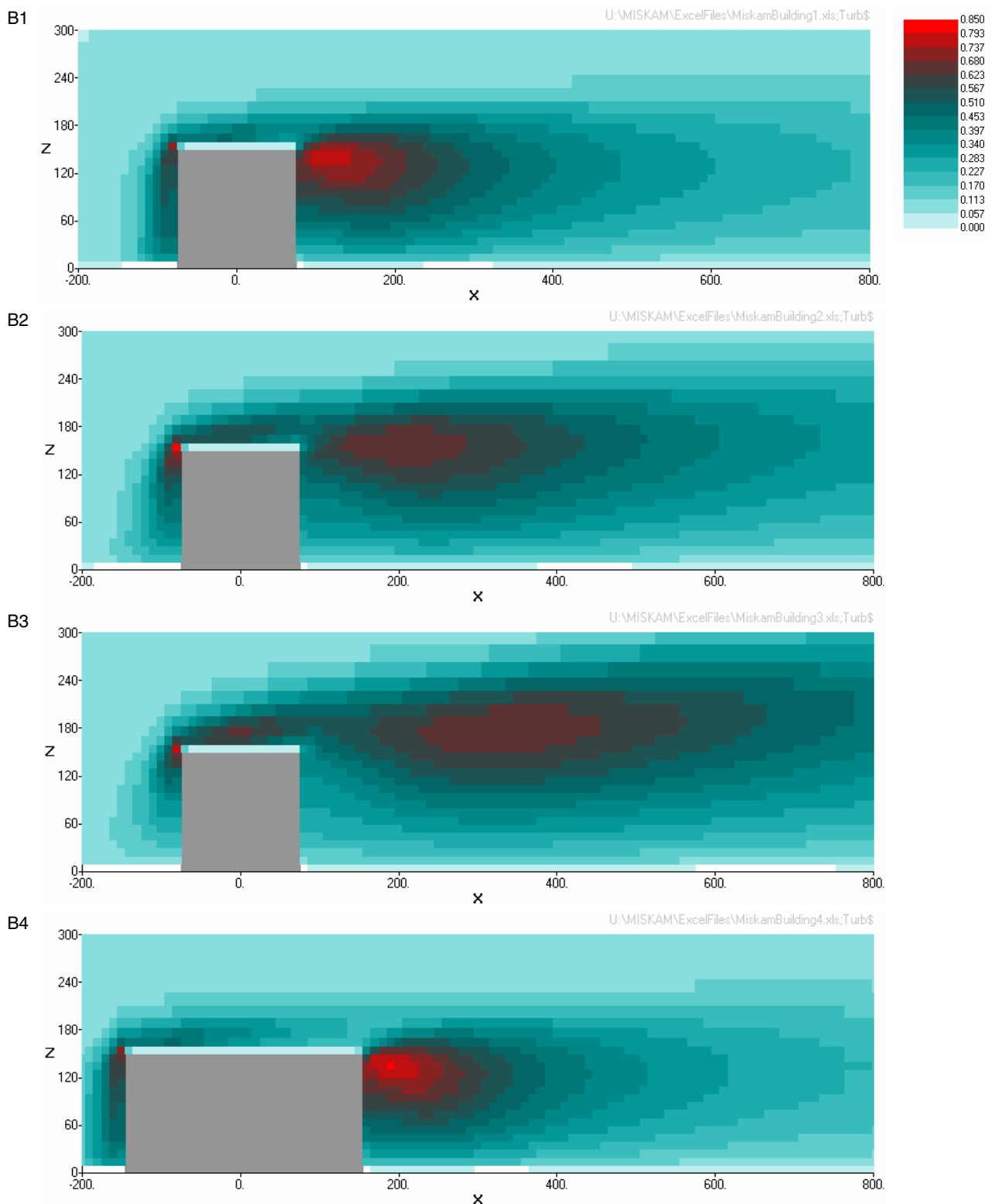


**Figure 6.9** Turbulent kinetic energy (TKE,  $m^2/s^2$ ), according to MISKAM for the four buildings in an x-z cross-section in the centre of the building.

Turbulence data as modelled by MISKAM are shown in Figure 6.9. The figure shows the Turbulent Kinetic Energy (TKE), which is the sum of variances of velocity fluctuations. In MISKAM, the turbulence is assumed to be isotropic, i.e. the velocity fluctuations in both x, y and z directions are considered to be the same. For all four building geometries MISKAM predicts enhancement of TKE in the region close to the top of the building, but with maximum at some distance from the leeward face of the building. This distance increases with increasing width of the

building. The length of a building does not seem to have any large influence on the field of TKE. This appears from the figure by comparing simulations for building B1 (cubic) and B4 (long). The turbulence data are crucial for dispersion modelling and it is therefore highly relevant to study the turbulence predictions by CFD models.

Thompson's data set does not allow a direct verification of MISKAM's turbulence predictions with measurements, so such verification must make use of other data sets. Although MISKAM is quite successful in predicting concentrations (Figure 6.7), some features of the behaviour of the turbulence field – notably the location of the maxima for TKE – as modelled by MISKAM can be questioned. This statement is based on a comparison with other measured data sets with measured turbulence fields. The question is a field of interest for further studies.

## 6.5 Discussion of building effects

As a very first conclusion to be drawn from the results presented in the previous section, it is clear that the presence of buildings has a dramatic influence on dispersion conditions. Comparing the wind tunnel results from experiments with and without buildings, one can see that in the case of building influenced dispersion the maximum ground level concentration is several times higher than in the case without buildings. Further, the location of maximum is much closer to the source. The building effect is still clearly visible at distances from the building larger than even 10 times building height.

Regarding the significance of the distance between stack and building, the building effect is largest for a stack located close to the building. When the distance between stack and building increases, the effect declines. For the results shown in the figures, the largest separation occurs for a stack located 4 building heights downwind of the building (row 7). With this separation, there is still a very clear effect of the building, in particular for the wide buildings. Thompson's data comprises results for larger separation distances. When the stack is 10 building heights downwind, and the stack top is at roof height, the effect of the building is still not negligible. In terms of the so-called Building Amplification Factor (BAF) - the ratio between maximum ground-level concentration *with* and *without* building - the BAF is around 1.5 for all four buildings.

The main drawback of the building algorithm implemented in the current standard version of OML is that the building effect is sharply cut off when the distance between the stack and the nearest building face becomes larger than or equal to 2 times the building height. Such a discontinuity is in contradiction with the observations from the wind tunnel experiments.

The more elaborate building algorithm used in AERMOD/PRIME does not show such a discontinuity, but the predicted ground level concentrations are still not well reproduced. The agreement between the modelled and measured concentrations be considered reasonable only at large distances from the building, and in this case the results are not much different from the current OML results (provided the building effect in OML is active). For AERMOD results, significant deviation compared to the

measured concentrations is observed for distances close to the building – more specifically, when the model predicts that the plume is within the building's near wake zone (recirculation zone). Thus, for buildings 1 and 4 in case of a low stack ( $H_s/H_b=1$ ), AERMOD produces considerable overpredictions close to the building.

The *sensitivity of results to a change of parameters* – stack height, building geometry and stack location – can be studied by comparing the various figures.

For  $H_s/H_b=1$  (Figure 6.5) concentrations modelled by AERMOD are much more sensitive to the *building geometry* than experimental data. Especially in the case of a stack centred on or adjacent to the building, the modelled concentrations decrease substantially with increasing width of the building. This is not the case for measured concentrations. See "Row 5" of the figure to get an impression of the discrepancy between modelled and observed behaviour.

The concentrations modelled by AERMOD are also more sensitive to the *location of the stack* with respect to the building than the measured concentrations. This can be seen by inspecting the differences from row to row in Figure 6.5.

For  $H_s/H_b=1.5$  (Figure 6.6), AERMOD has a tendency to underpredict the concentrations, and this underprediction is most pronounced when the stack is located close to or right on the building.

It is interesting to note that for this elevated stack, measurements show large sensitivity to building width, while AERMOD shows only little (Figure 6.6, row 5). This is the opposite behaviour compared to the situation with the low stack.

In other words, for a stack at roof height, building width is not crucial, whereas *for an elevated stack*, building width *does* matter. This behaviour is not replicated by AERMOD.

Results of simulations with the CFD model MISKAM (Figure 6.7) are in much better agreement with the wind tunnel measurements than results obtained with AERMOD. However, this should not be surprising, because AERMOD is an operational model using the PRIME module algorithm for simulation of building effects, while MISKAM is a numerical model based on solution of a set of equations describing the physical properties of the wind flow. The effect of buildings on the wind flow is directly described by these equations. The computational time required by MISKAM is several orders of magnitude larger than the time required by models like AERMOD or OML.

The dependence on building geometry is very well replicated by MISKAM. In the case of a source located at roof height at the building centre ( $H_s/H_b=1$ ), the modelled concentrations are not very sensitive to the width of the building, in accordance with measurements. For the source with  $H_s/H_b=1.5$ , the MISKAM model predicts concentrations which close to the building increase substantially with increasing width of the buildings. This is in good agreement with the experimental data.

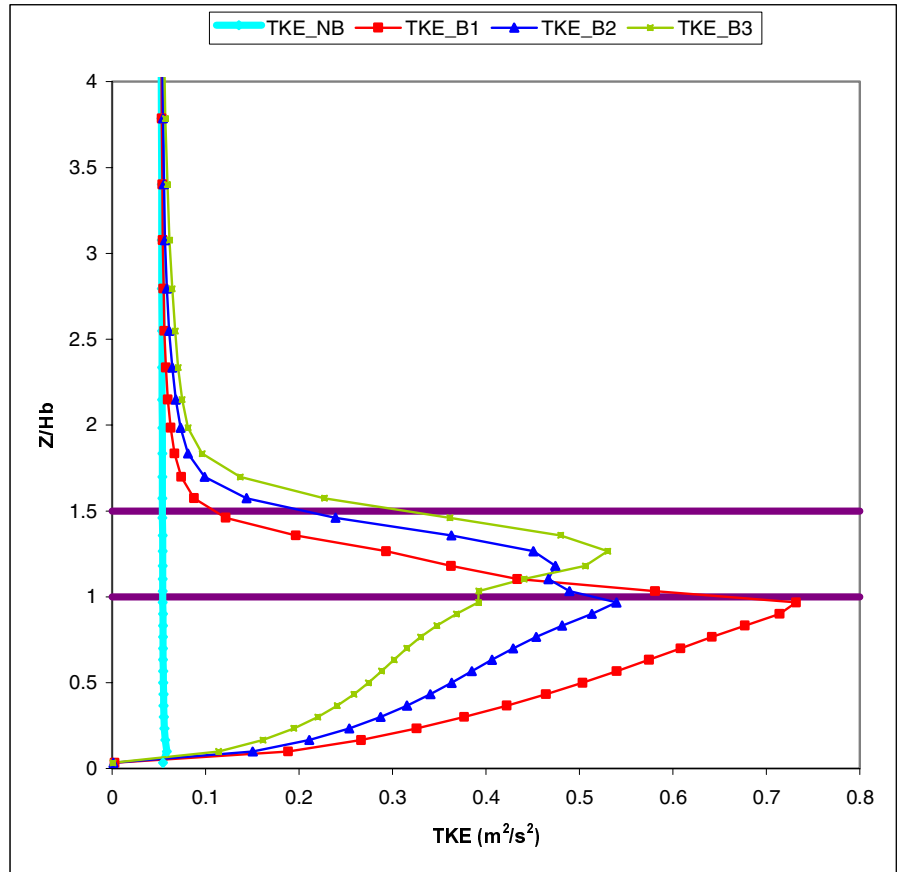


**Figure 6.10** The vertical profiles of the Turbulent Kinetic Energy (TKE) as modelled by MISKAM for the three buildings (B1 to B3) used in the wind tunnel experiments. The vertical cross-section is taken at the second model grid-point downwind of the building facade. The line labelled TKE\_NB represents the TKE level without building (ambient turbulence). The vertical axis is in units relative to the building height. The two horizontal lines indicate the source locations ( $H_s/H_b = 1$  and  $1.5$ , respectively).

The fact that MISKAM is able to reproduce, at least qualitatively, the dependence of the ground level concentrations on building geometry, makes it feasible to use this model in order to identify the main factors governing building effects on plume dispersion.

As it is seen from Figure 6.8, the wind flow above the building is not significantly influenced by the width of the building. The most apparent effect takes place below roof height, where the extent of the recirculation zone increases with increasing width of the building.

In the case of a source located right on top of a building at roof height ( $H_s/H_b=1$ ), the plume will be captured in the building wake and dispersed to the ground regardless of the building dimensions. This can explain the relatively weak dependence of ground level concentrations on building dimensions.

In the case of a source with  $H_s/H_b=1.5$  the wind flow cannot explain the observed differences in ground level concentrations for building with different width (e.g. Figure 6.7, right column). Here, the behaviour can more likely be attributed to the structure of the turbulence field (Figure 6.9). A more detailed picture of the turbulence field in a vertical cross-section, as modelled by MISKAM is shown in Figure 6.10. The figure shows the vertical profiles of the Turbulent Kinetic Energy (TKE) for the

three buildings (B1 to B3) used in the wind tunnel experiments. The vertical cross-section is taken at the second model grid-point downwind of the building facade. The line labelled TKE\_NB represents the TKE level without building (ambient turbulence). When considering a source with  $H_s/H_b=1.5$  it is seen that at this height the turbulence increases remarkably with increasing building width (from B1 to B3). The downward mixing of the plume will thus be more intense for a wider than for a narrow building. At a height of about 3-4 times building height, the turbulence decreases to approximately the ambient level, and the influence of building on plume dispersion can be expected to be marginal at this height. This indicates that a proper modelling of building influence on the turbulence field is crucial for modelling of plume dispersion.

The absolute values of TKE and some of the features predicted with MISKAM must, however, be taken with some care. Certain simplifications are made with regard to turbulence modelling (closure assumptions etc.). Such simplifications are common to many other similar CFD models.

## 6.6 Implications for OML development

When relating the discussion above to OML, we can note that the fact that AERMOD is sensitive to building shape while OML is not, does not in general make the performance of AERMOD better compared to that of OML. This is because AERMOD is not sensitive to building shape in the same way as observed data.

We can identify three major shortcomings of the standard OML building effect (see Olesen et al., 2005). Resolving the shortcomings by directly adopting an AERMOD approach would not in general lead to improved results, as model performance would in some instances be better, in others worse.

The shortcomings of the current standard OML model can be summarised as follows:

- The current algorithm results in an abrupt and discontinuous modification of plume dispersion. The building effect is totally neglected if the distance between the stack and the closest point of the building is larger than  $2 \times$  building height. An additional problem is that in the case when the stack is located upwind of the building, the increased dispersion is assumed to take place *immediately* when the plume leaves the stack, before it meets the building.
- In the model, the building effect is practically independent on the shape of the building. Essentially, building height is the only parameter used in the algorithm. It appears from the results above that building width and length *can* have a substantial influence (as exemplified in the case with an elevated stack,  $H_s/H_b=1.5$ , Figure 6.6, row 5). However, it does not necessarily have any large influence (as exemplified by the low stack, Figure 6.5). The current neglect of building geometry in OML leads to results which are often better

(i.e., less incorrect) than AERMOD's. The largest discrepancy between OML model results and measurements occur close to the building, while results are fair farther downwind.

- The plume height is treated in a simplistic manner in OML. The plume centreline remains unaffected at a constant height. For non-buoyant plumes, the only effect taken into account is the increased dispersion, which is simulated by an increase of the Gaussian plume dispersion parameters  $\sigma_z$  and  $\sigma_y$ . In reality, the plume material can be drawn down into the recirculation zone, which it leaves at a lower height than the original plume. For buoyant plumes, the OML model does account for a reduction in plume *rise* due to building effect, but there is no mechanism to bring plume height below stack height (here, we disregard the slight effect of *stack downwash*).
- The fact that OML simulates building effects mainly by increasing dispersion, often has the effect that the maximum ground-level concentrations occur in the "building influence zone" situated next to the building, and decline further away. An example can be seen in Figure 6.6, row 5 (elevated stack,  $H_s/H_b=1.5$ ). The OML graph is exactly the same for all four buildings, displaying a monotone decline of concentrations with distance. Measurements lead to four very different concentration graphs that depend very much on building width. The observed maximum does not occur next to the building, but downwind of it. Thus, the OML behaviour is not realistic. Nevertheless, for all four cases OML gives a better estimate for the maximum concentrations than AERMOD does.

Based on the discussion of results in the previous section, it can be concluded that directly adopting an AERMOD approach will in essence not result in a much more precise model for building effects. This is a very general statement, which deserves to be elaborated somewhat.

It is possible to develop quantitative model performance measures, as opposed to the qualitative approach that was used in the discussion in the previous sections. A model should be fit for purpose, so in order to develop such measures one would have to define the model objectives of interest: Which building geometries are important, which stack heights, which distance between stack and building, and at what distance from the stack are the concentrations to be evaluated?

But irrespective of all possible refinements in defining model objectives, performance measures will in part be based on the results shown. A quantitative approach may identify problems more precisely, but the fact remains that a user of either AERMOD or OML must accept rather large deviations between model predictions and observations for many situations. Predictions in the far field, away from the stack, are reasonable, but in the near field there can easily be overpredictions or underpredictions by a factor of 2 for both models. Such are the current limitations of the models.

The question remains as to whether other modelling approaches than that of AERMOD will be substantially more successful. Performance can

possibly be improved somewhat compared to AERMOD, but in view of the complexities involved, it seems inevitable that simple models must in many cases fail when challenged with the challenges of the real world.

If a modeller's purpose is an accurate prediction of concentrations close to a building, MISKAM is clearly superior to both OML and AERMOD. However, MISKAM is much more demanding in terms of required manpower, user skill and computer resources. Furthermore, even MISKAM has weaknesses.

It remains to be stated that one of the OML shortcomings - the one of neglecting building effect when the distance between stack and building becomes larger than 2 building heights - can probably be resolved by rather simple changes in the OML algorithm. This is a matter that should be addressed, while the remaining shortcomings are much more difficult to resolve. Obviously, performance problems cannot be successfully overcome by directly adopting the AERMOD/PRIME approach.

## 7 Conclusions

The present report serves as documentation for the concepts and parameterisations underlying the OML model - both the current standard version that was essentially developed during the 1980 and the new, modified Research Version, developed during a review of OML in 2005-06.

The Research Version was developed in order to resolve a number of problems that have been identified within the standard model in the course of time - and especially during the review process. These problems are summarised in Chapter 4.

Model performance has been evaluated on a number of research-grade data sets. It should be emphasized that model evaluation is by no means simple. There are numerous problems involved in evaluation, as it is explained in the supplementary report "OML: Model Validation" (Olesen et al., 2007). Briefly stated, some main difficulties are:

- Experimental data sets for validation are limited in many respects - they represent only few of the possible scenarios.
- Processing of experimental data sets is far from trivial. This statement refers to a wide range of problems, as indicated in the supplementary report.
- There are inherent uncertainties in the data due to the stochastic nature of the atmosphere. Even for a perfect model results will deviate from observations.

All of this means that it is often difficult to draw firm conclusions on model performance.

However, it appears from the studies that the Research Version of OML yields a better overall performance than the standard OML model. For certain situations, the performance improvements are substantial, while for others the difference is only marginal.

The Research Version is a candidate to replace the currently operational OML model. However, there may be inadequacies in some of the new parameterisations. Therefore, before replacing the operational model with the Research Version, it is recommended that additional model runs for a wide range of source conditions and meteorological scenarios are undertaken.

Furthermore, to the extent possible, it is desirable to conduct further evaluation studies with additional data sets, representing a wider range of physical conditions.

For most of the model validation undertaken, we have not only evaluated the performance of OML, but also of the US AERMOD model that resembles OML in many respects. Overall, the performance of the Re-

search Version of OML is similar to or better than that of AERMOD, when we consider cases *without* building effects.

A substantial effort has been devoted to the study of building effects. At the beginning of the model review it was anticipated that the building algorithm (PRIME) incorporated in AERMOD would be a candidate for inclusion within OML. PRIME is the result of a considerable development effort spent in the USA during the 1990's.

A much under-used data set - the Thompson wind tunnel data - has presented the opportunity to evaluate AERMOD for a range of building geometries and stack locations. Somewhat surprising, we can conclude that directly adopting an AERMOD approach in OML for building effect will in essence not result in a much more precise model for building effects. OML has shortcomings in respect to building effects, but so does AERMOD.

There are several recognised shortcomings of OML's building algorithm, and at the outset of the project the idea was to respond to them by adopting the AERMOD approach. However, this has proven not to be any solution to the problems. As it is, a user of either AERMOD or OML must accept rather large deviations between model predictions and observations for many situations with buildings. Predictions in the far field, away from the stack, are reasonable, but in the near field there can easily be overpredictions or underpredictions by a factor of 2 for both models. Such are the current limitations of the models.

It should be added that one of the shortcomings of OML probably can be alleviated with a rather simple change in the OML algorithm. This concerns a problem with abrupt cut-off of building influence when the stack is further than 2 building heights from the building.

The current state of affairs is that if a user wants predictions close to a building he can use a simple model, like OML or AERMOD, but he must then be willing to accept limited accuracy. Alternatively, the user can choose a model of a different category which is several orders of magnitude more demanding in terms of computer requirements. MISKAM is one such model that gives clearly better results than AERMOD and OML when buildings are present. MISKAM is also, however, much more demanding in terms of required man power and user skill and cannot be used for operational purposes in the same manner as the simpler models.

Summarising, it is recommended that the Research Version of OML, after a relatively short phase of consolidation, replace the current standard OML model. If possible within resource constraints, the existing OML building algorithm should be improved by eliminating the shortcoming of abrupt cut-off, as indicated above

As a long-term prospect, inclusion of a substantially better building algorithm is desirable. However, such an endeavour would require yet another major development effort, with no guarantee of success. Quality can probably be improved compared to the current OML or AERMOD, but in view of the complexities involved, it seems inevitable that any simple model must in some cases fail when facing real-world challenges.

As a side issue within the present project, the work with validation of OML has resulted in many findings of general interest for evaluation of atmospheric dispersion models. We have worked intensively with several research grade data sets. During the course of the work many pitfalls and problems with these data sets have been identified. Details of this work are explained in the supplementary report on model validation, referred to above.

## 8 Acknowledgements

The work presented here and conducted in 2005-06 was undertaken within the framework of the Danish research programme, *Action Plan for the Aquatic Environment III* (VMP III) under the Ministry of Food, Agriculture and Fisheries.

The current standard OML model, which forms basis for much of the work, was developed already in the 1980's within the project *Operational Meteorological Air Quality Models*. That project was carried out by the Air Pollution Laboratory under the National Agency of Environmental Protection with additional financial support from the Danish Technological Council and the Association of Danish Power Plants.

We wish here to acknowledge the other members of the original OML project group: Marie Bille, Nicky Brown, Högni Bäreñtsen, Knut Conradsen, Allan Bang Jensen, Jørgen S. Markvorsen, Ole Morsing, Synne Mølmark, Lars Bo Nielsen, Lars P. Prahm, Anne Marie Reiter.

Within the current project of reviewing the model, we have had valuable assistance from Matthias Ketzal of NERI who has contributed with MISKAM modelling work.

We appreciate the willingness of many individuals to provide experimental data to us. In particular, thanks to Steven Perry of the US EPA for providing the Thompson wind tunnel data, and to our colleagues at NERI and Risø National Laboratory for their help.

## 9 References

- Baerentsen, J. H. and Berkowicz, R. (1984): Monte-Carlo Simulation of Plume Dispersion in the Convective Boundary-Layer. *Atmospheric Environment* 18, 701-712.
- Barker, E. H. and Baxter, T. L. (1975): Computation of Atmospheric Surface-Layer Fluxes for Use in Numerical Modeling. *Journal of Applied Meteorology* 14, 620-622.
- Berkowicz, R., Olesen, H. R. and Torp, U. (1986): The Danish Gaussian air pollution model (OML): Description, test and sensitivity analysis in view of regulatory applications. 453-481.
- Berkowicz, R. and Prahm, L. P. (1982a): Evaluation of the Profile Method for Estimation of Surface Fluxes of Momentum and Heat. *Atmospheric Environment* 16, 2809-2819.
- Berkowicz, R. and Prahm, L. P. (1982b): Sensible Heat-Flux Estimated from Routine Meteorological Data by the Resistance Method. *Journal of Applied Meteorology* 21, 1845-1864.
- Berkowicz, R. and Prahm, L. P. (1984): Spectral Representation of the Vertical Structure of Turbulence in the Convective Boundary-Layer. *Quarterly Journal of the Royal Meteorological Society* 110, 35-52.
- Briggs, G. A. (1971): Some recent analyses of plume rise observations.
- Briggs, G. A. (1973): Diffusion estimation for small emissions. USDOC-NOAA. Environmental Res. Lab., Air Resources Atmos. Turb. & Diffusion Lab, Annual Report 1973 ATDL-106.
- Briggs, G. A. (1975): Plume rise predictions.
- Briggs, G. A. (1984): Plume Rise and Buoyancy Effects. 327-366.
- Businger, J. A., Wyngaard, J. C., Izumi, Y. and Bradley, E. F. (1971): Flux-Profile Relationships in Atmospheric Surface Layer. *Journal of the Atmospheric Sciences* 28, 181-&.
- Carpenter, S. B., Leavitt, J. M., Colbaugh, W. C. and Thomas, F. W. (1970): Principal plume dispersion models at TVA power plants.
- Caughey, S. J. and Palmer, S. G. (1979): Some aspects of turbulence structure through the depth of the convective boundary layer. *Quarterly Journal of the Royal Meteorological Society* 811-827.
- Cimorelli, A. J., Perry, S. G., Venkatram, A., Weil, J., Paine, R. J., Wilson, R. B., Lee, R. F., Peters, W. D., Brode, R. W. and Paumier, J. O. (2004): AERMOD: Description of model formulation. U.S. Environmental Protection Agency. EPA-454/R-03-004.

Davidson, G. A. (1989): Simultaneous Trajectory and Dilution Predictions from A Simple Integral Plume Model. *Atmospheric Environment* 23, 341-349.

Deardorf, J. W. (1972): Numerical Investigation of Neutral and Unstable Planetary Boundary-Layers. *Journal of the Atmospheric Sciences* 29, 91-115.

Eichhorn, J. (1996): Validation of a microscale pollution dispersal model. 539-548.

Gifford, F. A. (1961): Uses of routine meteorological observations for estimating atmospheric dispersion. *Nuclear Safety* 2, 47-51.

Gifford, F. A. (1975): Atmospheric dispersion models for environmental pollution applications.

Gifford, F. A. (1976): Turbulent Diffusion-Typing Schemes - Review. *Nuclear Safety* 17, 68-86.

Hanna, S. R. (1983): Lateral Turbulence Intensity and Plume Meandering During Stable Conditions. *Journal of Climate and Applied Meteorology* 22, 1424-1430.

Hanna, S. R., Briggs, G. A. and Hosker, R. P. Jr. (1982): Handbook on atmospheric diffusion. Technical information center. U.S. Department of Energy.

Hogstrom, U. (1996): Review of some basic characteristics of the atmospheric surface layer. *Boundary-Layer Meteorology* 78, 215-246.

Kaimal, J. C., Wyngaard, J. C., Haugen, D. A., Cote, O. R., Izumi, Y., Caughey, S. J. and Readings, C. J. (1976): Turbulence Structure in Convective Boundary-Layer. *Journal of the Atmospheric Sciences* 33, 2152-2169.

Løfstrøm, P., Jørgensen, H., Lyck, E. and Mikkelsen, T. (1994): A concentration fluctuation model for decision-makers based on joint tracer and lidar measurements from a non-buoyant elevated plume.

Løfstrøm, P., Jørgensen, H., Lyck, E. and Mikkelsen, T. (1996): Test of a New Concentration Fluctuation Model for Decision-Makers.

Løfstrøm, P. and Olesen, H. R. (1994): User's Guide for OML-Multi. An air pollution model for multiple point and area sources. National Environmental Research Institute. MST LUFT-A 126 (4th edition).

Markvorsen, J. S. (1982): Plume Rise (in Danish). National Environmental Research Institute. MST LUFT-A55.

Monin, A. S. and Obukhov, A. M. (1954): Dimensionless characteristics of turbulence in the atmospheric surface layer. *Dokl.Akad.Nauk.SSSR* 93, 223-226.

- National Environmental Research Institute (2005): OML-Multi 5.0 - getting started. National Environmental Research Institute.
- Nielsen, L. B., Prahm, L. P., Berkowicz, R. and Conradsen, K. (1981): Net Incoming Radiation Estimated from Hourly Global Radiation and Or Cloud Observations. *Journal of Climatology* 1, 255-272.
- Nieuwstadt, F. T. M. (1980): Application of Mixed-Layer Similarity to the Observed Dispersion from A Ground-Level Source. *Journal of Applied Meteorology* 19, 157-162.
- Olesen, H. R. (1993): User's Guide for OML-Point. An air pollution model for point sources. National Environmental Research Institute. MST LUFT-A125 (reprint).
- Olesen, H. R. (2005): User's Guide to the Model Validation Kit. National Environmental Research Institute. Research Notes from NERI 226.
- Olesen, H. R. (2006): Using the OML meteorological preprocessor - a practical guide.
- Olesen, H. R., Berkowicz, R. and Løfstrøm, P. (2007): OML: Model validation. National Environmental Research Institute. Technical Reports from NERI No. XXX (in preparation).
- Olesen, H. R. and Brown, N. (1992): The OML meteorological preprocessor - a software package for the preparation of meteorological data for dispersion models (2nd edition). National Environmental Research Institute. MST LUFT-A 122.
- Olesen, H. R. and Genikhovich, E. (2000): Building downwash algorithm for OML atmospheric dispersion model. National Environmental Research Institute. Research Notes from NERI 123.
- Olesen, H. R., Jensen, A. B. and Brown, N. (1992a): An operational procedure for mixing height estimation (2nd edition). National Environmental Research Institute. MST LUFT-A 96.
- Olesen, H. R., Løfstrøm, P., Berkowicz, R. and Jensen, A. B. (1992b): An improved dispersion model for regulatory use - the OML model. 29-38.
- Olesen, H. R., Løfstrøm, P., Berkowicz, R. and Ketzel, M. (2005): Regulatory odour model development: Survey of modelling tools and datasets with focus on building effects. National Environmental Research Institute. Technical Reports from NERI 541.
- Olesen, H. R. (1995a): Regulatory Dispersion Modeling in Denmark. *International Journal of Environment and Pollution* 5, 412-417.
- Olesen, H. R. (1995b): The Model Validation Exercise at Mol - Overview of Results. *International Journal of Environment and Pollution* 5, 761-784.
- Pasquill, F. (1961): The estimation of the dispersion of windborn material. *Meteorol.Mag.* 90, 33-49.

Paulsen, C. A. (1970): The mathematical representation of wind and temperature profiles in the unstable atmospheric surface layer. *Journal of Applied Meteorology* 9, 857-861.

Schulman, L. L. and Scire, J. S. (1980): Development of an air quality dispersion model for aluminium reduction plants. Environmental Research and Technology, Inc. Document P-7304 A.

Singer, I. A. and Smith, M. E. (1966): Atmospheric diffusion at Brookhaven National Laboratory. *International Journal of Water Pollution* 10, 125-135.

Strimaitis, D. G., Lavery, T. F., Venkatram, A., DiCristofaro, D. C., Greene, B. R. and Egan, B. A. (1985): EPA Complex terrain model development. Fourth Milestone Report - 1984. US EPA. EPA/600/3-84/110.

Taylor, G. I. (1921): Diffusion by continuous movements. *Proc.Londo.Math.Soc, Ser.2* 20, 196-202.

Tennekes, H. and Lumley, J. J. (1972): *A First Course in Turbulence*.

Thompson, R. S. (1993): Building Amplification Factors for Sources Near Buildings - A Wind-Tunnel Study. *Atmospheric Environment Part A-General Topics* 27, 2313-2325.

Turner, D. B. (1964): A diffusion model for an urban area. *Journal of Applied Meteorology* 3, 83-91.

Van der Hoven, I. (1976): A survey of field measurements of atmospheric diffusion under low wind speed inversion conditions. *Nuclear Safety* 17, 223-230.

Venkatram, A. (1992): Vertical Dispersion of Ground-Level Releases in the Surface Boundary-Layer. *Atmospheric Environment Part A-General Topics* 26, 947-949.

Weil, J. and Brower, R. P. (1982): The Maryland PPSP dispersion model for tall stacks. Martin Marietta Corp., Environmental Center. PPSP-MP-36.

Weil, J. and Corio, L. A. (1988): A Modification of the PPSP Dispersion Model for Highly Buoyant Plumes. Versar, Inc. PPRP-MP-60. NTIS No. PB88-231105/AS.

Willis, G. E. and Deardorf, J. W. (1974): Laboratory Model of Unstable Planetary Boundary-Layer. *Journal of the Atmospheric Sciences* 31, 1297-1307.

Willis, G. E. and Deardorff, J. W. (1976): Laboratory Model of Diffusion Into Convective Planetary Boundary-Layer. *Quarterly Journal of the Royal Meteorological Society* 102, 427-445.

Willis, G. E. and Deardorff, J. W. (1978): Laboratory Study of Dispersion from An Elevated Source Within A Modeled Convective Planetary Boundary-Layer. *Atmospheric Environment* 12, 1305-1311.

Willis, G. E. and Deardorff, J. W. (1981): A Laboratory Study of Dispersion from A Source in the Middle of the Convectively Mixed Layer. *Atmospheric Environment* 15, 109-117.

## Appendix A

### Treatment of area sources in the OML atmospheric dispersion model

Internal note from 1999

Department of Atmospheric Environment  
National Environmental Research Institute

By Per Løfstrøm and Helge Rørdam Olesen

## Area sources

The OML model is available in two main versions, OML-Point and OML-Multi. One of the features that distinguish OML-Multi is that it includes algorithms to handle area sources.

The area source algorithm in OML-Multi has undergone major changes from the version released in 1989-91 to the version to be released in year 2000. The present document presents the basic features of the old and new algorithms, and explains in some detail the considerations upon which the new version is based.

## Old version

### *Square area sources*

The original version of the area source algorithm was developed for modelling dispersion of emissions from uniformly distributed sources for individual domestic heating aggregated in large areas; and was used for mapping air pollution in entire cities. For this purpose the algorithms were constructed to consider only square areas with optional side length and emission height. From each square the dispersion was simulated as a non-buoyant point source, with initial dispersion parameters  $\sigma_{y,0}$  and  $\sigma_{z,0}$ . The point source was located at the centre of the square. In cases where the receptor was located inside the area, the point source was placed in the centre of the upwind part of the area, assuming that the square was always oriented with one side parallel to the wind direction.

### *Initial dispersion parameters*

The initial dispersion parameter  $\sigma_{y,0}$  was proportional to the side length  $L_s$  of the square area source:

$$\sigma_{y,0} = L_s / \sqrt{2\pi} \quad (0.1)$$

and  $\sigma_{z,0}$  was proportional to the emission height  $h_s$ , thereby simulating building effects on the initial dispersion:

$$\sigma_{z,0} = 0.5h_s \quad (0.2)$$

### *Total dispersion parameters*

The total dispersion parameters  $\sigma_y$  and  $\sigma_z$  depended on the downwind distance,  $x$ :

$$\begin{aligned} \sigma_y &= \max\{\sigma_{y,0}, \sigma_{y,p}(x)\} \\ \sigma_z &= [\sigma_{z,0}^2 + \sigma_{z,p}(x)^2]^{1/2} \end{aligned} \quad (0.3)$$

where  $\sigma_{y,p}(x)$  and  $\sigma_{z,p}(x)$  was determined as for a non-buoyant point source without any initial dispersion.

*Small area sources might result in correct centerline values, but problematic "tails"*

When downwind change in the vertical dispersion can be disregarded (such as for small area sources where  $\sigma_{z,0} \gg \sigma_{z,p}(x)$ ) and the horizontal dispersion  $\sigma_{y,p}(x)$  is small compared to the area side length, the value of  $\sigma_{y,0}$  from Eq. (0.3) ensures that the "correct" maximum

concentration is computed if we consider points at the centerline inside and just outside the area source - but only when the wind direction is parallel to the side of the real area source. The consequence of using the "correct" value for the maximum concentration is that the plume in the first phase of its travel becomes too wide, because the Gaussian crosswind concentration profile does not describe the correct shape of the plume for a square area; the correct shape is like a "top hat" (Fig A1), and the "tails" of the distribution are not well described by a Gaussian profile.

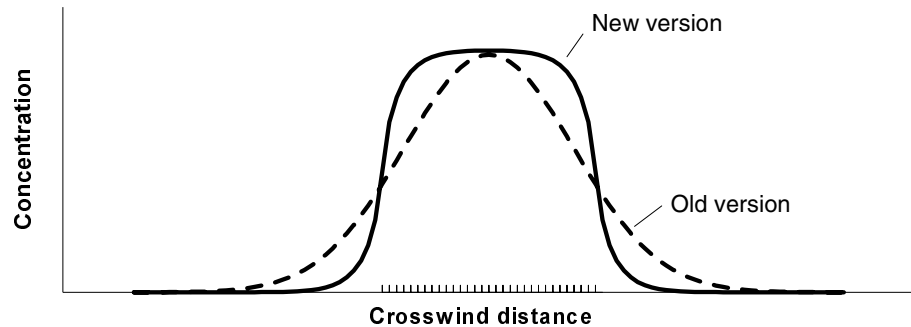


Fig. A1 Crosswind profile of concentration distribution resulting from a square area source, computed along a cross-section immediately downwind of the source. The curves show the profile according to the old OML algorithm, and the "top-hat" profile found in reality and predicted by the new algorithm.

*Problem:  $\sigma_y$  was assumed constant for a range of distances*

Furthermore, in the original algorithm  $\sigma_y$  was constant for downwind receptors at distances up to 2-5  $L_s$ , implying that the horizontal dispersion did not contribute to any change in the concentration levels. This gave rise to an error outside the area source; the maximum error at the centerline was up to about 30% (overprediction). Of course, these errors vanished further downwind.

*Large area sources might give incorrect results both for centerline and tails*

On the other hand, when the downwind change in the vertical dispersion cannot be disregarded (as for large area sources where  $\sigma_{z,0} \ll \sigma_{z,p}(x)$ ) and at distances less than 2-5  $L_s$  where  $\sigma_{y,p}(x) \ll \sigma_{y,0}$ , the centerline concentration errors could be large due to the non-linearity in the Gauss formula (the sum of many point sources gives a different result than one source in the centre). The errors have been estimated at the downwind edge of area sources ( $h_s=0$ ) at receptors 1.5 m above the ground level. The largest overprediction of about 35% was found for side lengths of 30-80 m depending on the stability, and the error decreased rapidly downwind. For large side lengths an underprediction was found, which increased as the side length increased. For a side length of 500 m a maximum error of -90% occurred, but this error decreased rapidly downwind, and 0.5  $L_s$  or 250 m downwind the error was -10% and possible  $\sigma_y$ -errors would dominate.

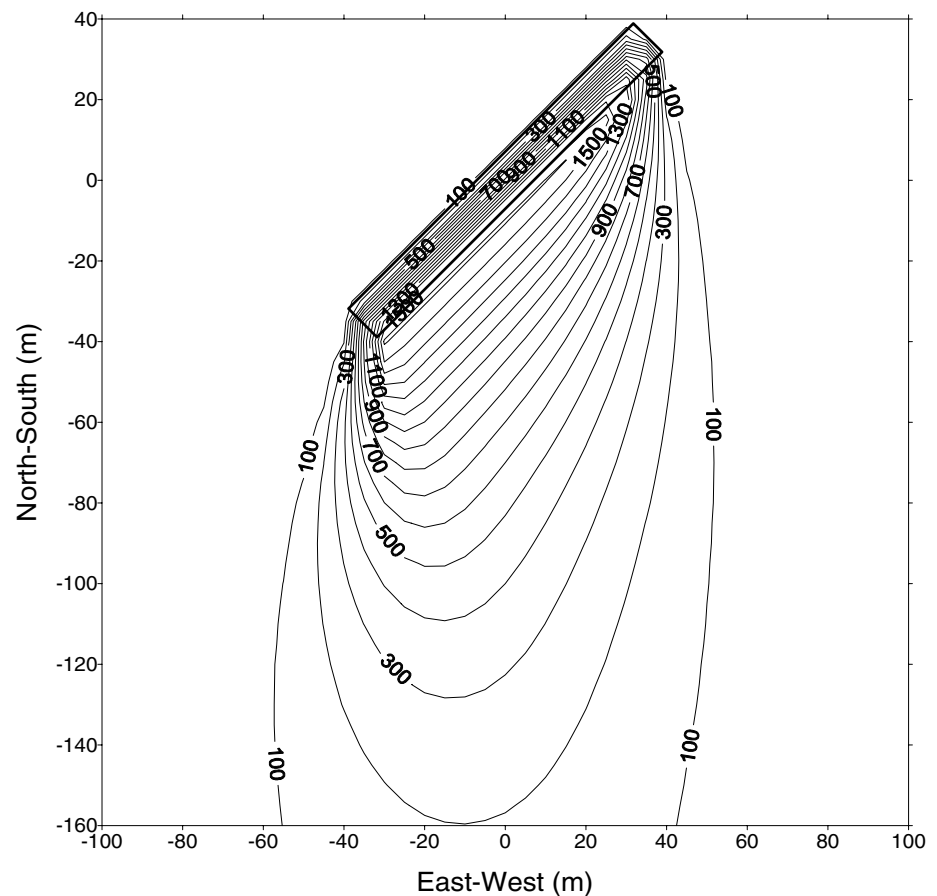
## The new version

*Rectangular sources allowed; orientation and release height are now user-specified*

In the new version of the area source algorithm, the plume is not any longer considered as a single point source with modified dispersion parameters; now, dispersion is modelled by integration over an area source with an infinite number of non-buoyant point source plumes

(cf. EPA, 1995). The former restriction, that only square areas sources could be treated, has been removed; now, rectangular areas sources are accepted which have aspect ratios (length/width) of up to 10, and a maximum and minimum side length of 1000 m and 1 m, respectively. The area orientation and release height are now optional parameters. Even though the area source algorithm models dispersion of uniform emission from a surface, it is also possible to model the dispersion of aggregated emissions from many point sources with building effects (domestic heating); for that purpose a general building height can be supplied by the user. The building height may influence the initial vertical dispersion of the point source plume. The plume dispersion parameters  $\sigma_y$  and  $\sigma_z$  and formulation for the effect of buildings in the vertical direction ( $\sigma_z$ ) are the same as those used in the OML model in general.

Fig. A2 shows an example of concentration contours computed with the new algorithm; the old algorithm could not directly handle a source of the type shown.



direction the integration is approximated using numerical methods, which include Romberg integration technique (Press et al., 1986). The numerical integration method is an iterative procedure where an integral  $I$  is estimated by a trapezoidal approximation with a doubling of the number of intervals  $N$  to  $2N$  at each new integration. The result makes use of a weighted average of the previous results:

$$I = I_{2N} + (I_{2N} - I_N)/3$$

The sequence of integration results  $I_i$  are treated as a polynomial in  $k$ , and a polynomial extrapolation of the result to zero interval-size is made. This means that the number of iterations (or the number of times the interval have been halved) must at least be  $k$  before the extrapolation is performed. The iteration is stopped when the change in successive integration results has converged to a certain level  $\epsilon$ , or when the maximum number of iterations  $N_x$  is reached. In the OML algorithm these integral parameter values are  $N_x=7$  (corresponding to  $1 + 2^{N_x-1} = 65$  finite line sources),  $k = 5$  and  $\epsilon = 0.0001$ . In comparison, the values for AERMOD/ISCST3 are  $N_x=10$ ,  $k = 4$  and  $\epsilon = 0.0001$ . Despite the fact that  $k$  is larger for OML, this choice of parameter values results in a 2.5 times faster calculation than the AERMOD parameter values (but still, the new more accurate procedure is approximately 14 times slower than the old OML algorithm). The numerical integration errors (mean and maximum errors) are almost the same as for AERMOD; although  $N_x$  is smaller in OML, the increased value of  $k$  has ensured that accuracy is retained. OML performs slightly better for side length up to about 100 m and slightly poorer for larger area sources.

*Far downwind, the source is approximated by a line source.*

At very far distances the numerical integration is replaced by an equivalent single line source for faster calculations. The line source is located at the centre of the area and is perpendicular to the wind direction; its width is the maximum of one of the following three candidates: (1) the average crosswind width of the area source and (2 and 3) the crosswind widths of each of the two sides. Three criteria for using the single line source should be met:  $x > 5 L_x$ ,  $\sigma_y > 0.5 L_x$ , and  $\sigma_z > 2 \sqrt{h_s z_r}$ , where  $x$  is the distance from the area centre to the receptor,  $L_x$  is the along-wind length of the area source,  $h_s$  is the release height, and  $z_r$  is the receptor height.

*Accuracy of numerical procedure*

The numerical errors have been estimated on the basis of runs for several different area sizes and aspect ratios, for 0 m release height and 1.5 m receptor heights; values calculated with the new algorithm and the parameter values specified above and have been compared with reference calculations where Romberg extrapolation is not performed, while  $N_x=10$  and  $\epsilon = 10^{-6}$ . One month of hourly meteorological data was used for concentration calculations at 360 receptors placed at different distances around the area sources. For the monthly maximum and mean concentrations, the relative error averaged over all receptors is approximately 0.6 % and 0.2 %, respectively. When looking at single receptors, the largest relative error for a single receptor (always located inside or adjacent to the area) is, respectively, approximately 3.8 % and 1.2 % for the maximum and monthly mean

concentration (this is an average for runs with various area configurations). The maximum errors decrease very rapidly within the first few tens of meters away from the area source.

### **References:**

EPA, 1995. User's Guide for the Industrial Source Complex (ISC3) dispersion models. Volume II - Description of model algorithms.

Press, W., Flannery, B., Teukolsky, S. and Vetterling, W. 1986. Numerical Recipes, Cambridge University Press, New York, 702 pp.

## **NERI National Environmental Research Institute**

DMU Danmarks Miljøundersøgelser

National Environmental Research Institute,  
NERI, is a part of  
University of Aarhus.

NERI's tasks are primarily to conduct  
research, collect data, and give advice  
on problems related to the environment  
and nature.

At NERI's website [www.neri.dk](http://www.neri.dk)  
you'll find information regarding ongoing  
research and development projects.

Furthermore the website contains a database  
of publications including scientific articles, reports,  
conference contributions etc. produced by  
NERI staff members.

Further information: [www.neri.dk](http://www.neri.dk)

National Environmental Research Institute  
Frederiksborgvej 399  
PO Box 358  
DK-4000 Roskilde  
Denmark  
Tel: +45 4630 1200  
Fax: +45 4630 1114

Management  
Personnel and Economy Secretariat  
Monitoring, Advice and Research Secretariat  
Department of Policy Analysis  
Department of Atmospheric Environment  
Department of Marine Ecology  
Department of Environmental Chemistry and Microbiology  
Department of Arctic Environment

National Environmental Research Institute  
Vejlsovej 25  
PO Box 314  
DK-8600 Silkeborg  
Denmark  
Tel: +45 8920 1400  
Fax: +45 8920 1414

Monitoring, Advice and Research Secretariat  
Department of Marine Ecology  
Department of Terrestrial Ecology  
Department of Freshwater Ecology

National Environmental Research Institute  
Grenåvej 14, Kalø  
DK-8410 Rønde  
Denmark  
Tel: +45 8920 1700  
Fax: +45 8920 1514

Department of Wildlife Ecology and Biodiversity

## NERI Technical Reports

NERI's website [www.neri.dk](http://www.neri.dk) contains a list of all published technical reports along with other NERI publications. All recent reports can be downloaded in electronic format (pdf) without charge. Some of the Danish reports include an English summary.

- Nr./No. 2006**
- 600 Assessing Potential Causes for the Population Decline of European Brown Hare in the Agricultural Landscape of Europe – a review of the current knowledge.  
By Olesen, C.R. & Asferg, T. 30 pp.
  - 599 Beregning af naturtilstand ved brug af simple indikatorer. Af Fredshavn, J.R. & Ejrnæs, R. 93 s.
  - 598 Klimabetingede effekter på marine økosystemer. Af Hansen, J.L.S. & Bendtsen, J. 50 s.
  - 597 Vandmiljø og Natur 2005. Tilstand og udvikling – faglig sammenfatning. Af Boutrup, S. et al. 50 s.
  - 596 Terrestriske Naturtyper 2005. NOVANA. Af Bruus, M. et al. 99 s.
  - 595 Atmosfærisk deposition 2005. NOVANA. Af Ellermann, T. et al. 64 s.
  - 594 Landovervågningsoplande 2005. NOVANA. Af Grant, R. et al. 114 s.
  - 593 Smådyrfaunaens passage ved dambrugsspærringer. Af Skriver, J. & Friberg, N. 33 s.
  - 592 Modelling Cost-Efficient Reduction of Nutrient Loads to the Baltic Sea. Model Specification Data, and Cost-Fnctions. By Schou, J.S. et al. 67 pp.
  - 591 Økonomiske konsekvenser for landbruget ved ændring af miljøgodkendelsen af husdyrbrug. Rapport fra økonomiudredningsgruppen. Af Schou, J.S. & Martinsen, L. 55 s.
  - 590 Fysisk kvalitet i vandløb. Test af to danske indices og udvikling af et nationalt indeks til brug ved overvågning i vandløb. Af Pedersen, M.L. et al. 44 s.
  - 589 Denmark's National Inventory Report – Submitted under the United Nations Framework Convention on Climate Change, 1990-2004. Emission Inventories. By Illerup, J.B. et al. 554 pp.
  - 588 Agerhøns i jagtsæsonen 2003/04 – en spørgebrevundersøgelse vedrørende forekomst, udsætning, afskydning og biotoppleje. Af Asferg, T., Odderskær, P. & Berthelsen, J.P. 47 s.
  - 587 Målinger af fordampning af pesticider fra jord og planter efter sprøjtning.  
Af Andersen, H.V. et al. 96 s.
  - 586 Vurdering af de samfundsøkonomiske konsekvenser af Kommissionens temastrategi for luftforurening. Af Bach, H. et al. 88 s.
  - 585 Miljøfremmede stoffer og tungmetaller i vandmiljøet. Tilstand og udvikling, 1998-2003.  
Af Boutrup, S. et al. 140 s.
  - 584 The Danish Air Quality Monitoring Programme. Annual Summary for 2005.  
By Kemp, K. et al. 40 pp.
  - 583 Naturgenopretning af søerne i Vejlerne – en vurdering af effekterne på yngle- og trækfugle.  
Af Clausen, P., Holm, T.E. & Kjeldsen, J.P. 122 s.
  - 582 Arter 2004-2005. NOVANA. Af Søgaard, B., Pihl, S. & Wind, P. 145 s.
  - 581 Physical and biological oceanography in West Greenland waters with emphasis on shrimp and fish larvae distribution. By Søderkvist, J., Nielsen, T.G. & Jespersen, M. 54 pp.
  - 580 Habitatmodellering i Ledreborg Å. Effekt af reduceret vandføring på ørred.  
Af Clausen, B. et al. 58 s.
  - 579 Aquatic and Terrestrial Environment 2004. State and trends – technical summary.  
By Andersen, J.M. et al. 136 pp.
  - 578 Limfjorden i 100 år. Klima, hydrografi, næringsstofflørsel, bundfauna og fisk i Limfjorden fra 1897 til 2003. Af Christiansen, T. et al. 85 s.
  - 577 Limfjordens miljøtilstand 1985 til 2003. Empiriske modeller for sammenhæng til næringsstofflørsler, klima og hydrografi. Af Markager, S., Storm, L.M. & Stedmon, C.A. 219 s.
  - 576 Overvågning af Vandmiljøplan II – Vådområder 2005. Af Hoffmann, C.C. et al. 127 s.
  - 575 Miljøkonsekvenser ved afbrænding af husdyrgødning med sigte på energiudnyttelse. Scenarieanalyse for et udvalgt opland. Af Schou, J.S. et al. 42 s.
  - 574 Økologisk Risikovurdering af Genmodificerede Planter i 2005. Rapport over behandlede forsøgsudsætninger og markedsføringsager.  
Af Kjellsson, G., Damgaard, C. & Strandberg, M. 22 s.
  - 573 Monitoring and Assessment in the Wadden Sea. Proceedings from the 11. Scientific Wadden Sea Symposium, Esbjerg, Denmark, 4.-8. April 2005. By Laursen, K. (ed.) 141 pp.
  - 572 Søerne i De Vestlige Vejler. Af Søndergaard, M. et al. 55 s.

OML is a local-scale operational air pollution model for estimating dispersion from point sources and area sources. Based on the original OML model, several model versions have been developed over the years to treat different regulatory aspects in Denmark, including assessment of industrial air pollution, regulation of odour and assessment of ammonia deposition. The model was reviewed in 2005-06, and model performance was evaluated with more experimental data than previously. A number of problems were identified, and various issues have been resolved with introduction of new parameterisations in certain parts of the model. The outcome of the process is a revised model, referred to as the "Research Version" of OML.